

Flow and Sediment-POM transport in stream with vegetation

HO-SEONG JEON

Advisor : Professor Tetsuro TSUJIMOTO

Special Forefront Studies program

Department of Civil Engineering

NAGOYA UNIVERSITY

Japan

TABLE OF CONTENTS

CHAPTER 1: INTRODUCTION

1.1 Background	1
1.2 Literature Review.....	4
<i>1.2.1 Flow through vegetation</i>	4
<i>1.2.2 Sediment transport through vegetation</i>	7
<i>1.2.3 Particulate organic matter through vegetation</i>	10
1.3 Study Object and Method.....	11
1.4 Contents.....	12
References	14

CHAPTER 2: LABORATORY EXPERIMENTS FOR FLOW AND TRANSPORT AND DEPOSITION PROCESS OF SEDIMENT AND POM

2.1 General.....	23
2.2 Laboratory experiments	24
<i>2.2.1 Overview of laboratory experiment</i>	24
<i>2.2.2 Longitudinal transition in riparian vegetation</i>	25
<i>2.2.3 Transverse dispersion in riparian vegetation</i>	33
2.4 Concluding Remarks.....	39

References	4 0
------------------	-----

CHAPTER 3: DISCUSSION ON 2D DEPTH AVERAGE MODEL FOR FLUVIAL PROCESS WITH VEGETATION

3.1 General	4 3
--------------------------	-----

3.2 Conventional method	4 4
--------------------------------------	-----

<i>3.2.1 Outline of Numerical analysis method</i>	4 4
---	-----

<i>3.2.2 Flow model</i>	4 5
-------------------------------	-----

<i>3.2.3 Sediment and bed variation model</i>	4 7
---	-----

<i>3.2.4 Numerical grid and basic of discretization of governing equations</i>	5 0
--	-----

<i>3.2.5 Fractional step method</i>	5 2
---	-----

<i>3.2.6 Interpolation technique</i>	5 5
--	-----

3.3 Discussion of flow and sediment transport with vegetation	5 7
--	-----

3.4 Concluding Remarks	5 9
-------------------------------------	-----

References	6 0
------------------	-----

CHAPTER 4: CONCEPT OF BED ROUGHNESS BOUNDARY LAYER IN VEGETATED AREA

4.1 General	6 3
--------------------------	-----

4.2. Concept and formulation of Boundary layer thickness	6 4
---	-----

<i>4.2.1 Experiment data of Liu</i>	6 5
---	-----

<i>4.2.2 Interaction formula</i>	6 7
--	-----

4.2.3 Friction velocity in the vegetation	6 9
4.2.4 Velocity Distribution in bed roughness boundary layer in vegetated area	7 1
4.2.5 Resistance law in vegetated area	7 3
4.2.5.1 Velocity distribution and kinematic eddy viscosity in bed roughness boundary layer in vegetated area	7 3
4.2.5.2 Lateral mixing of momentum and lateral distribution of depth averaged velocity	7 4
4.3 Discussion on resistance law in vegetated area.....	7 5
4.4 Concluding Remarks.....	7 6
References	7 7
 CHAPTER 5: APPLICATION OF BED ROUGHNESS BOUNDARY LAYER CONCEPT	
5.1 General.....	7 9
5.2 Flow and sediment transport with non submerged vegetation in 1D scheme	8 0
5.2.1 Uniform flow in a stream with Non submerged vegetation	8 1
5.2.2 Description of sediment transport in vegetated stream	8 4
5.2.3 Secondary flow and dynamic equilibrium bed profile at a bend in vegetated stream	8 6
5.3 Comparison with bed load deposition in decelerated area in vegetation	8 8
5.3.1 Laboratory experiment (full width vegetation)	8 8

5.3.2 Simulation of depth-averaged flow and comparison with flume experiment (full width vegetation)	8 8
5.3.3 Bed load transport and deposition in vegetated area (full vegetation)	9 1
5.3.4 Laboratory experiment (half width vegetation)	9 3
5.3.5 Simulation of depth-averaged flow and comparison with flume experiment (half width vegetation)	9 3
5.3.6 Bed load transport deposition in vegetated area(half vegetation)	9 5
5.4 Suspended sediment concentration in bed roughness boundary layer..	9 7
5.4.1 Ratio of depth averaged concentration and bottom concentration	9 8
5.4.2 Comparison of suspended sediment concentration profile	1 0 2
5.5 Concluding Remarks.....	1 0 4
References	1 0 8
 CHAPTER 6: TRANVERSE MIXING IN FLOW AND SUSPENDED SEDIMENT IN STREAM WITH VEGETATION ZONE	
6.1 General.....	1 1 1
6.2 Lateral mixing between flow and suspended sediment between areas without and with non submerged vegetation	1 1 2
6.2.1 Lateral mixing of momentum and lateral distribution of depth-averaged velocity	1 1 2
6.2.2 Lateral mixing of suspended sediment and lateral distribution of depth averaged concentration of suspended sediment	1 1 3

6.3 Transverse distribution of depth-averaged flow in stream with vegetation	1 1 3
.....	
<i>6.3.1 Transverse diffusion coefficient for flow with vegetation</i>	1 1 3
<i>6.3.2 Kinematic eddy viscosity investigated by k-ϵ model</i>	1 1 6
6.4 Transverse distribution of depth-averaged concentration of suspended sediment in stream with vegetation	1 2 0
6.5 Suspended sediment transport deposition in vegetated area	1 2 4
6.6 Concluding Remarks	1 2 9
References	1 3 0
 CHAPTER 7: TRANSPORT OF POM WITH SEDIMENT	
7.1 General	1 3 1
7.2 Field observation	1 3 2
<i>7.2.1 Overview of field observation</i>	1 3 2
<i>7.2.2 Deposition characteristic in the field</i>	1 3 3
<i>7.2.3 Sedimentation test</i>	1 3 6
7.3 Deposition process of POM transported with sand	1 3 8
<i>7.3.1 Flume experiment</i>	1 3 8
<i>7.3.2 Deposition process of POM Transported with Sand</i>	1 4 0
7.4 Modeling of POM deposition with ripple	1 4 1
<i>7.4.1 Model concept</i>	1 4 1

7.4.2 Simulation of CPOM deposition and comparison with flume experiment....	1	4	4
7.5 Concluding Remarks.....	1	4	5
References	1	4	6
CHAPTER 8: GENERAL SUMMARY AND CONCLUSIONS			
8.1 General.....	1	4	9
8.2 Experimental studies	1	5	0
8.2.1 Longitudinal transition in riparian vegetation	1	5	0
8.2.2 Transverse dispersion in riparian vegetation	1	5	1
8.3 Numerical studies	1	5	1
8.3.1 Development of numerical analysis method	1	5	1
8.3.2 boundary layer thickness	1	5	2
8.3.3 Comparison with bed load deposition in decelerated area in vegetation	1	5	3
8.3.4 Comparison with transverse distribution in stream with vegetation	1	5	5
8.3.5 Transport of POM with sediment.....	1	5	5
A.1 General	1	5	7
A.2 Discretization of basic equation	1	5	7
A.3 Momentum equation of u, w	1	5	9
A.4 Solution of discretized equation	1	6	0
B.1 Bed load transport formulas	1	6	5

B.1.1 Meyer-Peter Mueller(1948)	1 6 5
B.1.2 Frijlink(1952)	1 6 6
B.1.3 Bagnold(1966)	1 6 6
B.2 Suspended load transport rates	1 6 9
B.2.1 Einstein(1950)	1 6 9
B.2.2 Bijker(1971)	1 7 0
B.2.3 Van Rijn(1984)	1 7 1
References	1 7 2

CHAPTER 1

INTRODUCTION

1.1 Background

A river basin is the portion of land drained by a river and its tributaries. It encompasses all of the land surface dissected and drained by many streams and creeks that flow downhill into one another, and eventually into one river. The final destination is an estuary or an ocean and it sends all the water falling on the surrounding land into a central river and out to the sea as shown Fig. 1.1. Not only water but also sediment and several materials are transported along a river, and they support many kinds of organic matters.

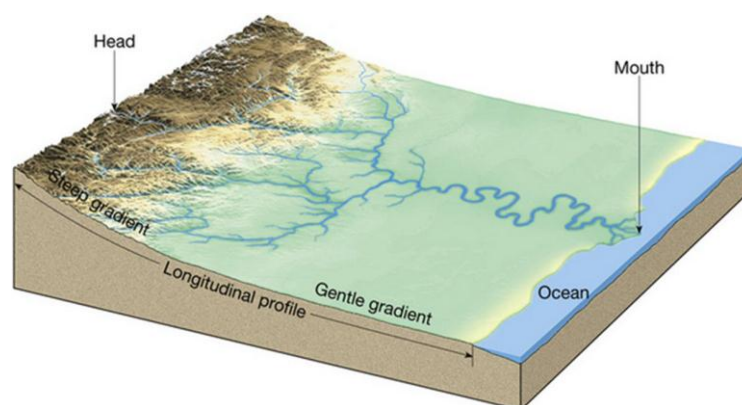


Fig. 1.1 Concept and organization of river basin

Source: bc.outcrop.org

Hydrological cycle in a river basin is a conceptual model that describes the storage and movement of water between the hydrosphere, atmosphere and biosphere. It is also takes a role not only transporting water but also sediment and various materials including biophilic elements. In conveyance process of biophilic elements, they will change from inorganic to organic matters, and they sometimes form biomass. In this sense the hydrological cycle drives even bio-aspects related to various organisms.

Recently, Such as river basins are developed in order to achieve certain objectives, among which are the control of floods; the generation of power; the supply of water for municipal, industrial, and agricultural use; opportunities for fishing; improved transportation; and recreation. River basin development is closely related to these processes and river basin management is a key for sustainability of human activity. In particular, management of rivers must be efficient where the above processes are dynamic. Since the revision of river law in 1997, ecosystem conservation has become one of the objectives of river management, and we need to understand the research topics how to recognize the mechanism of river ecosystem. River ecosystem is recognized as an interrelating system among (A) physical basement, (B) biota and (C) biophilic elements cycle by tsujimoto (2008): When fluxes(water, sediment, materials, temperature, etc.) pass through the above system, the interactions in the system become active, and various ecosystem functions appear as shown in Fig. 1.2.

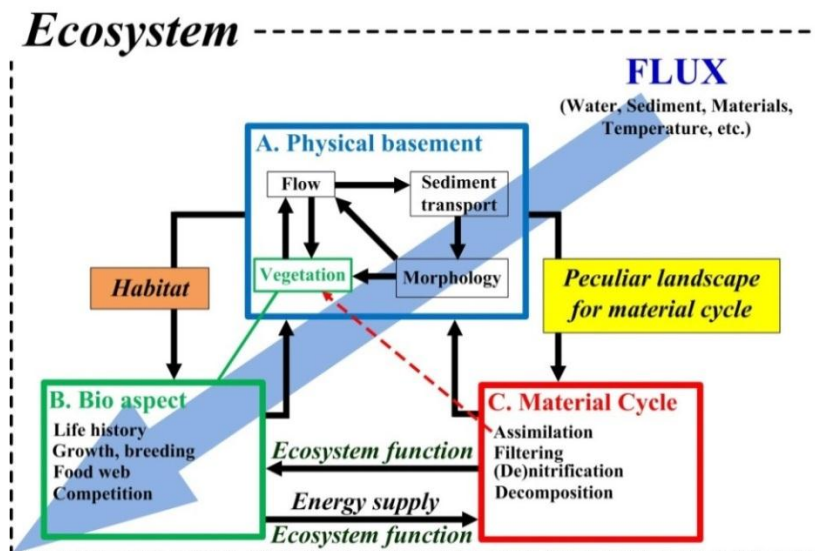


Fig. 1.2 Landscape expressed by interrelating system

As for the subsystem(A), the vegetation plays many essential roles in the functioning of river ecosystem, including: flow regulation: the vegetation slows the flow of water, both by physically blocking the passage of water, and by absorbing the water into its root systems. water quality regulation: the vegetation acts as a buffer or filter between nutrients, sediments, contaminants, and bacteria from the surrounding land and air, and the river channel itself. habitat provision: the riparian vegetation zone is an important habitat for many plants and animals, because it is an area of transition between the land and the river. These relatively steep environmental gradients (moisture, temperature, topography, and soil) generally support higher levels of biodiversity than more homogeneous areas. Especially, vegetation plays an important role in fluvial processes, and fluvial processes in streams with vegetation have become hot topics in river hydraulics. Vegetation significantly affects flow, sediment transport and bed morphology, while morphology governs growth and decay of vegetation with flow regime. Since the vegetation affects flood flow with higher resistance, vegetation dynamics and its control are critical issue from flood management as well as ecosystem management. Habitat suitability is another topics in ecohydraulics. Combining it with the knowledge of population dynamics, some aspect of biota can be described. As for biota (B), life cycle and food web are especially focused on. Habitat of some species should be considered in relation to their characteristic life cycle and energy supply based on food web. and it is described as population dynamics of organisms, where that for one species is related to those for other species in its food web. Production and respiration in population dynamic are intimately related to biophilic element material cycle(C). As for the subsystem(C), In aquatic ecosystems, most particulate organic matters (POM) with smaller specific weight are suspended in water, and gradually settles. In particular, many different types of material are collected together by currents, and much material settles in slowly flowing areas, and its role is great on river ecosystem.

Recently depth-averaged analysis of flow and sediment transport has become familiar and powerful means in river management. To date, many kinds of hydraulic model have been performed to analyze hydrodynamical and geomorphological characteristics of riparian vegetation zone, but several issues remained in numerical modeling in depth-average scheme. The objective of the this study is to describe the detailed characteristics of flow through rigid vegetation, considering new resistance law and to find out complicated sediment transport processes including particulate organic matters (POM).

Chapter 1 describes as follows. The first is existing research related to this study,

second is subject and methodology of study third is structure of this thesis.

1.2 Literature Review

1.2.1 Flow through vegetation

Many researchers have attempted to identify the effect of vegetation using a resistance parameter. Early researcher attempt to describe vegetation roughness use the Chezy coefficient, C (Leliavsky (1959), Chow (1959), Strupczewski (1996), Strupczewski and Szymkiewicz (1989, 1996)), Manning roughness coefficient, n (Arcement and Schneider (1989), De Doncker et al. (2009), Petryk and Bosmajian (1975), Sepaskhah and Bondar (2002), Limerinos (1970), Li and Zhang (2001), Morvan et al. (2008)). And the Darcy-weisbach friction factor, f (Kouwen (2000), Fathi-Moghadam (1997), Chen (1976), Aberle et al. (2010)).

It is also common for hydraulic conductivity to be estimated using empirically derived formulas. Out of all hydraulic parameters involved in the process, roughness coefficients represent is a key for a practical numerical simulation of vegetated open channel flows, but remain especially difficult to determine (Kidson et al. (2005), Thorndy craft et al. (2005), Zhu and Zhang (2009)) and the roughness coefficients are influenced by many kinds of factor (Chow (1959), Aldridge and Garrett (1973)). James et al. (2004) addresses the necessity to find methods other than the conventional roughness formulations to describe flow in presence of vegetation. They also made mention of conventional resistance equations (such as those of Manning, Chezy and Darcy-Weisbach) are inadequate for flow through emergent vegetation, where resistance is exerted originally by stem drag throughout the flow depth rather than by shear stress at the bed.

Some research attempt to describe the problem of roughness parameter estimation was extensively examined by using the various simulation optimization models((Becker and Yeh, 1972, 1973; Wasantha Lal, 1995; Ramesh et al., 2000; Ding et al., 2004; Nguyen and Fenton, 2004; Ding and Wang, 2005; Waichler et al., 2005; Tang et al., 2010; Ayvaz and Genç, 2012).

To improve resistance relationships, many researchers have been conducted vegetation with:

- **Submerged and non-submerged(rigid vegetation)**

In the vegetation resistance, the height of the vegetation according to the water depth is important because it influence the flow velocity profile. The flow velocity profile about submerged and non-submerged vegetation is very different so these kinds of condition are deal with separately. In the case of flow over fully submerged vegetation, the vegetation does not interrupt the velocity at the upper part of the water depth. After flow become stable, The velocity becomes a logarithmic profile. Fully submerged vegetation can be described as a roughness and therefore can be approximated by Manning roughness coefficient (Augustijn et al. 2008).

Second case is flow through non submerged vegetation. The mean velocity of non submerged vegetation is easier to calculate than submerged vegetation. Near the channel bed, the velocity is lower, due to bottom roughness. Petryk and Bosmaian (1975) derived an equation using the resistance acting on the flow balanced with the drag force. The resistance acting on the flow are; gravity, shear forces on the boundary caused by viscosity and wall roughness and drag forces on the vegetations. Stone and Shen (2002) also derived an equation to determine the vegetation resistance verified by their laboratory experiment for submerged and emergent rigid vegetation with stems of various sizes and densities. They started with the momentum balance in streamwise direction. Hoffmann (2004) developed a space-time averaged form of the Navier-Stokes equation treating the vegetation as a porous media. He averaged the Navier-Stokes equation in time and volume. And he defined the closure term needed in the time and volume averaged Navier-Stokes equation. This closure term depicts the interaction of the flow with the porous media and consider the extra drag exerted on the fluid according to the presence of the vegetation stems, based on the macroscopic variables.

Third case is flow through submerged vegetation. In this case, due to higher velocities in the surface layer above the vegetation, a shearing effect in the vegetation layer occurs. Because of the difference in velocity in these two layers, vegetation depiction for submerged vegetation are often based on a two-layer approach. The two-layer approach depicts the velocity inside the vegetation layer separately from the velocity inside the layer above the vegetation. The averaged velocity inside the vegetation (U_v) is often assumed to be constant (Klopstra et al., 1997 and Huthoff, 2007). Above the vegetation often a logarithmic profile is assumed for the velocity distribution in the surface layer (U_s). Borovkov and Yurchuk (1994) derived an equation for the resistance of submerged vegetation using the theory and laboratory

investigations from Tai (1973), Kouwen et al. (1969), Chow (1959). The method of Klopstra et al. (1997) is included in the two-dimensional WAQUA models, which is used in the Netherlands for modeling. The turbulent length scale α of Van Velzen et al. (2003) is empirically determined. There are also other authors who derived an equation for this parameter. Meijer (1998b) used the results of 56 flume tests and derived empirically the following relation. Another formula for the turbulent length scale is defined by Huthoff (2007). He found the highest coefficient of correlation for the relation. Van Velzen et al. (2003) assumed a flow velocity in the vegetation layer that is unaffected by surface layer flow. Stone and Shen (2002) is used to describe the mean velocity inside the vegetation layer using the submergence fraction. From the momentum balance for flow through submerged vegetation Baptist et al. (2006) derived a formula for the velocity inside the surface layer using genetic programming. Genetic programming is a technique that can be used to find the symbolic form of an equation, including a set of coefficients. Using scaling assumptions, Huthoff (2007) derived an analytical expression for bulk flow through and over vegetation.

• Flexible vegetation

Flexible vegetation elements are distinguished from that of rigid vegetation elements because the drag coefficient of flexible vegetation decreases when the vegetation is bending. It is less difficult to describe a theoretical equation for the resistance of rigid vegetation than for the resistance caused by flexible vegetation. The behavior of flexible vegetation depends on the flow conditions making it more complex than rigid vegetation. For submerged vegetation, bending of the vegetation influences the averaged velocity. For submerged flexible vegetation, three different configurations (stiff, bending, prone) can be distinguished depending on the flow velocity and the plant characteristics (Kouwen et al., 1969; Gourlay, 1970, Carollo et al., 2005). If the flow velocity is small, the flexible vegetation shows a rigid behavior. In the case of bending and prone situation, the behavior of the vegetation depends not only on the flow velocity but also on the bending stiffness of the vegetation. Kutija and Hong (1996) demonstrated that formulas developed for rigid vegetation could be extended to include the effects of plant flexibility by an iterative method using a simple cantilever beam theory. Similar methods have been proposed by Thompson and Roberson (1976) and Manz and Westhoff (1998). However, characterized by the flexibility of the stem and the connected deflected vegetation height is very complicated. Most explanations use the elasticity of the vegetation to calculate the

deflected vegetation height. For example, Kouwen and Unny (1973) suggested to establish values of mEI (stem density, elasticity, stem area's second moment of inertia) empirically to define the deflected vegetation height. However, there are a lot of arguments against such methods: Fischenich (2000) mentioned that the mEI value has been proven to be difficult to measure in the field, and has no direct physical meaning. Wilson (2007) argued that the flexibility of an individual grass blade is difficult to determine and highly variable; variations in modulus of elasticity of up to 100% can occur between samples. Moreover, densely packed groups of blades will have different bending properties compared to a single blade, hence correlating deflected height as a function of bending stiffness may be inappropriate. Most of these research efforts focus on determining drag coefficients and empirical formulas for resistance under various vegetation configurations. While it is important to develop empirical solutions to vegetative resistance, it is also important to understand the detailed characteristics of the flow through vegetation. Recently, several studies have focused on velocity profiles and turbulent characteristics of vegetated channels (Shimizu and Tsujimoto, 1994; Tsujimoto et al., 1992; Naot et al., 1996; Nepf, 1999; López and Garcí'a, 2001, 2004; Stephan and Gutknecht, 2002).

1.2.2 Sediment transport through vegetation

The influence of vegetation on hydraulics and sediment transport depends on characteristics like height (emergent, submergent), location (on river banks, on floodplains, aquatic vegetation), arrangement, density, and flexibility (grass, reeds, bushes, trees). In conjunction with the water discharge it controls hydraulic parameters like flow velocity, water depth, and energy slope. Thus, vegetation has a direct impact on sediment transport processes. Due to the transport processes bed roughness and bed slope are changed looping back to the geometry and the hydraulic of the river. Also sediment transport processes and in this context bed stability and bed form development have been investigated since many years.

• Bed-load transport through vegetation

Many approaches and equations have been proposed for relating the rate of sediment transport to flow characteristics, but these cannot be applied directly for flow through vegetation stems. Within stands of vegetation, drag on the stems increases overall flow resistance and reduces the shear stress (James et al., 2002;

Jordanova and James, 2003; Watanabe et al., 2002) applied to the bed, resulting in reduced capacity for bed load transport and increased propensity for trapping, deposition, and stabilization of sediment. A number of studies such as those by Hirano et al. (1987), Hirano (1992), Mizuhara (1995), Ishikawa et al. (1998), Jordanova and James (2004), Kao and Barfield (1978), Klaassen and van der Zwaard (1974), Kouwen and Moghadam (1996), Li and Shen (1973), Nepf and Vivoni (1998), Nepf (1999), and Thompson and Roberson (1976), have been carried out for estimating the flow resistance due to drag of the stems. Mizuyama et al. (1989) on the evaluated of the surface roughness coefficient on flows through riparian forests related to accelerating sedimentation.

Detailed experimental studies of how bed load is transported through vegetation have only recently been carried out by Specht (2002). Specht (2002) investigated in a series of laboratory experiments how vegetation influences bed load transport rates in compact river channels. Based on these experiments he derived a coefficient which can be used with various bed load transport formulae to account for the effect of both symmetrical and asymmetrical bank vegetation. Besides the altered transport rates, Specht (2002) found that vegetation significantly influences the geometry of sand dunes, which became steeper and more regular in length. In the study, shear stress exerted on the bed was calculated by subtracting the total stem drag from the total force applied by the flow in the flow direction.

A paper by Parker and Klingeman (1982) proposed the idea of equal mobility. Equal mobility refers to a small range of discharge that moves a large range of bedload; In other words, when a threshold discharge is reached, the armor layer is disrupted and a large percentage of the bed load is moved. Although this was only to be used as a first approximation for transportation rates, the idea of equal mobility has been challenged, supported, and dismissed as nonsense. Komar and Shih (1992) refute the idea of equal mobility and, through calculations, show that equal mobility cannot occur. A compromise between these two views is given by Jackson and Beschta (1982). Their two-phase bed load transport includes both equal mobility and differential movement.

Numerical models for the assessment of morphological development of river reaches have been developed by Tsujimoto (1999) and Baptist (2005). Successful numerical simulations of the transportation of fine sediments through emergent vegetation have been carried out by Lopez & Garcia (1998) and Choi & Kang (2004) on the basis of experimental data of Tollner et al. (1982) and another numerical modeling studies by Hirano et al. (1997) and Hashimoto et al. (1997) on the drag

coefficient of riparian trees and sedimentation characteristics at times of sediment inflow.

• **Suspended sediment through vegetation**

A lot of research efforts have been put into the effects of vegetation on hydraulic roughness, but the effects of vegetation on suspended sediment transport are less known and even less is known about the effects of vegetation on bed load transport. Several studies have been carried out on the interaction of vegetation and suspended sediment. These include field and laboratory measurements as well as numerical modelling (Nakagawa *et al.* 1992, Watanabe & Hoshi 1996, Houwing *et al.*, 2000, Teeter *et al.* 2001, Madsen *et al.* 2001).

The altered turbulent flow field around plants and the reduced bulk flow velocity may result in enhanced deposition of suspended sediments. However, vegetation may have also a destabilising effect on the sediments due to high local turbulent intensities and vertical velocity components in their wake. In this context, Choi & Kang (2004) concluded that the use of an isotropic turbulence model results in a significant underestimation of suspended sediment load for open-channel flow with emergent vegetation.

Lopez and Garcia (1998; 2001) also used computational turbulence modelling to determine the velocity and kinematic eddy viscosity distributions for one-dimensional flow through vegetation stems, and then one-dimensional diffusion-convection theory to determine the vertical suspended sediment concentration distributions. The transverse transfer of sediment from a non vegetated channel to adjacent vegetated zones is more complex, and requires description of the transverse distribution of velocity and the transverse eddy viscosity. Tsujimoto and Shimizu (1994) used a similar approach to that of Lopez and Garcia (1998; 2001) to simulate the vertical and transverse distributions of suspended sediment concentration in simple and compound channels with vegetation zones in the cross-sections. Their model is able to predict deposition within a vegetation strip and its dependence on stem density.

An alternative to turbulence modelling for determining sediment diffusivity values is empirical evaluation for appropriate conditions. As part of a study of fine sediment settling within emergent vegetation, Elliott (2000) determined vertical diffusivities in an array of 6.4 mm diameter cylindrical rods set at a density of 3667 rods/m² in a 6 m long, 0.29 m wide flume, by measuring concentration variations of injected dye. The diffusivity varied with velocity, slope and flow depth, but the concentration

distributions were consistent with constant values over the depth. Nepf (1999) used measurements of dye dispersion to determine transverse diffusivities in flows through arrays of cylindrical rods. She found transverse diffusivities to vary with stem characteristics and flow velocity.

1.2.3 Particulate organic matter through vegetation

Low-order forested streams, where light limitation restricts primary production, rely upon the input of organic matter from the riparian zone to fuel in-stream processes (Vannote et al., 1980). Thus, benthic coarse particulate organic matter (CPOM; e.g. leaves, wood and twigs) is a pivotal component of the functioning of these streams. It often forms the basis of the trophic structure of streams, being the major source of organic matter and energy in woodland stream ecosystems (Cummins et al., 1989). The decomposition of this organic matter is a key ecosystem-level process integrating the activities of both microbial and invertebrate decomposers (Gessner and Chauvet, 1994; Suberkropp, 1998; Graca, 2001; Hieber and Gessner, 2002).

Organic matter storage within stream sediments has received less attention than at the surface of sediments. However large standing stocks of particulate organic matter (POM) may occasionally be buried in sediments and significantly contribute to hyporheic metabolism (Metzler and Smock, 1990; Sobczak et al., 1998), and therefore to the overall ecological functioning of headwater streams. Relatively little work has attempted to quantify POM buried in the sediments of headwater streams as usually it occurs following spates or other depositional events (Leichtfried, 1985, 1988; Metzler and Smock, 1990; Smock, 1990; Bretschko, 1991; Wagner et al., 1993; Jones et al., 1995; Naegeli et al., 1995).

The quantity of organic matter deposited on the stream substratum was greatly increased, this being true of both fine particulate organic matter (FPOM) and coarse particulate organic matter (CPOM, particles >1 mm in diameter) (Koetsier and McArthur, 2000). Many researchers have addressed the role of grain size and organic matter of sediments (Borovec, 2000; Wen et al., 2001; Lu and Allen, 2001; Vignati and Dominik, 2003).

1.3 Study Object and Method

In order to manage river from the viewpoints of flood mitigation, water resources utilization and ecosystem conservation, river flow and morphological changes there would be fairly understood and reasonably described. In particular, vegetation developed in riparian area recently is a key because it affects flow, sediment transport and morphological change. In addition, behavior of particulate organic matter (POM) including plants seeds in river ecosystem is also important to understand how POM drifts are different from sediment behavior in riparian vegetation, because it influences vegetation productivity and supports diversity through riverine biogeochemical process.

From the view point of flow in vegetated area, the velocity profile is deviated from log-law. Transport and deposition behavior of sand and POM are somehow similar with different specific weight of particles but they are mutually related each other. Though mechanics of sediment transport has been developed well to describe fluvial process, the complicated processes including behaviors of POM has not been well understood yet. It is focused on that riparian vegetation plays an important role there and the behavior of sand and POM there is quite complicated. In this study, transport and deposition of sand and POM in vegetated area are focused on and investigated by using a fundamental flume experiment and numerical calculation scheme.

The 2-Dimensional numerical model made by Nagoya hydraulic(hereafter, NHSED2D), which is able to simulate flow fields-vegetation-bed variation interaction directly, is used to investigate fluvial process and mechanics of sediment transport in vegetated area. The NHSED2D model is basically based on the model developed by (Goto et al., (2002)). New model (which can analyze the suspend sediment and specific fluvial process) will be developed.

Several issues remained in numerical modeling in depth-averaged scheme has been discussed using newly developed numerical model: how the boundary layer develops near the bed in vegetated area and how particles with different specific weights behave with mutual interaction.

This study will perform overall evaluation about fluvial process and behavior of sediment and POM in vegetated area with the detailed purpose. And it will be discussed concretely.

1.4 Contents

Though fundamental flume experiment and numerical simulation, this study will be discussed hydrodynamic characteristics and behavior of sediment and POM in vegetated area. The research contents are as follows.

Chapter 1 will describe background, purpose and method, and contents of the research, as well as literature review.

Chapter 2 will describe the fundamental flume experiments in a laboratory for flow and transport and deposition process of sediment and POM through experiment set-up and result. And it will be discussed what cannot be described in the conventional 2D scheme, and what should be modified for application in the conventional model.

Chapter 3 will describe discussion on 2D depth averaged model for flow and fluvial process with vegetation. Flow can be described by the momentum equation, continuity equation, resistance law and advection-diffusion equation. The time variation of the bed elevation can be described bed shear stress, bed load sediment and suspended sediment. Ambiguous aspects remained in numerical modeling has been discussed: velocity distribution and bed shear stress in flow with vegetation, transverse mixing of flow with vegetation, suspended sediment concentration profile in vegetation area.

Chapter 4 will discuss concept of bed roughness boundary layer in vegetation area. the bed roughness boundary layer in vegetated area through Liu et al. (2008). This chapter consist of favorable formula to estimate the bed roughness boundary layer thickness, velocity distribution in bed roughness boundary layer in vegetated area and resistance law in vegetated area.

Chapter 5 will discuss application of bed roughness boundary layer concept. In this chapter discuss about flow and sediment transport with non submerged vegetation in 1D scheme. Second, application to bed load transport and it will compare with experiment data of bed load deposition in decelerated area in vegetation. Third discuss about ratio of averaged concentration and bottom concentration and comparison of suspended sediment concentration profile using bed roughness boundary layer concept.

Chapter 6 will discuss transverse mixing in flow and suspended sediment in stream with vegetation zone. Lateral mixing of momentum and lateral distribution of depth averaged velocity are introduced and discuss transverse mixing of kinematic eddy viscosity, diffusion coefficient, depth averaged concentration and suspended sediment transport deposition in vegetated area.

Chapter 7 will discuss transport of POM with sediment. In this chapter POM discuss about interference with sediment using hydraulic experiment. And it is compare with 2D numerical analysis model.

Finally we draw an overall conclusion of this research and some recommendations for further researches relating to this topic are made in Chapter 8. Concluding remarks are also made at the end of each chapter base on results obtained in different phase of the research within the framework of the objectives.

The frame of the research phases presented in this dissertation with the relationship among them is delineated with a Fig. 1.3.

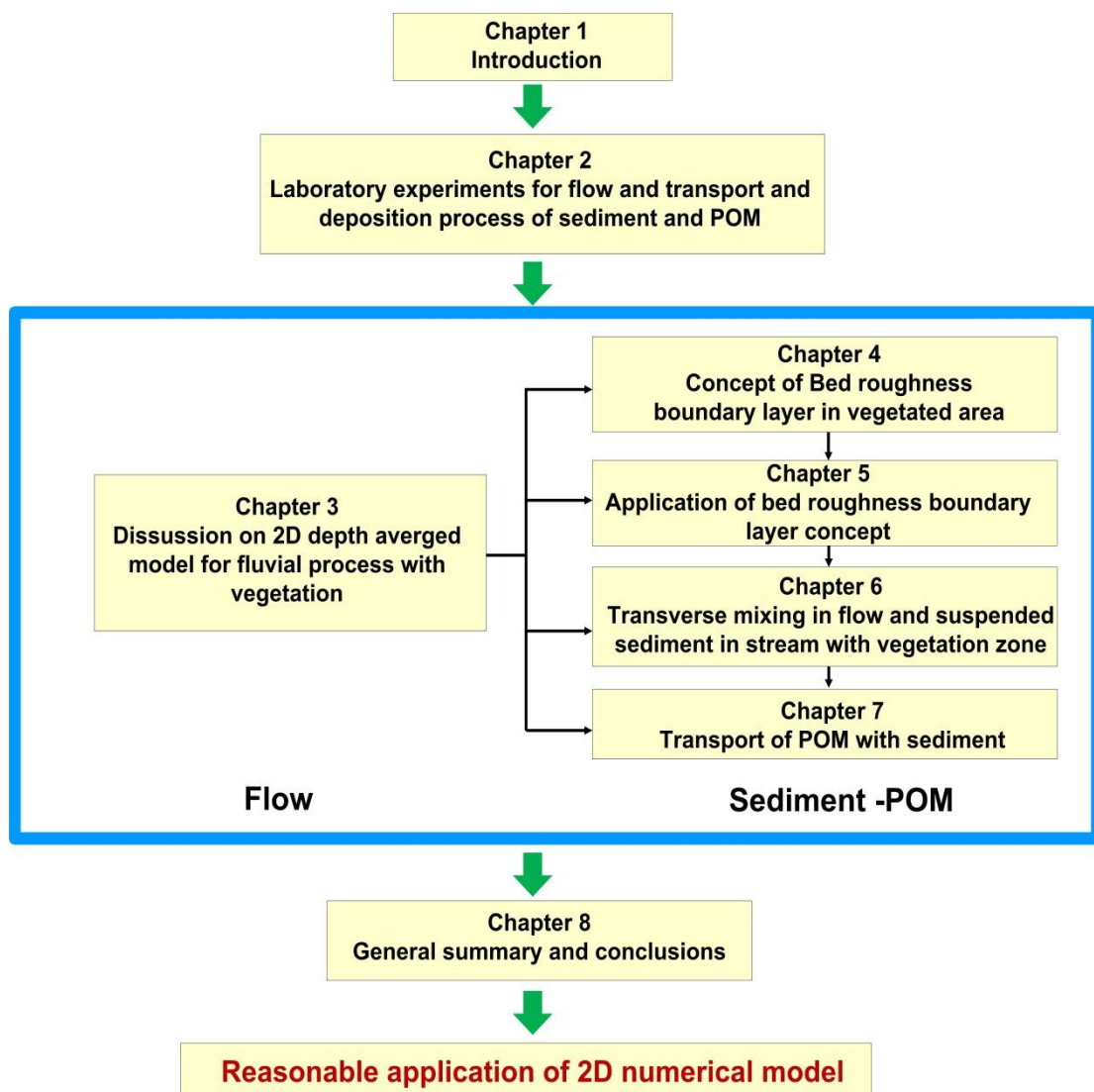


Fig. 1.3 Graphical representation of dissertation framework

References

1. Aberle, J., Järvelä, J., Schoneboom, T., Dittrich, A. (2010) Flow resistance of rigid and flexible emergent vegetation revisited. *Proceedings of the 1st European IAHR Congress*, 4–6 May, 2010, Edinburgh, 6 pp.
2. Aldridge, B.N., Garrett, J.M. (1973) Roughness Coefficients for Stream Channels in Arizona. *US Geological Survey Open-File Report*, 87 pp.
3. Arcement, G.J., Schneider, V.R. (1989) Guide for Selecting Manning's Roughness Coefficients for Natural Channels and Flood Plains.
4. Augustijn, D.C.M, Huthoff, F., & Velzen, van E.H. (2008) Comparison of vegetation roughness descriptions. *River flow 2008*; international conference on fluvial hydraulics.
5. Ayvaz, M.T., Genç, O. (2012) Optimal estimation of Manning's roughness in open channel flows using a linked simulation-optimization model, BALWOIS 2012. *International Conference on Water, Climate and Environment*, May 28–June 2, Ohrid, Macedonia.
6. Baptist, M. (2005) Modelling floodplain biogeomorphology. PhD thesis. Delft: Technical University of Delft.
7. Baptist, M.J., Babovic, V., Rodrigues Uthurburu, J., Keijzer, M., Uittenbogaard, R.E., Verway, A., & Mynett, A.E. (2006) On inducing equations for vegetation resistance. *Journal of Hydraulic Research*, 45(4), pp. 435-450.
8. Becker, L., Yeh, W.W.-G. (1972) Identification of parameters in unsteady open channel flows. *Water Resour. Res.* 8 (4), pp. 956–965.
9. Borovkov, V.S. and Yurchuk, M. (1994) Hydraulic resistance of vegetated channels. *Hydrotechnical Construction*, 8, 28.
10. Borovec, Z. (2000) Elements in size fractioned bottom sediments of the Elbe river in its Czech part. *Aquat. Sci.*, 62, pp. 232-251.
11. Bretschko G. (1991) The limnology of a low order alpine gravel stream (Ritrodat-Lunz study area, Austria). *Verh. Internat. Verein. Limnol.*, 24, pp. 1908–1912.
12. Carollo, F.G., Ferro, V. and Termini, D. (2005) Flow resistance law in channels with flexible submerged vegetation. *Journal of Hydraulic research* 131, pp. 554-564.
13. Chen, C. (1976) Flow resistance in broad shallow grassed channels, *J. Hydraul. Div. Am. Soc. Civ. Eng.*, 102(HY3), pp. 307– 322.
14. Choi, S.-U. & Kang, H. (2004) Reynolds stress modeling of vegetated open-channel flows. *J. Hydr. Res.* 42(1): pp. 3–11.

15. Chow, V.T. (1959) Open-channel Hydraulics. McGraw-Hill, New York. 680 pp.
16. Cummins K.W., Wilzbach M.A., Gates D.M., Perry J.B. and Taliaferro W.B. (1989) Shredders and riparian vegetation. *Bioscience*, 39, pp. 24–30.
17. De Doncker, L. et al. (2009) Determination of the Manning roughness coefficient influenced by vegetation in the river Aa and Biebrza river. *Environ. Fluid Mech.* 9, pp. 549–567.
18. Ding, Y., Jia, Y., Wang, S.S.Y. (2004) Identification of Manning's roughness coefficients in shallow water flows. *J. Hydraul. Eng.-ASCE* 130 (6), pp. 501–510.
19. Elliott, A.H. (2000) Settling of fine sediment in a channel with emergent vegetation. *J. Hydr. Engrg.* 126(8): pp. 570–577.
20. Fathi-Maghadam, M., Kouwen, N. (1997) Non rigid, non submerged, vegetative roughness on floodplains. *Journal of Hydraulic Engineering* 123 (1), pp. 51–57.
21. Fischenich, C. (2000) Resistance due to vegetation. EMRRP Technical Notes, ERDC TNEMRRP-SR-07, Us Army Engineer Research and Development Center, Vicksburg, MS.
22. Garcia, M. H., F. Lopez, C. Dunn, and C. V. Alonso. (2004) Flow, turbulence, and resistance in a flume with simulated vegetation, in *Riparian Vegetation and Fluvial Geomorphology*, edited by S. J. Bennett et al., pp. 11 –27, AGU, Washington, D. C.
23. Gessner M.O. and Chauvet E. (1994) Importance of microfungi in controlling breakdown rates of leaf litter. *Ecology*, 75, pp. 1807–1817.
24. Goto, T., T. Tsujimoto and T. Kitamura. (2002) Numerical model for simulating channelization and its validation, *Advances in Fluid Modeling & Turbulence Measurements*, Edited by H. Ninokata et al., *World Scientific*, pp.127-134.
25. Gourlay, M.R. (1970) Discussion of 'Flow retardance in vegetated channels' by N. Kouwen, T.E. Unny and H.M. Hill. *Journal of Irrigation Drainage Engineering*. 96, 351-357.
26. Grac, a M.A.S. (2001) The role of invertebrates on leaf litter decomposition in streams – a review. *Int. Rev. Hydrobiol.*, 86, pp. 383–393.
27. Hashimoto H, Hirano H, Tamamatsu J, Kusaba K. (1997) Sediment deposition by hyper-concentrated flows in stream forests (in Japanese). *Proceedings of annual meeting of Jpn Soc Erosion Cont Eng*, pp 186–187.
28. Hieber M. and Gessner M.O. (2002) Contribution of stream detritivores, fungi, and bacteria to leaf breakdown based on biomass estimates. *Ecology*, 83, pp.

- 1026–1038.
29. Hirano Y, Mizuhara K, Ohte K. (1987) Studies on the flow resistance and the sediment transport in vegetated channels (in Japanese with English summary). *J Jpn Soc Erosion Cont Eng* 40(3): pp. 4–10
 30. Hirano M, Hashimoto H, Tagawa H, Tamamatsu J. (1997) Drag forces of solid-liquid mixture flows on multiple rows of cylinders (in Japanese with English summary). *Proceedings of Hydraulic Engineering* 41, Jpn Soc Civil Engineers, pp 699–704
 31. Hirano Y. (1992) Studies on vegetated channels (in Japanese). PhD thesis, Kyoto Prefectural University, Japan
 32. Hoffmann, M.R. (2004) Application of a simple space-time averaged porous media model to flow in densely vegetated channel. *Journal of porous media*, 7(3), pp. 183-191.
 33. Houwing, E.J., Tanczos, I.C., Kroon, A. & De Vries, M.B. (2000) Interaction of submerged vegetation, hydrodynamics and turbidity; analysis of field and laboratory results. *Proceedings of the INTERCOH conference 2001*.
 34. Huthoff, F. (2007) Modelling hydraulic resistance of floodplain vegetation, PhD Thesis, Department of Water Engineering, University Twente.
 35. Ishikawa Y, Fujita H, Mizuhara K, Narutomi Y. (1998) Bed-load sediment transport in woody vegetated channels (in Japanese with English summary). *J Jpn Soc Erosion Cont Eng* 51(3): pp. 35–43.
 36. Jackson, W.L. and Beschta, R.L. (1982) A model of two-phase bedload transport in an Oregon Coast Range stream. In *Earth surface processes and landforms*, vol. 7, pp. 517-527. New York: John Wiley & Sons
 37. James CS, Jordanova AA and Nicolson CR. (2002) Flume experiments and modelling of flow-sediment-vegetation interactions. In *Structure, Function and Management Implications of Fluvial Sedimentary Systems* (Dyer FJ, Thoms MC and Olley JM (eds)). IAHS Press, Wallingford, pp. 3–9.
 38. James, C. S., Birkhead, L., Jordanova, A. A., and O'Sullivan, J. J. (2004). “Flow resistance of emergent vegetation” *Journal of Hydraulic Research*, 42(4).
 39. Jones J.B., Fisher S.G. & Grimm N.B. (1995) Vertical hydrologic exchange and ecosystem metabolism in a Sonoran Desert stream. *Ecology*, 76, pp. 942–952.
 40. Jordanova AA and James CS. (2003) Experimental study of bed load transport through emergent vegetation. *Journal of Hydraulic Engineering ASCE* 129(6): pp. 474–478.
 41. Kao, D. T. Y., and Barfield, B. J. (1978) “Prediction of flow hydraulics for

- vegetated channels.” *Trans. ASAE*, 21~(3), pp. 489–494.
42. Kidson, R., Richards, K.S., Carling, P.A. (2005) Reconstructing the ca. 100-year flood in Northern Thailand. *Geomorphology* 70 (3–4), pp. 279–295.
 43. Klaassen, G. J., and van der Zwaard, J. J. (1974) “Roughness coefficients of vegetated flood plains.” *J. Hydraul. Res.*, 12(1), pp. 43–63.
 44. Klopstra, D., Barneveld, H.J., Van Noortwijk, J.M. and Van Velzen, E.H. (1997) Analytical model for hydraulic roughness of submerged vegetation. *Proceedings of the 27th IAHR Congress theme A Managing Water: Coping with Scarcity and Abundance*, San Fransisco, pp. 775-780.
 45. Koetsier P, McArthur JV. (2000) Organic matter retention by macrophyte beds in 2 south eastern USA, low-gradient, headwater streams. *Journal of the North American Benthological Society* 19: pp. 633–647.
 46. Komar, P.D. and Shih, S.M. (1992) Equal mobility versus changing bed load grain sizes in gravel-bed streams. In *Dynamics of gravel-bed rivers*, ed. P. Billi, R.D. Hey, C.R. Thorne, and P. Tacconi; pp. 73-106. Chichester, U.K.: John Wiley & Sons Ltd.
 47. Kouwen, N., Unny, T.E., and Hill, H.M. (1969) Flow retardance in vegetated channels. *Journal of Irrigation Drainage Engineering*, 95(2), pp. 329-344.
 48. Kouwen, N. and Unny, T. E. (1973) Flexible roughness in open channels. *Jouarnal of the Hydraulics Division, ASCE*, HY5, pp. 713-728.
 49. Kouwen, N. and Moghadam, F. (1996) “Friction factor for vegetation.” *Proc., 2nd Symposium on Habitat Hydraulics*, Quebec, pp. 251-A257.
 50. Kouwen, N., Fathi-Moghadam, M. (2000) Friction factors for coniferous trees along rivers. *Journal of Hydraulic Engineering* 126 (10), pp. 732–740.
 51. Kutija, V. and Hong, H.T.M. (1996) A numerical model for assessing the additional resistance to flow introduced by flexible vegetation. *Journal of Hydraulic Research*, 1, pp. 99-114.
 52. Leichtfried M. (1985) Organic matter in gravel streams (Project Ritrodat-Lunz). *Verh. Internat. Verein. Limnol.*, 22, pp. 2058-2062.
 53. Leichtfried M. (1988) Bacterial substrates in gravel beds of a second order alpine stream (Project Ritrodat-Lunz). *Verh. Internat. Verein. Limnol.*, 23, pp. 1325–1332.
 54. Leliavsky, S. (1959) *Irrigation and Hydraulic Design*. Vol. I, Chapman & Hall, London, UK.
 55. Li, R.-M., and Shen, H. W. (1973) “Effect of tall vegetations on flow and sediment.” *J. Hydraul. Div., Am. Soc. Civ. Eng.*, 99(5), pp. 793–814.

56. Limerinos, J.T. (1970) Determination of the Manning coefficient from measured bed roughness in natural channels.
57. Liu, D., Diplas, P., Fairbanks, J., Hodges, C. (2008) An experimental study of flow through rigid vegetation. *Journal of Geophysical Research: Earth Surface*(2003-2012) 113 (F4).
58. López, F. & García, M.H. (1998) Open-channel flow through simulated vegetation: Suspended sediment transport modeling. *Water Resour. Res.* 34(9): pp. 2341–2352.
59. Lo'pez, F., Garcí'a, M.H. (2001) Mean flow and turbulence structure of open-channel flow through non-emergent vegetation. *J. Hydraulic Eng.* 127 (5), pp. 392–402.
60. Lu, Y. and H.E. Allen. (2001) Partitioning of copper onto suspended particulate matter in river waters. *Sci. Tot. Environ.*, 277(1-3), pp. 119-132.
61. Madsen, J.D, Chambers, P.A., James, W.F., Koch, E.W. & Westlake, D.F. (2001) The interaction between water movement, sediment dynamics and submersed macrophytes. *Hydrobiologia* 444: pp. 71- 84. Kluwer Academic Publishers.
62. Manz, D.H. and Westhoff, D.R. (1988) Numerical analysis of the effects of aquatic weeds on the performance of irrigation conveyance systems. *Can. J. Civil Engineering*, 15, pp. 1-13.
63. Meijer, D.G. (1998b) Model pro even over stroomde vegetatie. Technical report PR121, HKV Consultants, Lelystad, The Netherlands.
64. Metzler G.M. and Smock L.A. (1990) Storage and dynamics of subsurface detritus in a sand bottomed stream. *Can. J. Fish. Aquat. Sci.*, 47, pp. 588–594.
65. Mizuhara K. (1995) A study on flow resistance in woody vegetated channels. *Proceedings of the International Sabo Symposium*, Jpn Soc Erosion Cont Eng, pp 205–211
66. Mizuyama T, Amada T, Kurihara J, Kobayashi M. (1989) Resistance and sedimentation by trees (in Japanese with English summary). *J Jpn Soc Erosion Cont Eng* 42(4): pp. 18–22
67. Morvan, H., Knight, D., Wright, N., Tang, X., Crossley, A. (2008) The concept of roughness in fluvial hydraulics and its formulation in 1D, 2D and 3D numerical simulation models. *J. Hydraul. Res.* 46 (2), pp. 191–208.
68. Naegeli M.W., Hartmann U., Meyer E.I. and Uehlinger U. (1995) POM-dynamics and community respiration in the sediments of a floodprone prealpine river (Necker, Switzerland). *Arch. Hydrobiol.*, 133, pp. 339–347.
69. Nakagawa, H., Tsujimoto, T. & Shimizu, Y. (1992) Sediment Transport in

- Vegetated Bed Channel. *Conference Proceedings of the 5th International Symposium on River Sedimentation*, Karlsruhe.
70. Naot, D., Nezu, I., Nakagawa, H. (1996) Unstable patterns in partly vegetated channels. *J. Hydraulic Eng.* 122 (11), pp. 671–673.
71. Nepf, H. M. (1999) Drag, turbulence, and diffusion in flow through emergent vegetation, *Water Resour. Res.*, 35(2), pp. 479 – 489
72. Nepf, H. A., and Vivoni, E. R. (1998) “Drag and diffusivity within emergent vegetation, *Proc., Wetlands Engineering River Restoration Conf.*, ASCE, Denver.
73. Obana, M, T. Uchida & T. Tsujimoto. (2012) Deposition of Sand and particulate organic matter in ri-parian vegetation, *Advances in River Eng., JSCE*, pp.47-52 (in Japanese).
74. Parker, G., Klingeman, P.C., and McLean, D.G. (1982) Bed load and size distribution in paved gravel-bed streams. *Proceedings of the American Society of Civil Engineers*, Jour. Hydraulics Division 108(HY1): pp. 585-587.
75. Petryk, S. and Bosmajian, G. (1975) Analysis of flow through vegetation. *Journal of the Hydraulic Division of the American Society of Civil Engineers*. 101(HY7): pp. 871-884.
76. Petryk, S., Bosmajian III, G. (1975) Analysis of flow through vegetation. *J. Hydraul. Div.* 101(HY7), pp. 871–884.
77. Ramesh, R., Datta, B., Bhallamudi, S.M., Narayana, A. (2000) Optimal estimation of roughness in open-channel flows. *J. Hydraul. Eng.-ASCE* 126 (4), pp. 299–303.
78. Sepaskhah, A.R., Bondar, H. (2002) Estimation of Manning roughness coefficient for bare and vegetated furrow irrigation. *Biosyst. Eng.* 82 (3), pp. 351–357.
79. Shimizu, Y., Tsujimoto, T. (1994) Numerical analysis of turbulent open-channel flow over a vegetation layer using a k-3 turbulence model. *J. Hydrosci Hydraulic Eng* 11 (2), pp. 57–67.
80. Smock L.A. (1990) Spatial and temporal variation in organic matter storage in low-gradient, headwater streams. *Arch. Hydrobiol.*, 118, pp. 169–184.
81. Sobczak W.V., Hedin L.O., and Klug M.J. (1998) Relationships between bacterial productivity and organic carbon at a soilstream interface. *Hydrobiologia*, 386, pp. 45–53.
82. Specht, F.-J. (2002) Einfluß von Gerinnebreite und Uferbewuchs auf die hydraulisch-sedimentologischen Verhältnisse naturnaher Fließgewässer. *Mitt. des Leichtweiß- Instituts für Wasserbau*, Heft 153. TU Braunschweig.

83. Stephan, U., Gutknecht, D. (2002) Hydraulic resistance of submerged flexible vegetation. *J. Hydrol.* 269 (1/2), pp. 27–43.
84. Stone, B. M., and H. T. Shen. (2002) Hydraulic resistance of flow in channels with cylindrical roughness, *J. Hydraul. Eng.*, 128(5), pp. 500–506.
85. Strupczewski, W. G. & Szymkiewicz, R. (1989) On direct applicability of the Chezy formula to natural channels. In: *Proc. Int. Conf. on Channel Flow and Catchment Runoff*, (University of Virginia, USA), pp. 350–361..
86. Strupczewski, W. G. (1996) Warning of application of the Chezy-Manning formula regardless of channel.
87. Strupczewski, W. G. & Szymkiewicz, R. (1996) Analysis of paradoxes arising from the Chezy formula with constant roughness: II. Flow area-discharge curve. *Hydrol. Sci. J.* 41(5).
88. Suberkropp K. (1998) Microorganisms and organic matter processing. In: Naiman R.J. and Bilby R.E. (eds.), *River Ecology and Management: Lessons from the Pacific Coastal Ecoregion*, Springer-Verlag, New York, pp. 120–143.
89. Tai, N. (1973) Investigation of Hydraulic Resistances in Vegetated Channels. Candidate Dissertation Abstract, MGMI, Moscow.
90. Tang, H.-W., Xin, X.-K., Dai, W.-H., Xiao, Y. (2010) Parameter identification for modeling river network using a genetic algorithm. *J. Hydrodyn.* 22 (2), pp. 246–253
91. Teeter, A.M., Johnson, B.H., Berger, C., Stelling, G., Scheffner, N.W., Garcia, M.H. & Parchure, T.M. (2001) Hydrodynamic and sediment transport modelling with emphasis on shallow-water, vegetated areas (lakes, reservoirs, estuaries and lagoons). *Hydrobiologia* 444: pp. 1-23. Kluwer Academic Publishers.
92. Thompson, G.T. and Roberson, J.A. (1976) A theory of flow resistance for vegetated channels. *Trans. ASAE*, 19, pp. 288-293.
93. Thorndycraft, V.R., Benito, G., Rico, M., Sopeña, A., Sánchez, Y., Casas, A. (2005) A long-term flood discharge record derived from slackwater flood deposits of the Llobregat River, NE Spain. *J. Hydrol.* 313 (1–2), pp. 16–31.
94. Tollner, E.W., Barfield, B.J. & Hayes, J.C. (1982) Sedimentology of erect vegetal filters. *J. Hydr. Div. ASCE* 108(12): pp. 1518–1531.
95. Tsujimoto, T., Y. Shimizu, T. Kitamura, and T. Okada. (1992), Turbulent open-channel flow over bed covered by rigid vegetation, *J. Hydrosoci. Hydraul. Eng.*, 10(2), pp. 13–25.
96. TSUJIMOTO T and SHIMIZU Y. (1994) Flow and suspended sediment in a

- compound channel with vegetation. *Proc. 1st Int. Symp. on Habitat Hydraulics*. Held in Trondheim, Norway, August. pp. 357-370.
97. Tsujimoto, T. (1999) Fluvial processes in streams with vegetation. *J. Hydr. Res.* 37(6): pp. 789–803.
98. Tsujimoto, T. (2008) River management for ecosystem conservation: policy making support though mathematical modeling. *Proc. JST Presto Symposium.*, No.136, pp. 32-41.
99. Van Velzen, E.H., Jesse, P. Cornelissen, P., and Coops, H. (2003) Stromingsweerstand vegetatie in uiterwaarden; Handboek. Part 1 and 2. RIZA Reports, 2003.028 and 2003.029, Arnhem, The Netherlands.
100. Vannote R.L., Minshall G.W., Cummins K.W., Sedell J.R. and Cushing C.E. (1980) The river continuum concept. *Can. J. Fish. Aquat. Sci.*, 37, pp. 130–137.
101. Vignati, D. and J. Dominik. (2003) The role of coarse colloids as a carrier phase for trace metals in riverine systems. *Aquat. Sci.*, 65, pp. 129-142.
102. Wagner R., Schmidt H.H. and Marxsen J. (1993) The hyporheic habitat of the Breitenbach, spatial structure and physicochemical conditions as a basis for benthic life. *Limnologica*, 23, pp. 285–294.
103. Waichler, S.R., Perkins, W.A., Richmond, M.C. (2005) Hydrodynamic Simulation of the Columbia River, Hanford Reach, Pacific Northwest National Laboratory Technical, Report, PNNL-15226.
104. Wasantha Lal, A.M. (1995) Calibration of riverbed roughness. *J. Hydraul. Eng.* ASCE 121 (9), pp. 664–671.
105. Watanabe, Y. & K. Hoshi. (1996) Influence of vegetation on flow velocity and suspended load. *International Workshop on Interactive Issues of Flood and Environment in Cold Regions*, 3-6 October 1996, Trento, Italy.
106. Watanabe K, Nagy HM and Noguchi H. (2002) Flow structure and bed-load transport in vegetation flow. *Proceedings of the 13th Congress of the Asia/Pacific Division of the International Association of Hydraulic Engineering and Research* pp. 214– 218. World Scientific Publishing Company.
107. Wen, X., L. Wu and H. Tang. (2001) Adsorption of copper on polluted river sediment. *Bull. Environ. Contam. Toxicol.*, 67(6), pp. 913-920.
108. Wilson, C.A.M.E., (2007) Flow resistance models for flexible submerged vegetation. *Journal of Hydrology*, 342, pp. 213-222
109. Zhu, C.J., Zhang, J. (2009) Prediction of roughness coefficient using

multivariate forecast model. *In: Luo, Q. (Ed.), ETP/IITA World Congress in Applied computing, Computer Science and Computer Engineering*. ACC, Sanya, pp. 319–322.

CHAPTER 2

Laboratory experiments for flow and transport and deposition process of sediment and POM

2.1 General

The POM in rivers is derived from both allochthonous and autochthonous sources, which include litter from the riparian zone, breakdown of large organic matter, transport from upstream reaches, algae, bacteria, and aquatic plants (Wallace & Grubaugh, 1996). POM is a component of the carbon budget of a basin, and the transport of organic matter from headwater channels is important in providing food resources for aquatic biota in downstream reaches (Webster & Golladay, 1984).

Recently, the transport and deposition of particulate organic matter (POM) in river streams has received much attention as one of important ecological process in rivers. The complicated processes including behaviors of POM has not been well understood yet, despite a wealth of measurements of POM in transport and in storage in stream sediments (Fisher (1997), Golladay et al (1987), Webster et al (1990)). Capture of POM there must be significant in ecosystem and it is important to understand how POM drifts are different from sediment behavior in riparian vegetation, because it influences vegetation productivity and supports diversity through riverine biogeochemical processes.

We focused on interacted behaviors of suspended sediment and POM in vegetated area on sand bars. The purpose of Chapter 2 to clarify the characteristics of deposition

of POM with suspended sediment on sandbars with riparian vegetation through laboratory experiments.

2.2 Laboratory experiments

2.2.1 Overview of laboratory experiment

To observe the deposition mechanisms of sediments and POM which has two properties such as the shape and specific gravity that differ from the sediments during flood stage, a laboratory experiment was conducted by focusing on two kinds of basic fluvial processes as mentioned above. The experiment using an open channel with 20 m of length, 0.5 m of width and 0.3 m of height was carried out. The channel bed is rigid by laying 2 mm diameter of sediments. The vegetation model was created by using bamboo skewers that was inserted into staggered form on an acrylic board with diameter $D=0.25\text{cm}$ and spacing $\lambda=0.25\text{cm}^{-2}$ (number of cylinders in unit area), Their condition in the experiment is non-submerged (Fig. 2.1)

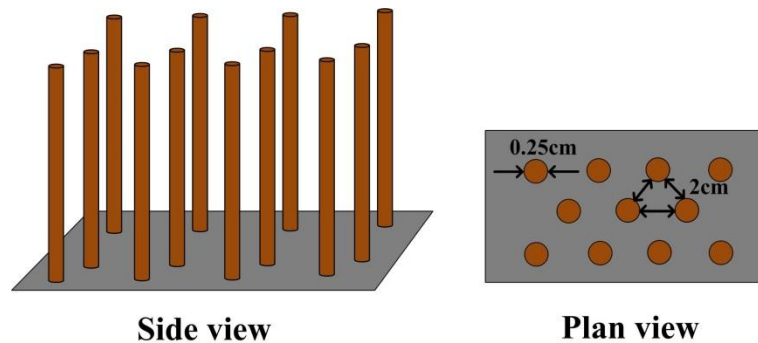


Fig. 2.1 Vegetation model

The 2 kinds of sediment, 1.25 mm (coarse sand) and 0.25 mm (fine sand) diameter, and the 2 kinds of PVC pellets assumed as POM model adjusted as the specific weight 1.26 were used through this laboratory experiment. In general, POM derives from the surface litter of forests, from peat, and it has various shapes. Hence each PVC that has various shapes was selected and distinguished a coarse particulate organic matter (CPOM) from fine particulate organic matter (FPOM) by their size (Yoshimura, 2006).

The Fig. 2.2 and Table 2.1 shows these details of experimental materials. We selected each experimental condition to change each material from movement or bed-

load transport to non-movement or suspended transport.

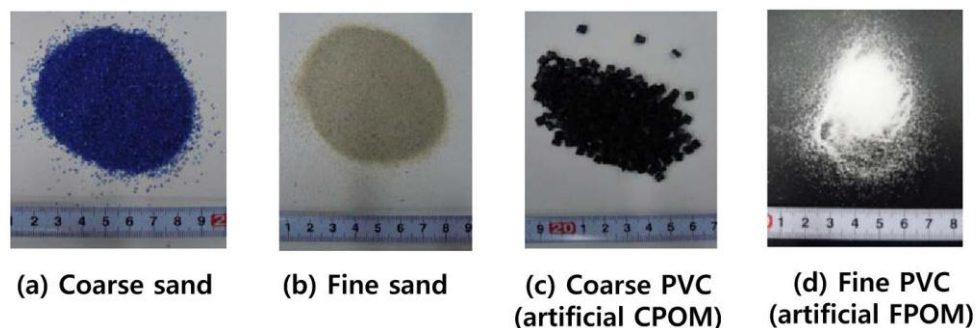


Fig. 2.2 Experimental materials

Table 2.1 Detail of each experimental sample

	d ₅₀ (mm)	Specific weight	w _f (cm/s)
Coarse sand	1.25	2.65	11.1
Fine sand	0.25	2.65	3.13
CPOM (using PVC)	1.50	1.26	5.5
FPOM (using PVC)	0.15	1.26	0.47

2.2.2 Longitudinal transition in riparian vegetation

To observe the deposition mechanism of each sediment and POM in riparian vegetation, the experiment was carried out by using 2 of 4 kinds of samples, e.g. fine sand and CPOM. The vegetation model was laying on all width and 5 m length of the open channel from 6 m lower of the upstream of the channel as shown in Fig. 2.3.

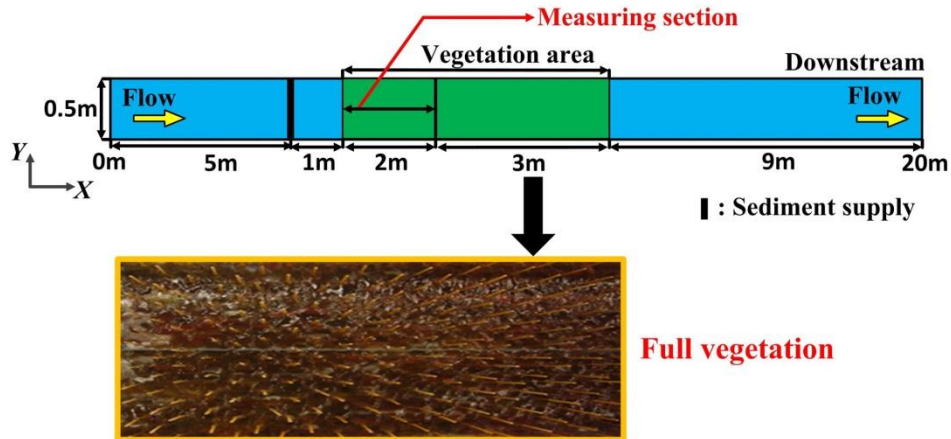


Fig. 2.3 Plan view of experiment channel (full vegetation)

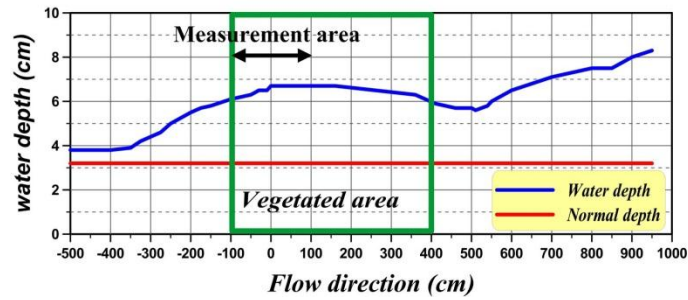


Fig. 2.4 Water depth and normal depth (full vegetation)

Fig. 2.4 shows water depth and normal depth. Measurement area of 2 m from the beginning of vegetation area was confirmed the condition of uniform flow. Fig. 2.5 shows depth averaged velocities in open channel can also be affected by vegetation.

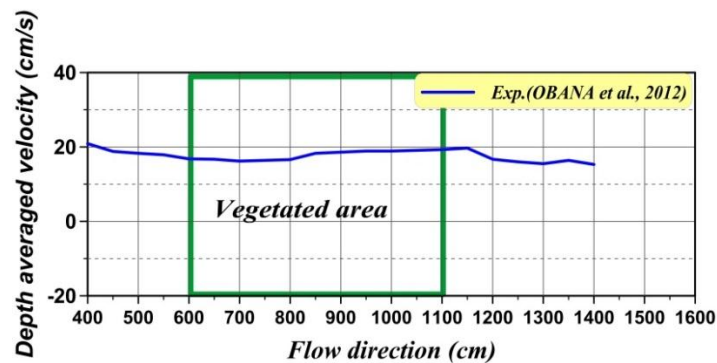


Fig. 2.5 Depth averaged velocity (full vegetation)

And the water discharge was controlled so that the vegetation is non-submerged. Table 2.2 shows the concentration of the sediment and POM supplied by each case.

Table 2.2 Concentration of sediment and POM

	Sediment	CPOM	Inserting time
	Concentration(mg/l)	Concentration(mg/l)	Min
Case1	900		20
Case2	900	60.0	20

The 2 kinds of experimental cases were run to observe each fluvial process of sediment and POM. Case-1 was to provide only fine sand, the other Case-2 was to provide both of fine sand and CPOM. Both of sediment and POM were provided at 2 m upper part from vegetation area with constant density during 20 minutes for all cases. The experimental hydraulic condition is listed in Table 2.3.

Table 2.3. Experimental hydraulic condition about full vegetation

$Q(\text{cm}^3/\text{s})$	I_b	I_f	h_0 (cm)	u_{*0} (cm/s)	u_{*v} (cm/s)	λ	$S(\text{kg})$
6940	1/150	1/185	3.5	4.3	2.3	0.00625	7.5

In which Q is the water discharge, I_b is the bed slope, I_f is the energy slope, u_{*0} is the friction velocity in non-vegetation area, u_{*v} is the friction velocity in vegetation area, λ is the vegetation density and S is the quantity of sediment supply. Friction velocity(u_{*v}) of each sample is determined as follow; The energy slope(I_f) was calculated using the Equation (2.2) has been altered Equation (2.1).

$$v = \frac{1}{n} R^{\frac{2}{3}} I_f^{\frac{1}{2}} = \frac{1}{n} h_0^{\frac{2}{3}} I_f^{\frac{1}{2}} \quad (2.1)$$

$$I_f = n^2 v^2 h_0^{-\frac{4}{3}} \quad (2.2)$$

Where, v : depth averaged velocity(m/s), R : hydraulic mean depth(m), I_f : energy slope, h_0 : normal depth(m), n : manning's roughness coefficient(=0.02), v , h_0 is using the observed value. Friction velocity of non-vegetation is obtained using Equation

(2.3).

$$u_{*0} = \sqrt{gh_0I} \quad (2.3)$$

The u_{*v} was calculated by multiplying the ratio of u_{*0} and the bottom velocity after measuring each bottom velocity in vegetation area and non-vegetation area.

$$\alpha = \frac{u_{*0}}{v_p} \quad (2.4)$$

$$u_{*v} = \alpha v_{pi} \quad (2.5)$$

Where, v_p : measuring bottom velocity(m/s), v_{pi} : bottom velocity in the vegetated area(m/s).

The movement form of each sample is judged on Shields diagram ($\tau^* \sim R_e^*$ plane; τ^* =dimensionless shear stress, and R_e^* =grain size Reynolds number) as shown in Fig. 2.6

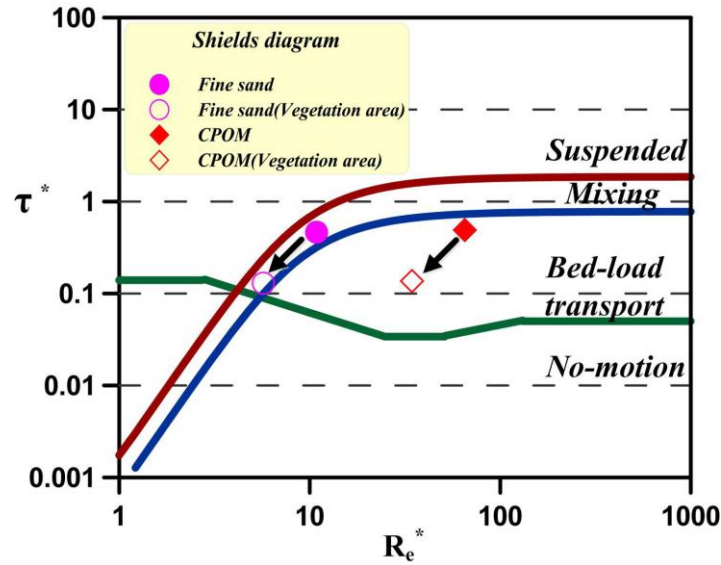


Fig. 2.6 Shields diagram in longitudinal transition(full vegetation)

Fig. 2.6 is different whether the vegetation area is existed. Fine sand is not transported in vegetation area but CPOM is transported as bed-load under this

hydraulic condition.

The longitudinal profiles of deposition of fine sand were measured during 20 min and depicted in Fig. 2.7.

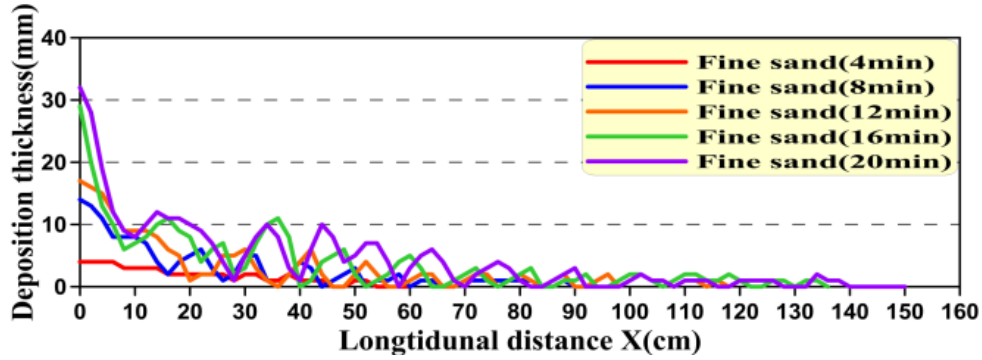


Fig. 2.7 Longitudinal profile of deposition of case1

The beginning of X axis indicates the upstream part of vegetation area. We observed that sediment deposition was occurred at the beginning of vegetation area. Longitudinal profile of deposition after 20min have some undulations with wave length L ($L=8-10\text{cm}$, $L=d=300-500$), and they were regarded as ripples from the experimental conditions on the Shields diagram.

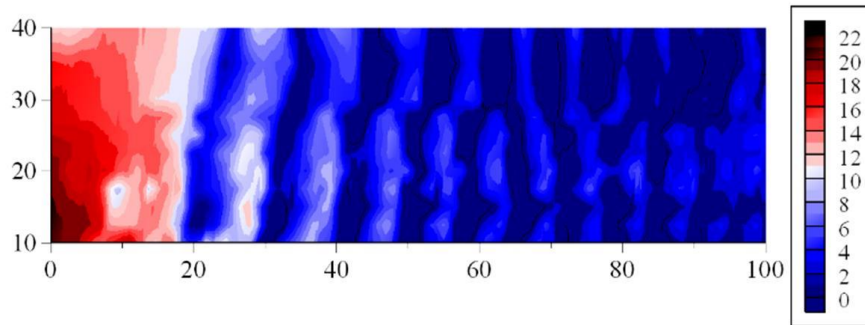


Fig. 2.8 Contour of the sediment thickness (after 14min)

Contour of sediment thickness after 14min as shown in Fig. 2.8. In this figure, we can confirm that the shape of ripple and tendency of deposition tendency are constant

with transverse direction.

Fig. 2.9 shows the temporal change of deposition thickness and number of CPOM deposited during 20 minutes.

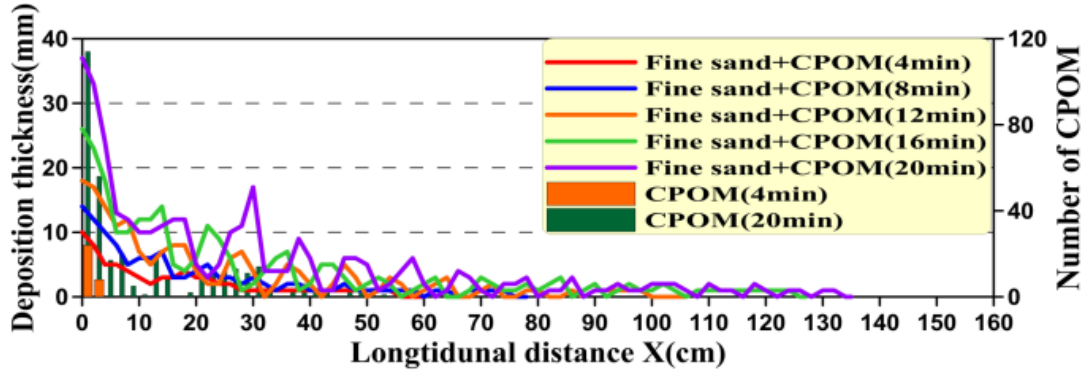


Fig. 2.9 Temporal change of deposition thickness and number of CPOM deposited

The beginning of x axis indicates the upstream part of vegetation area. We observed that sediment deposition was occurred at the beginning of vegetation area in both of cases; ripples were formed by fine sand and propagated it with time progress. In contrast, CPOM isn't deposited by itself in vegetated area but it deposited with fine sand. Firstly fine sand formed ripples. CPOM is deposited behind crest of fine sand. Second, fine sand is deposited on CPOM depositions, finally new CPOM is coming and deposited behind crest and the steps are then repeated (Fig. 2.10).

In Fig. 2.10, we can confirm that CPOM deposition is increasing and propagating with the development of ripples. Therefore, the places where CPOM can easily deposit are formed by the development of ripples in vegetated area.



Fig. 2.10 Deposition mechanism of CPOM

Fig. 2.11 shows sediment thickness of case1 and case2 after 20 minutes. It seems clear that wavelength of ripple and length of deposition zone is different.

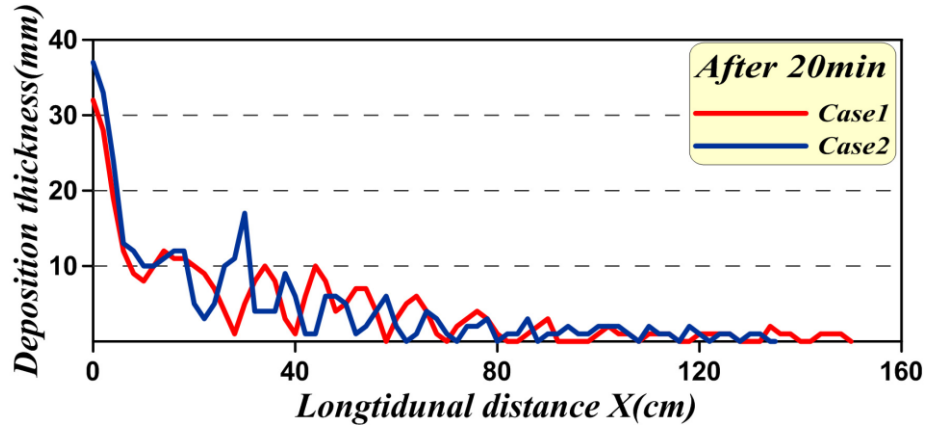


Fig. 2.11 Sediment thickness of case1 and case2

Fig. 2.12~15 shows maximum deposition thickness, wave length of ripple, length of deposition, and wave height of ripple during time. Wave length of ripple is the average value and length of deposition is continuously deposited sediment. The temporal change of wave length and height of each case at 40-60 cm downstream part from the beginning of vegetation area was compared as shown in Fig. 2.13 and Fig. 2.15.

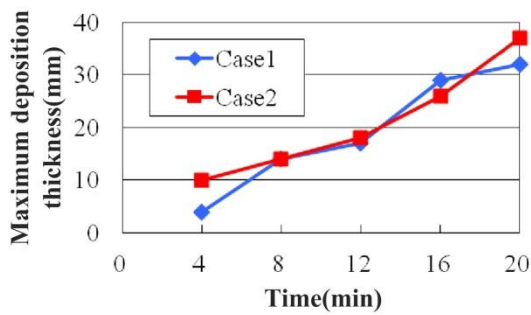


Fig. 2.12 Maximum deposition thickness

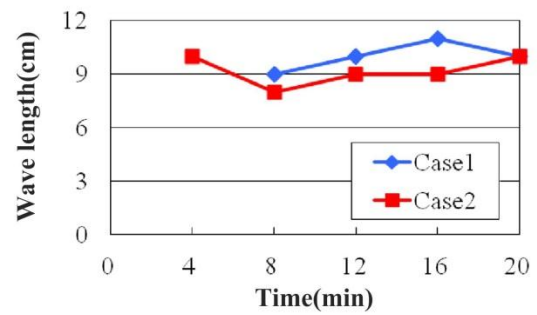


Fig. 2.13 Wave length

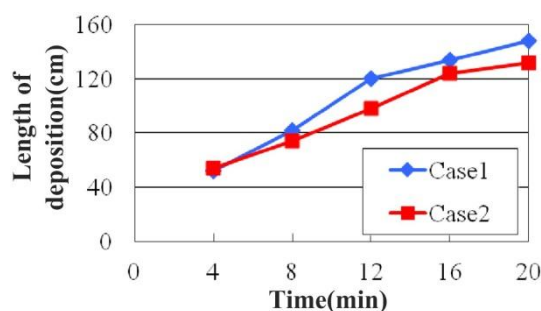


Fig. 2.14 Length of deposition

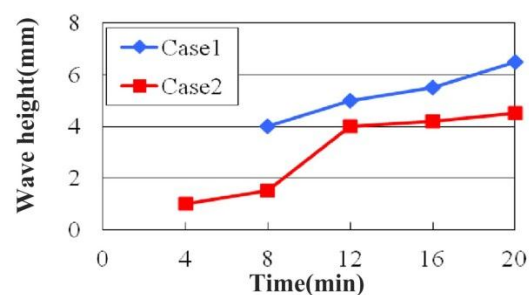


Fig. 2.15 wave height

In case1 and case2, the maximum deposition thickness of the sediments is not significantly different. We can assume that maximum deposition thickness according to CPOM is not affected by CPOM. The wave length is constant with time progress; however the wave height is tend to develop. In particular, the wave height of Case-2 is lower than Case-1 because the phenomena is caused by multifunction of sand and CPOM deposition. When the fine sand go through from up to down in vegetation area with CPOM, the ripples are firstly formed by fine sand, and CPOM are captured by trough of ripples formed by wave action. The fine sand is transported to downstream part so that ripples are developed with time progress. Hence, the decrease of wave height are affected by the quantity of fine sand transported into vegetation area whether CPOM exist or not. According to comparison of the progress speed of wave length measured of each case, Case-1 was faster twice than Case-2 because of the influence of CPOM deposited in trough of ripple. Table 2.4 show details.

Table 2.4 Comparison of wave length, height and propagation velocity of ripple

x=40-60cm	Case-1	Case-2
Wave length: L(cm)	10	9
Wave height: H(cm)	0.65	0.45
Propagation velocity: U_w (cm/s)	0.021	0.019

2.2.3 Transverse dispersion in riparian vegetation

To observe each mechanism of invasion and deposition of sediment and POM into the vegetated zone by transverse dispersion by neighboring faster flow with slower flow in vegetated zone along a bank, the experiment was carried out by installing the vegetation model on one side bank, using 4 kinds of samples as shown in Table 2.1.

The vegetation model was laying on 7 m length and 0.25 m width from 6 m lower of the upstream of the channel as shown in Fig. 2.16 Measurement section is determined at 5.3m point from the beginning of vegetation area by confirming equilibrium condition. The Table 2.5 shows the experimental hydraulic condition for these cases.

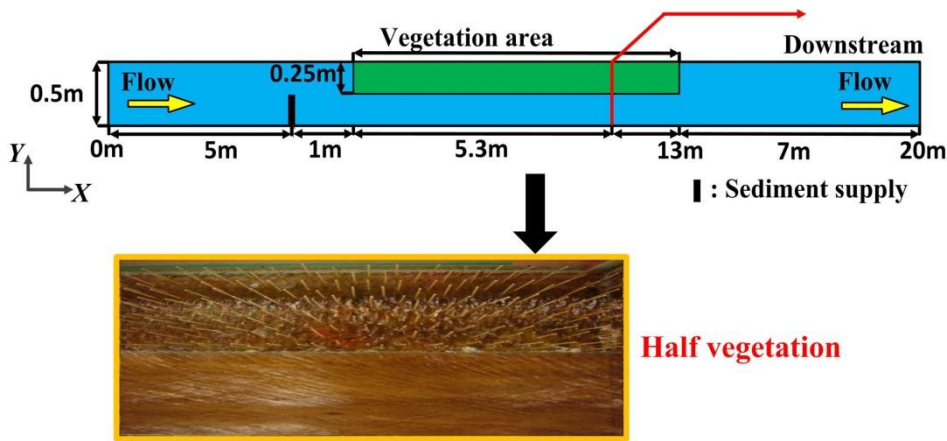


Fig. 2.16 Plan view of experiment channel (half vegetation)

Table 2.5 Experimental hydraulic condition about half vegetation

$Q(\text{cm}^3/\text{s})$	I_b	I_f	$h_0(\text{cm})$	$u_{*0}(\text{cm/s})$	$u_{*v}(\text{cm/s})$	λ
6940	1/150	1/185	3.4	6.5	1.2	0.00625

In which Q is the water discharge, I_b is the bed slope, I_f is the energy slope, u_{*0} is the friction velocity in non-vegetation area, u_{*v} is the friction velocity in vegetation area, λ is the vegetation density. The u_{*v} was calculated by using same method as mentioned above. The movement form of each sample described by shields diagram as shown in Fig. 2.17 is different whether the vegetation area is existed.

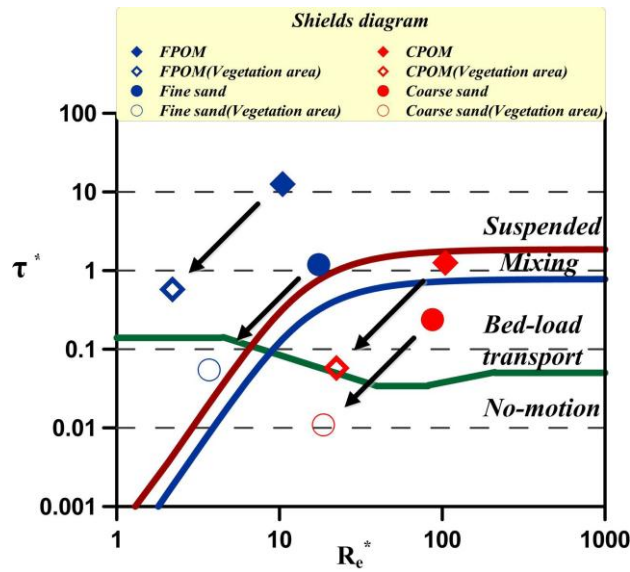


Fig. 2.17 Shields diagram in longitudinal transition (half vegetation)

In the experiment, two kinds of sand: coarse sand ($d = 1.25\text{mm}$, $\sigma/\rho = 2.65$); fine sand ($d = 0.25\text{mm}$, $\sigma/\rho = 2.65$) and two kinds of POM: CPOM model ($d = 1.50\text{mm}$, $\sigma/\rho = 1.26$); FPOM model ($d = 0.15\text{mm}$, $\sigma/\rho = 1.26$): were employed, and their movement in non-vegetated and vegetated zones was judged as shown in Table 2.6

Table 2.6 Movement of particles

Particle	Non-vegetated zone	Vegetated zone
CS(Coarse sand)	Bed load motion	No motion
FS(Fine sand)	Suspension	No motion
CPOM	Bed load+suspension	Bed load motion
FPOM	Suspension	Suspension

In this laboratory experiment, 6 cases were prepared to observe critical mechanism of deposition characteristics of 2 kinds of POM according to the sand deposition as shown in Table 2.7.

Table 2.7 Experimental cases with various blend of particles

Case	Blending of supplied particles(mg/l)				Supplied amount per 20min(kg)
	CS	FS	CPOM	FPOM	
3	1578		78.9		8.0
4		1262	98.6		8.0
5	789	789	98.6		12.0
6	1669			250	12.0
7		1819		273	12.0
8	947	947		284	12.0

CS, FS, CPOM and FPOM were supplied 1m upstream from vegetation area with various blends. As shown in Fig. 2.18, Measurement section is determined at 4.5m-6.0m from the beginning of vegetation area by confirming equilibrium condition. Fig 2.19 shows depth averaged velocity in transverse direction at 5.3m from the beginning of vegetation area. Water depth is 3.4m and vegetation model is non submerged in this point.

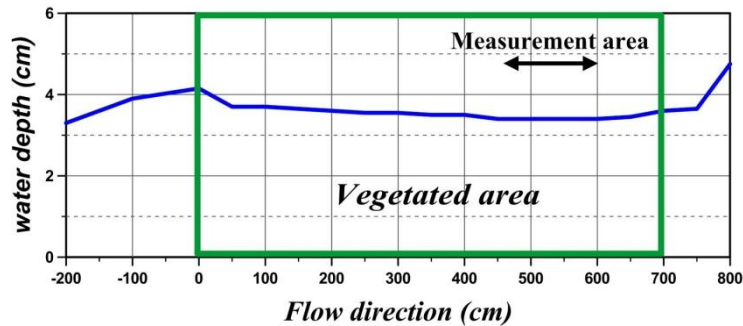


Fig. 2.18 Water depth in the vegetated area (half vegetation)

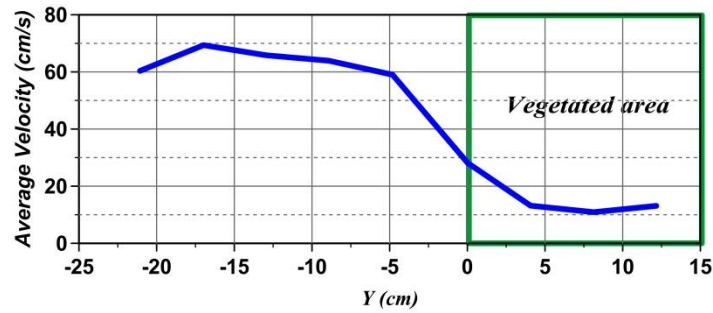
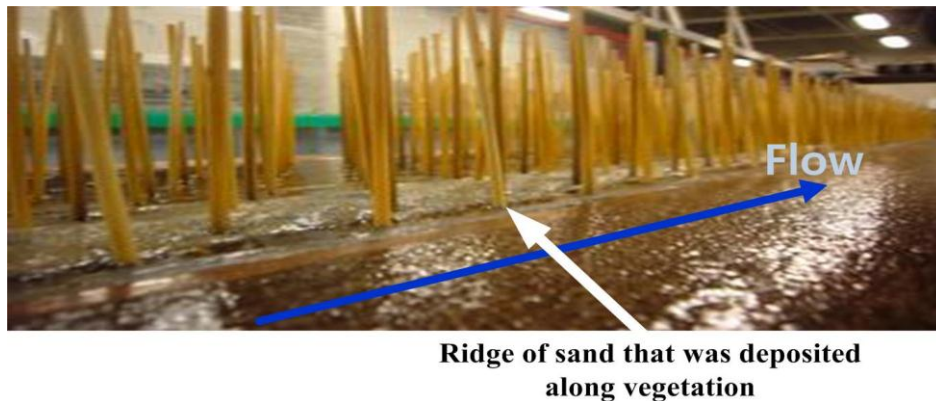


Fig. 2.19 Depth averaged velocity (half vegetation)

We measured the thickness of sand deposition and the width of deposition layer from the boundary of vegetation area. However CPOM run through with bed-load transport without depositing into vegetation area, we found that they invaded into vegetation. So that the invasion rate of CPOM was measured, and FPOM deposited with sediment was also measured by conducting the sieve analysis test.

As for the temporal change of sand deposition of each case at measurement section ($x=530$ cm, see Fig. 2.16), the Fig. 2.20 shows their deposition characteristics. In this hydraulic condition, coarse sand is transported as bed-load, and fine sand is transported as suspended formation. The beginning of x axis represents the beginning of vegetation area in lateral direction. The result of every case showed ridge of sediment that was deposited along the boundary of vegetation, and it develop with time progress.



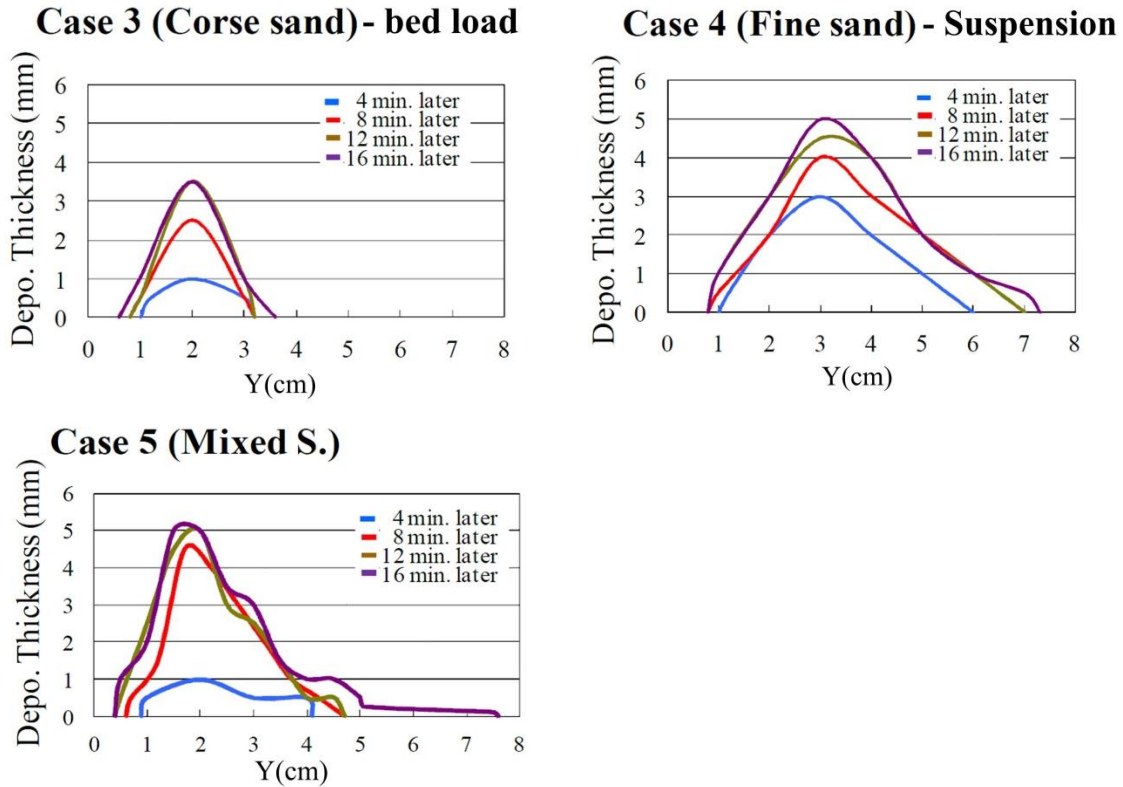


Fig. 2.20 Temporal change of sand deposition of each case

The deposition thickness and width is increased from coarse to fine sand according to their grain size. Many researches which had already conducted about the deposition of suspended sediment in one side bank of vegetation pointed out that the deposition mechanisms of coarse and fine sand are differ (Lau et al, 1977, Webel et al, 1984). The movement of suspended sediment transport has good followability with fluid motion, hence it predominate in transverse dispersion into vegetation area. This is the reason why the deposition width of suspended sediment became twice as wide as bed-load.

On the other hand, deposition of bed-load on boundary layer of vegetation caused by wave action by neighboring faster flow with slower flow in vegetated zone along a bank (Ikeda et al., 1992, Tsujimoto et al., 1994). The wave action that caused the active movement of transverse dispersion could change the quantity of bed-load in lateral direction. The proportion of suspended and bed-load sediment in mixed sand deposited was 9 to 1. Moreover, the bed-load was transported more wide than it was transported by itself.

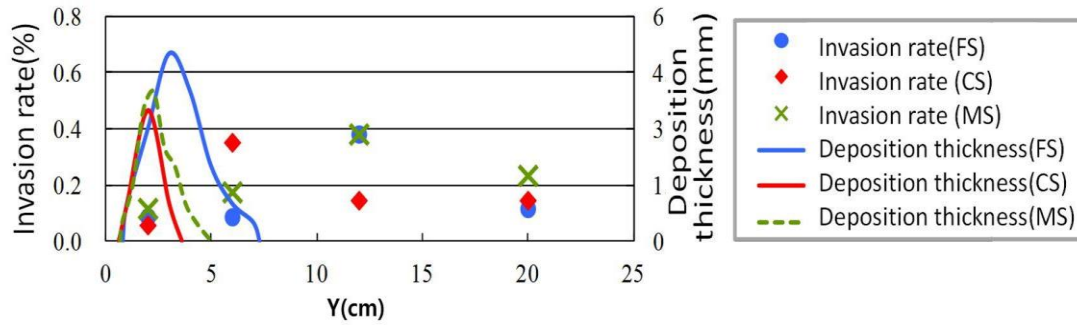


Fig. 2.21 CPOM invasion rate of each case (20min later)

Fig. 2.21 shows the CPOM invasion rate into vegetation area of each case after 20 minutes later. The CPOM number which passed through each section of the area within vegetation was comparatively displayed to all the CPOM input. Their range of movement is expanded according to height of sediment deposition. The height and width of sediment deposition is developed with time progress, on the other hand tractive force to transport sediment and CPOM in lateral direction was decreased according to the development of ridge of sediment. We assumed that these multifunctions changed the invasion rate of CPOM into vegetation area.

The deposition thickness of FPOM was shown in Fig. 2.22. Their result showed that the deposition of FPOM is increased with coarser sand. In fact, we found that FPOM are captured by porosity in sediment and deposited, in particular FPOM is tend to deposit at backward from the top of ridge of sediment. The reason was assumed that the movement of FPOM has good followability with fluid motion as same as the movement of suspended sediment. The ridge of sediment deposition on boundary layer is decreased the velocity in lateral direction, at same time the tractive force is also decreased in backward from top of ridge. However, we have not illustrated their movement mechanism so that it is important to consider more details by observing the FPOM mechanisms with many trial cases.

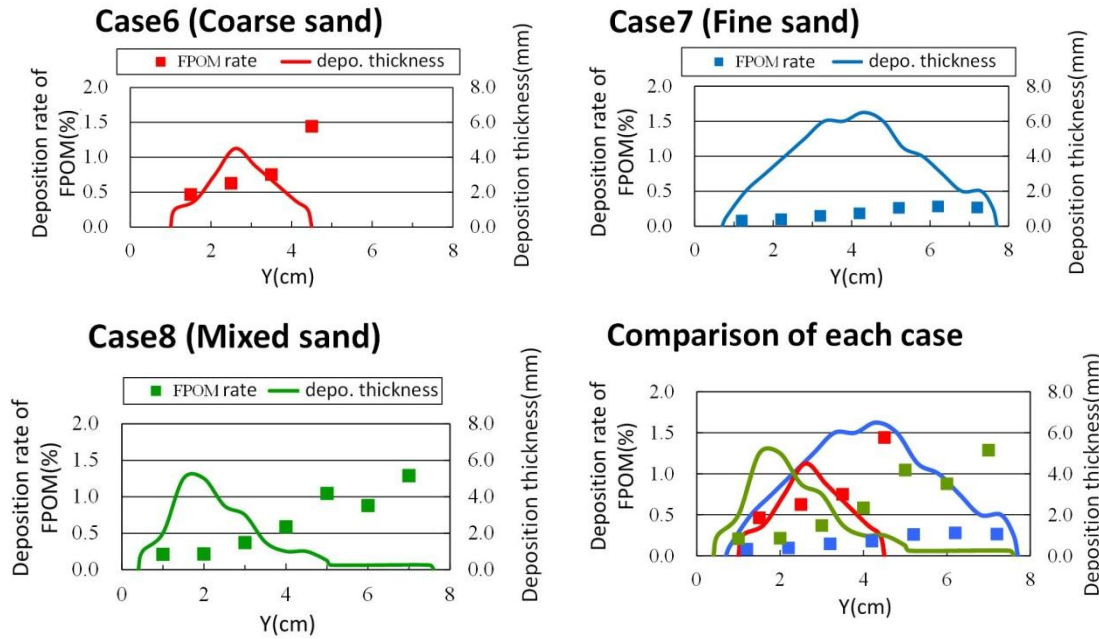


Fig. 2.22 Deposition thickness of FPOM

2.4 Concluding Remarks

Flood mitigation and ecosystem conservation are simultaneously required in recent river management, and understanding and analysis of flow and river morphology in a stream with vegetation have become important topics in river hydraulics.

In this study, we investigated the deposition mechanisms of sediment and POM through a laboratory experiment. After we observed the deposition mechanisms by the laboratory experiment focusing on two kinds of empirical hydraulic processes.

Deposition mechanisms of sediment and POM by the laboratory experiment can be described as below:

1. In case of longitudinal transition in riparian vegetation, ripples are formed by fine sediment that was deposited in riparian vegetation. And CPOM is captured by trough of ripples formed by wave action. In contrast, their multifunction of movement of both sample were decreased the propagation velocity of wave height and length of ripples.
2. In case of transverse dispersion with vegetated zone, ridges of respective size

sediment are formed along the boundary of vegetation. CPOM and FPOM are not deposited by themselves in vegetation area (without sediment motion) but their ranges of movement are expanded by transverse diffusion promoted by sand ridges of sediment deposition.

Although the results of this study add to rather limited empirical knowledge base, more research regarding the connectivity between the phenomenon caused on the field and the deposition mechanisms observed in the laboratory, the development of POM model (Chapter 8) based on the deposition mechanisms and numerical model (Chapter 4-7) presented in this study is clearly needed.

References

1. Fisher, S. G. (1977) Organic matter processing by a stream-segment ecosystem: Fort river, massachusetts, usa. *Internationale Revue der gesamten Hydrobiologie und Hydrographie* 62 (6), pp. 701–727.
2. Golladay, S., Webster, J., Benfield, E. (1987) Changes in stream morphology and storm transport of seston following watershed disturbance. *Journal of the North American Benthological Society*, pp. 1–11.
3. Ikeda, S., Ohta, K., & Hasegawa, H. (1992) Periodic vortices at the boundary of vegetated area along river bank, *Journal of JSCE*, No.443/II-18, pp.47-54.
4. Lau, Y.L., & Krishnappan, B.G. (1977) Transverse dispersion in rectangular channels, *Journal of Hydraulic Engineering, ASCE*, vol.103, No. HY 10, pp.1173-1189.
5. Tsujimoto, T., Kitamura, T., & Nakagawa, H. (1996) Lateral bed-load transport and sorting near vegetation zone along side wall, *Journal of JSCE*, No.503/II-29, pp.99-108..
6. Wallacc, J. B. & Grubaugh, J. W. (1996) Transport and storage of FPOM. *Methods in Stream Ecology* (ed. By F. R. Hauer & G. A. Lamberti), pp. 191-215. Academic Press. New York, USA.
7. Webel, G., & Schatzmannm M. (1984) Transverse mixing in open channel flow, *Journal of Hydraulic Engineering, ASCE*, vol.110, No. 4, pp.423-435.
8. Webster, J., Golladay, S., Benfield, E., D'Angelo, D., Peters, G. (1990) Effects of forest disturbance on particulate organic matter budgets of small streams. *Journal of the North American Benthological Society*, pp. 120–140.

9. Webster, J. R. & Golladay, S. W. (1984) Seston transport in streams at Coweeta Hydrologic Laboratory, North Carolina, USA. *Verhondlungen der Internotionalen Vereinigung fur Theoretische und Angewandte Limnologie* 22, pp. 1911-1919.
10. Yoshimura, C., Tanida, K., Furumai, H., & Nakajima, F. (2006) Various particulate organic matter (POM) supporting stream ecosystems, *Ecol. Civil Eng.* 9(1), pp. 85-101.

CHAPTER 3

DISCUSSION ON 2D DEPTH AVERAGE MODEL FOR FLUVIAL PROCESS WITH VEGETATION

3.1 General

In order to manage river from the viewpoints of flood mitigation, water resources utilization and ecosystem conservation, river flow and morphological changes there would be fairly understood and reasonably described. In particular, Riparian vegetation is an important feature of many streams and rivers, because it may significantly affect river flow, sediment transport and morphological changes.

Numerical models have been extensively used in simulating and predicting velocity and solute transport fields in open channels, rivers and other water bodies, most models are developed based on the finite volume method, the finite element method, the finite difference method. The models developed for vegetated open-channel flows. Range from simplified one-dimensional models to fully three-dimensional models.

Yoshida and Dittrich presented a 1D steady-state flow simulation model with evaluating the roughness parameters due to the surface roughness of the main channel and floodplains, riparian forests on the floodplains. Vegetation is regarded as dispersive obstacles represented by form drag, and it is expected to apply to description of fluvial process in a stream with vegetation (Tsujimoto 1999). Nadaoka and Yagi developed large eddy simulation (LES) models to simulate the hydrodynamic behavior of turbulent flow in open channels with domains of vegetation. David and Horritt used TELEMAC-2D to simulate a flood event of the River Severn, UK. Vionnet et al. calculated the values of the flow resistance and eddy viscosity coefficients in channel and floodplain areas using a 1D model based on the lateral distribution method and incorporated the results into a 2D numerical model.

Wu and López proposed a depth-averaged two-dimensional k-e model for computing the flow and sediment transport in vegetated open channels based on the finite volume method. (Shimizu and Tsujimoto (1994); Darby (1999); Lopez and Garcia (2001); Neary (2003); see review by Simon et al. (2004)). These latter models can accurately resolve local flow and turbulence phenomena due to the presence of vegetation. To address fluvial processes at larger time and length scales, Tsujimoto (1998) and Van de Wiel and Darby (2004) developed depth averaged two-dimensional (2-D) models of flow and sediment transport in straight and meandering tree-lined channels under steady flow conditions.

There are many kinds of study conducted to find out hydraulic characteristics and morphological change of vegetated area using numerical modeling. However ambiguous aspects remained in numerical modeling. In conventional method, the numerical modeling consider just spatially averaged drag due to vegetation. it is comparatively well described the flow behavior, but lack of bed roughness resistance law in vegetated area must bring inaccurate description of fluvial processes. Inaccurate description of fluvial process in depth average scheme has been discussed: how the bed roughness boundary layer developed near the bed in vegetated area, how the transverse mixing occurred with vegetation, how the bed load transport rate changed in vegetated area, how the suspended sediment concentration profile distributed in vegetated area and secondary flow in vegetation.

Chapter 3 provides detailed description on numerical model which was developed to analyze flow and sediment transport with vegetation.

3.2 Conventional method

3.2.1 Outline of Numerical analysis method

In this study, a 2-Dimensional numerical model made by Nagoya hydraulics (hereafter, NHSED2D), which is able to simulate flow fields-vegetation-bed variation interaction directly, is used to investigate fluvial process and mechanics of sediment transport in vegetated area.

The NHSED2D model is basically based on the model developed by Goto et al., (2002). The NHSED2D model is consist of two main part, the flow model and bed variation model. In the numerical analysis, at first the velocity components and water depth are computed over an initial bed configuration. and next time step are calculated using the QUICK scheme until it converges. Then the sediment transport and result of bed variation are calculated with the flow field. After the bed

configuration is renewed, the flow field is calculated again on the renewed bed configuration. These procedures are repeated to obtain successive bed deformation in the vegetation area. The numerical model is modified in depth- averaged simulation scheme for get the accuracy of calculation of deposition profile.

It includes the following features:

- 1) Boundary-fitted non-orthogonal grids
 - Easily and effectively applicable to practical problems with complicated boundaries in rivers
- 2) To prevent numerical oscillation due to collocated grid arrangement, the idea according to (Chow and Rhie,1982) to interpolate the flux of mass at the cell surface is used.
- 3) The fractional step method to solve the Poisson equation of water surface elevation is employed in order to obtain the stable and accurate flow field (Ferziger and Peric, 1996).
 - Relatively stable and cost-effective compared to simple time developing scheme
- 4) Finite volume method for discretization of the governing equations
 - Easily understandable for engineers
- 5) Semi-coupling of surface and subsurface flow
- 6) Unsteady inlet discharge is available

In the present short report, the solving technique in the NHSED2D model is explained briefly.

3.2.2 Flow model

$$\frac{\partial hU}{\partial t} + \frac{\partial(hU^2)}{\partial x} + \frac{\partial(hUV)}{\partial y} = -gh \frac{\partial(H)}{\partial x} + D_x - F_x h - \frac{\tau_{bx}}{\rho} \quad (3.1)$$

$$\frac{\partial hV}{\partial t} + \frac{\partial(hUV)}{\partial x} + \frac{\partial(hV^2)}{\partial y} = -gh \frac{\partial(H)}{\partial y} + D_y - F_y h - \frac{\tau_{by}}{\rho} \quad (3.2)$$

$$\frac{\partial h}{\partial t} + \frac{\partial(hU)}{\partial x} + \frac{\partial(hV)}{\partial y} = 0 \quad (3.3)$$

Equation (3.1)-(3.2) is the momentum equations and Equation (3.3) is the continuity equation. where t is time, x and y are Cartesian coordinate system, U, V are

the depth-averaged velocity components in x and y direction, respectively. h is the water depth, g is the gravitational acceleration, ρ is the density of water. τ_{bx} , τ_{by} are the bed shear stress in x and y direction as following Equation (3.4)-(3.5). where C_f is the resistance coefficient of bed-surface.

$$\tau_{bx} = \rho C_f U \sqrt{U^2 + V^2} \quad (3.4)$$

$$\tau_{by} = \rho C_f V \sqrt{U^2 + V^2} \quad (3.5)$$

D_x , D_y are the turbulent diffusion term of momentum in x and y direction. The momentum fluxes due to horizontal turbulent diffusion are modeled with using eddy viscosity ν_T as following Equation (3.6)-(3.8).

$$D_x = \frac{\partial}{\partial x} \left[\nu_t \frac{\partial(hU)}{\partial x} \right] + \frac{\partial}{\partial y} \left[\nu_t \frac{\partial(hU)}{\partial y} \right] \quad (3.6)$$

$$D_y = \frac{\partial}{\partial x} \left[\nu_t \frac{\partial(hV)}{\partial x} \right] + \frac{\partial}{\partial y} \left[\nu_t \frac{\partial(hV)}{\partial y} \right] \quad (3.7)$$

$$\nu_T = \alpha u_* h \quad (3.8)$$

F_x , F_y are the spatially averaged drag due to vegetation per unit horizontal area in x and y direction.

$$F_x = \frac{1}{2} C_d \lambda \frac{l}{h} U \sqrt{U^2 + V^2} \quad F_y = \frac{1}{2} C_d \lambda \frac{l}{h} V \sqrt{U^2 + V^2} \quad (h > l) \quad (3.9)$$

$$F_x = \frac{1}{2} C_d \lambda U \sqrt{U^2 + V^2} \quad F_y = \frac{1}{2} C_d \lambda V \sqrt{U^2 + V^2} \quad (h \leq l) \quad (3.10)$$

where C_D is the drag coefficient by vegetation, and $\lambda (= N_0 * D)$ is projected area of vegetation to flow on a unit horizontal area, l is the vegetation height, N_0 is the number of vegetation unit per unit horizontal area, D is the diameter of vegetation stem. Equation (3.11) is employed as the resistance law by using the equivalent sand roughness k_s that varies according to the exposure height of sand.

$$\frac{U}{u_*} = \sqrt{\frac{1}{C_f}} = \frac{1}{\kappa} \ln \frac{11.0 * h}{k_s} \quad (3.11)$$

Where U denotes the depth-average velocity and u_* denotes bed shear velocity.

When the water depth is less than critical value that is comparable to sediment diameter at the riverbed in the surface flow region, the following governing equations for subsurface flow are solved instead of that for surface flow.

$$\frac{\partial \zeta}{\partial t} + \text{div}(C_{sub} \text{grad} \zeta) = 0 \quad (3.12)$$

$$C_{sub} \equiv \frac{K(\zeta - z_{sub})}{n_e} \quad (3.13)$$

where K = permeability of subsurface layer; z_{sub} =elevation of the bottom of subsurface layer; and n_e =porosity of subsurface layer.

3.2.3 Sediment and bed variation model

Sediment transport and bed variation model based on the above mentioned depth-averaged flow model. Morphological computation involves a combination of flow fields, sediment transports, and bed elevation associated with vegetation area. After resolving the flow fields, the sediment transport fields are computed from the expression of bed load and suspended load. Finally, the change in the bed topography due to total load are determined. Bed-load transport is related to the bed shear stress or the shear velocity. The time variation of the bed elevation can be described by the following sediment continuity equation.

$$\frac{\partial z}{\partial t} + \frac{1}{(1-\lambda)} \left\{ \frac{\partial q_{bx}}{\partial x} + \frac{\partial q_{by}}{\partial y} \right\} = 0 \quad (3.14)$$

The bedload in depth-averaged velocity direction q_b can be calculated by the following (Ashida and Michiue, 1972) formula.

$$q_{b*} \equiv \frac{q_b}{\sqrt{(\sigma/\rho - 1)gd^3}} = 17\tau_*^{3/2} \left(1 - \frac{\tau_{*c}}{\tau_*} \right) \left(1 - \sqrt{\frac{\tau_{*c}}{\tau_*}} \right) \quad (3.15)$$

where q_{b*} is the dimensionless bedload transport rate; q_b is the bedload transport rate(substantial volume per unit width per unit time) σ , ρ is the mass densities of

sediment and fluid, respectively; d is the sand diameter, τ_* is the dimensionless bed shear stress (Shields number), τ_{*c} is the dimensionless critical tractive force.

$$\tau_* \equiv \frac{u_*^2}{(\sigma / \rho - 1) g d} \quad (3.16)$$

In the horizontally 2D scheme, the transport rate is divided into the longitudinal and transverse directions according to the direction of bed-load motion and the transverse bed slope as follows.

$$q_{bx} = q_b \cos \varphi \quad q_{by} = q_b \sin \varphi \quad (3.17)$$

φ is the angle of bedload movement. The effect of transverse bed slope on the sediment transport is taken into account following (Nakagawa and Murakami, 1986). The angle of bedload movement φ is expressed by the following equation.

$$\tan \phi_L = - \sqrt{\frac{1}{\mu_d \mu_f} \frac{\tau_{*c}}{\tau_*} \frac{\partial z_b}{\partial n}} \quad (3.18)$$

where ϕ_L is the effect of transverse slope, μ_d , μ_f is dynamic and static friction coefficients of sand, n is the axis perpendicular to the main-flow. After calculating bed variation, the bed slope angles $\tan^{-1} (\partial z / \partial x)$ and $\tan^{-1} (\partial z / \partial y)$ between adjacent grids on the bed are compared with the angle of repose ϕ . In the case that the bed slope angle is greater than the angle of repose ϕ , the bed is assumed to collapse with the angle ϕ .

A large number of investigations have tried to find a single equation to describe the total transport, even if several authors believe that this is basically impossible, since movement in suspension follows principles which are entirely different from those which govern bedload transport (Einstein 1950; Hu and Guo 2010). Several authors affirm (Nikora and Goring 2002) that there are too many theories and a few experimental validation on suspended load. Nowadays, with better methods of investigation, especially images analysis (ADV or PIV), several new empirical approaches on suspended load are led. The most common method to approach the suspended sediment transport is based on the integration of the advection/diffusion equation of suspended load in steady uniform flow conditions (Fang and Wang 2000;

Lane and Kalinske 1941; Rouse 1937; Van Rijn 2007).

The spatial distribution of depth-averaged concentration is described by the flowing equation.

$$\frac{\partial hC}{\partial t} + \frac{\partial}{\partial x} \left(hCU - \beta v_{th} h \frac{\partial C}{\partial x} \right) + \frac{\partial}{\partial y} \left(hCV - \beta v_{th} h \frac{\partial C}{\partial y} \right) = \Xi_{\Theta} \quad (3.19)$$

Where Ξ_{Θ} = difference between deposition and entrainment from the bed to be expressed by $(C_{Be} - C_B)w_0$ and it represents the bed deformation; and the horizontal diffusion coefficient of suspended sediment is assumed to be βv_{th} .

Entrainment of suspended sediment at bottom Ξ_{Θ} is described by the flowing equation.

$$\Xi_{\Theta} = (C_{be} - C_b)w_0 \quad \text{When bed is covered by sand} \quad (3.20)$$

$$\Xi_{\Theta} = \begin{cases} (C_{be} - C_b)w_0 & (C_{be} - C_b) < 0 \\ 0 & (C_{be} - C_b) > 0 \end{cases} \quad \text{When bed is not covered by sand} \quad (3.21)$$

Where, C_b = bottom concentration, C_{be} = bottom concentration under equilibrium, and w_0 = settling velocity of sand.

Settling velocity of sand is described by Rubey's equation. It is balance of drag and submerged weight.

$$w_{0*} \equiv \frac{w_0}{\sqrt{(\sigma / \rho - 1)gd}} = \sqrt{\frac{2}{3} + \frac{36}{d_*}} - \sqrt{\frac{36}{d_*}} \quad (3.22)$$

$$d_* = (\sigma / \rho - 1)gd^3 / \nu^2 \quad (3.23)$$

Drag coefficient for natural sand, as Equation (3.24)

$$C_D = 2.0 + \frac{24\nu}{w_0 d} \quad (3.24)$$

The value given for Turbulent diffusion coefficient of suspended sediment, as follows:

$$\varepsilon_s = \beta \nu_T \quad (3.25)$$

$1/\beta$ =turbulent Schmidt number, ν_T =Kinematic eddy viscosity

$$\beta \equiv \frac{\varepsilon_s}{\nu_T} = 1 + 1.54 \left(\frac{w_0}{u_*} \right)^2 \quad (3.26)$$

Equation (3.26) compared between diffusion theory and stochastic approach by Tsujimoto 1986.

The equilibrium suspended sediment concentration distributes along the depth in the area without vegetation and the profile $c(z)$ is written as follows (Lane & Kalinske 1941) by substituting Equation (3.27).

$$\frac{c(z)}{C_B} = \exp \left(- \frac{6w_0}{\beta \kappa u_*} \frac{z}{h} \right) \quad (3.27)$$

Then, the depth averaged suspended sediment concentration C is written by

$$\frac{C}{C_B} \equiv \frac{6w_0 h}{\beta \kappa u_*} \left[1 - \exp \left(- \frac{6w_0 h}{\beta \kappa u_*} \right) \right] \quad (3.28)$$

The equilibrium bottom concentration, C_{be} , is related to the shear velocity.

$$C_{be} = A_{s1} \left(\frac{u_*}{w_0} \right)^{A_{s2}} \left(1 - \frac{\tau_{*c}}{\tau_*} \right)^{A_{s3}} \quad (3.29)$$

Where, $A_{s1}=0.002$, $A_{s2}=2$, $A_{s3}=1.5$

3.2.4 Numerical grid and basic of discretization of governing equations

In the NHSED2D model, the boundary fitted non-orthogonal grid system (Ferziger and Peirc, 1997) is employed. The example of the grid arrangement is shown in Fig.

3.1. As shown in Fig. 3.1, shape of each cell is quadrilateral and all of the quantities in a cell are represented by the quantities at the geometrical center of the cell (collocated grid, Ferziger and Peirc, 1997). Each cell is surrounded by four cells that are represented as E, W, N, S, respectively. The cell surface values are expressed as e, w, n, s, respectively.

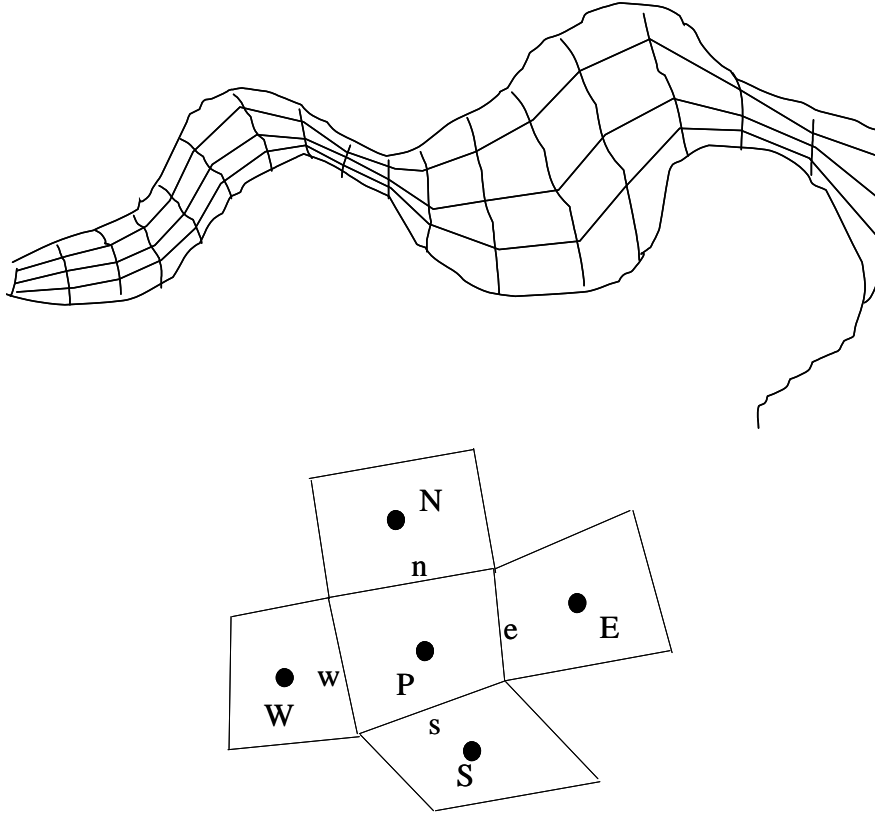


Fig. 3.1 Grid system

The FVM (Finite Volume Method, Ferziger and Peirc, 1997) is employed to discretize the governing equations in the NHSED2D model. All of the governing equations are integrated within a cell that has area ΔA . We basically use the following approximation for discretizing each term.

$$\iint \varphi dA \approx \varphi_p \Delta A \quad (3.30)$$

$$\iint \text{div} \mathbf{V} dA = \int (\mathbf{V}_c \cdot \mathbf{n}_c) dS \approx \sum (\mathbf{V}_c \cdot \mathbf{n}_c) S_c \quad (3.31)$$

where ϕ =physical quantity(scalar); V =physical quantity(vector); n_c =unit vector normal to cell surface; S =cell surface length; and subscript P and C represent the cell center value and cell surface value, respectively.

3.2.5 Fractional step method

How to couple the momentum equations with the continuity equation is the key technique when one solves the flow field stably and accurately. The fractional step method (Ferziger and Peirc, 1997) with solving Poisson equation on water-surface elevation is introduced here.

The integrated momentum equation for x-direction within a cell is as follows:

$$\left. \frac{\partial q_x}{\partial t} \right|_P = -(\mathbf{C}_{xP} - \mathbf{D}_{xP} + \mathbf{P}_{xP} + \mathbf{F}_{xP}) \quad (3.32)$$

$$\mathbf{C}_{xP} \equiv \frac{1}{\Delta A} \iint \text{div} \left(q_{xP} \frac{\mathbf{q}_P}{h_P} \right) dA \approx \frac{1}{\Delta A} \sum_c \left(q_{xc} \frac{\mathbf{q}_c \cdot \mathbf{n}_c}{h_c} \right) S_c \quad (3.33)$$

$$\mathbf{D}_{xP} \equiv \frac{1}{\Delta A} \iint \text{div} \left(\frac{\mathbf{T}_{xP}}{\rho} \right) dA \approx \frac{1}{\Delta A} \sum_c \left(\frac{\mathbf{T}_{xc} \cdot \mathbf{n}_c}{\rho} \right) S_c \quad (3.34)$$

$$\mathbf{P}_{xP} \equiv \frac{1}{\Delta A} \iint gh \frac{\partial \zeta}{\partial x} dA \approx gh \left. \frac{\partial \zeta}{\partial x} \right|_P \quad (3.35)$$

$$\mathbf{F}_{xP} \equiv \frac{1}{\Delta A} \iint \left(\frac{C_f}{h^2} + \frac{C_D \lambda}{h} \right) q_x |\mathbf{q}| dA \approx \left(\frac{C_f}{h^2} + \frac{C_D \lambda}{h} \right) q_x |\mathbf{q}| \Big|_P \quad (3.36)$$

Equation (3.32) is discretized with finite time step Δt as follows:

$$q_{xP}^* = q_{xP}^{n-1} - \Delta t (\mathbf{C}_{xP}^{n-1} - \mathbf{D}_{xP}^{n-1} + \mathbf{F}_{xP}^{n-1}) \quad (3.37)$$

$$q_{xP}^n = q_{xP}^* - \Delta t gh_P^{n-1} \left. \frac{\partial \zeta}{\partial x} \right|_P \quad (3.38)$$

where superscript n represents time-step and superscript means interim value. The momentum equation for y-direction is discretized with the same manner.

$$q_{yP}^* = q_{yP}^{n-1} - \Delta t (\mathbf{C}_{yP}^{n-1} - \mathbf{D}_{yP}^{n-1} + \mathbf{F}_{yP}^{n-1}) \quad (3.39)$$

$$q_{yP}^n = q_{yP}^* - \Delta t g h_p^{n-1} \left. \frac{\partial \zeta}{\partial y} \right|_P^n \quad (3.40)$$

After Equations (3.38) and (3.40) are inserted into Equation (3.3), the following Poisson equation is derived.

$$\left. \frac{\partial \zeta}{\partial t} \right|_P + \text{div} \mathbf{q}_P^* - \text{div} (\Delta t g h_p^{n-1} \text{grad} \zeta_P^n) = 0 \quad (3.41)$$

After integrating the above equation within a cell and discretized with finite time step Δt , the following is derived.

$$\frac{\Delta A}{\Delta t} (\zeta_P^n - \zeta_P^{n-1}) + \mathbf{Q}_P - \mathbf{R}_P = 0 \quad (3.42)$$

$$\mathbf{Q}_P \equiv \iint \text{div} \mathbf{q}_P^* dA \approx \sum_c (\mathbf{q}_c^* \cdot \mathbf{n}_c) S_c \quad (3.43)$$

$$\mathbf{R}_P \equiv \iint \text{div} (\Delta t g h_p^{n-1} \text{grad} \zeta_P^n) dA \approx \sum_c (\Delta t g h_c^{n-1} \text{grad} \zeta_c^n \cdot \mathbf{n}_c) S_c \quad (3.44)$$

The term $\text{grad} \zeta_c^n \cdot \mathbf{n}_c$ is approximated as follows (see Fig. 3.2): For the east side cell surface;

$$\text{grad} \zeta_e^n \cdot \mathbf{n}_e = \frac{\zeta_E^n - \zeta_P^n}{|\mathbf{d}_{PE} \cdot \mathbf{n}_e|} \quad (3.45)$$

where d_{PE} =vector of point P to E.

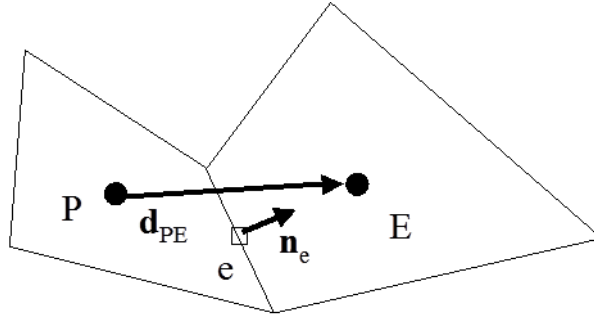


Fig. 3.2 Approximation of gradient of water-surface elevation

Considering the above approximation, the following algebraic equation can be derived finally:

$$a_P \zeta_P^n = a_E \zeta_E^n + a_W \zeta_W^n + a_N \zeta_N^n + a_S \zeta_S^n + b_0 \quad (3.46a)$$

$$a_P \equiv a_E + a_W + a_N + a_S + b_P \quad (3.46b)$$

$$a_E \equiv \frac{\Delta t g h_e^{n-1} S_e}{|d_{PE} \cdot n_e|} \quad (3.46c)$$

$$a_W \equiv \frac{\Delta t g h_w^{n-1} S_w}{|d_{PW} \cdot n_w|} \quad (3.46d)$$

$$a_N \equiv \frac{\Delta t g h_n^{n-1} S_n}{|d_{PN} \cdot n_n|} \quad (3.46e)$$

$$a_S \equiv \frac{\Delta t g h_s^{n-1} S_s}{|d_{PS} \cdot n_s|} \quad (3.46f)$$

$$b_P \equiv \frac{\Delta A}{\Delta t} \quad (3.46g)$$

$$b_0 \equiv -\sum_c (q_c^* \cdot n_c) S_c + \frac{\Delta A}{\Delta t} \zeta_P^{n-1} \quad (2.46h)$$

For each time step, firstly Equations (3.37) and (3.39) are solved, then Equation (3.46) is solve using calculated q^* to get water-surface elevation. Finally, Equations (3.38) and (3.40) are solved. This procedure will be repeated until converged solution appears. When the water depth is less than critical value, q_x and q_y are simply set as zero and the following discretized equation for subsurface flow is solved instead of Equation (3.46).

$$a_P \zeta_P^n = a_E \zeta_E^n + a_W \zeta_W^n + a_N \zeta_N^n + a_S \zeta_S^n + b_0 \quad (3.47a)$$

$$a_P \equiv a_E + a_W + a_N + a_S + b_P \quad (3.47b)$$

$$a_E \equiv \frac{C_{sub,e}^{n-1} S_e}{|d_{PE} \cdot n_e|} \quad (3.47c)$$

$$a_W \equiv \frac{C_{sub,w}^{n-1} S_w}{|d_{PW} \cdot n_w|} \quad (3.47d)$$

$$a_N \equiv \frac{C_{sub,n}^{n-1} S_n}{|\mathbf{d}_{PN} \cdot \mathbf{n}_n|} \quad (3.47e)$$

$$a_S \equiv \frac{C_{sub,s}^{n-1} S_s}{|\mathbf{d}_{PS} \cdot \mathbf{n}_s|} \quad (3.47f)$$

$$b_P \equiv \frac{\Delta A}{\Delta t} \quad (3.47g)$$

$$b_0 \equiv \frac{\Delta A}{\Delta t} \zeta_P^{n-1} \quad (3.47h)$$

3.2.6 Interpolation technique

The cell surface value of each physical quantity ϕ is approximated as the following set of equations (see Fig. 3.3): For east side cell surface;

$$\phi_e = \phi_{e'} + \text{grad} \phi_{e'} \cdot \mathbf{d}_{ee'} \quad (3.48)$$

$$\phi_{e'} = (1-f) \phi_P + f \phi_E \quad (3.49)$$

$$\text{grad} \phi_{e'} = (1-f) \text{grad} \phi_P + f \text{grad} \phi_E \quad (3.50)$$

$$f = \frac{|\mathbf{d}_{Pe}|}{|\mathbf{d}_{Pe}| + |\mathbf{d}_{eE}|} \quad (3.51)$$

where $d_{ee'}$, d_{Pe} , d_{eE} = vector of point e to e' , P to e , e to E , respectively.

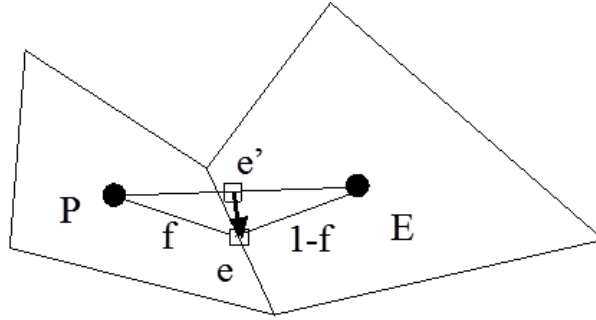


Fig. 3.3 Interpolation of cell surface value

We assume that the gradient of ϕ at cell center can be approximated as follows (see Fig. 3.4):

$$\left. \frac{\partial \varphi}{\partial x} \right|_p \approx \frac{1}{\Delta A} \iint \frac{\partial \varphi}{\partial x} dA \approx \frac{1}{\Delta A} \sum_c \varphi_c S_{xc} \quad (3.52)$$

$$\left. \frac{\partial \varphi}{\partial y} \right|_p \approx \frac{1}{\Delta A} \iint \frac{\partial \varphi}{\partial y} dA \approx \frac{1}{\Delta A} \sum_c \varphi_c S_{yc} \quad (3.53)$$

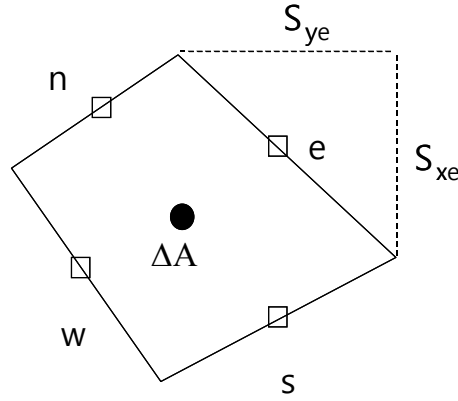


Fig. 3.4 Approximation of gradient

The above interpolation technique is applied to all of the quantities except the convection term C in the momentum equations.

To prevent the numerical oscillation and unstableness, the following equation is employed to interpolate the cell surface value (see Fig. 3.5): For east side cell surface;

$$(\mathbf{q}_e \cdot \mathbf{n}_e) S_e = (\mathbf{q}_e \cdot \mathbf{n}_e) S_e - \Delta t g h_e \left[\left(\frac{\zeta_E - \zeta_P}{|\mathbf{d}_{PE} \cdot \mathbf{n}_e|} \right) - \left\{ \frac{1}{2} (\text{grad} \zeta_E + \text{grad} \zeta_P) \right\} \cdot \mathbf{n}_e \right] \quad (3.54)$$

$$q_e = \begin{cases} q_P + \text{grad} q_P \cdot \mathbf{d}_{Pe} & (\mathbf{q}_e \cdot \mathbf{n}_e > 0) \\ q_E + \text{grad} q_E \cdot \mathbf{d}_{Ee} & (\mathbf{q}_e \cdot \mathbf{n}_e < 0) \end{cases} \quad (3.55)$$

The idea of Equation (3.54) comes from Rhie and Chow (1983), which can prevent the numerical oscillation due to collocated grid arrangement. The method to interpolate in Equation (3.55) is equivalent to QUICK method (Ferziger and Peirc, 1997).

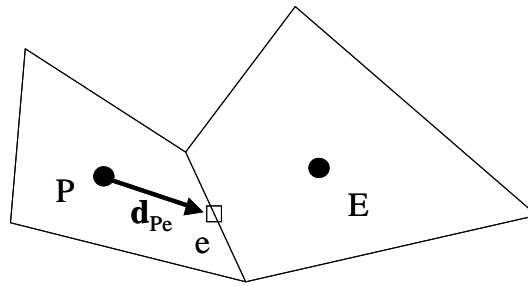


Fig. 3.5 Upwind scheme

3.3 Discussion of flow and sediment transport with vegetation

Spatial variation of flow discharge is related to flood and water resources management. Especially various landscape created by fluvial process is related to river ecosystem. In rivers flow is mainly governed by river morphology and it drives sediment transport.

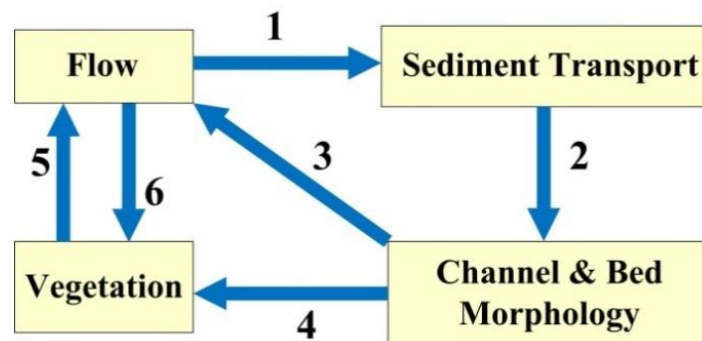


Fig. 3.6 Interrelating system in river

When we are interested in ecosystem, various morphology provides place of vegetation invasion and growth and they provides habitat to various organisms. As mentioned above, the interaction among flow, sediment transport, river morphology and vegetation (see Fig. 3.6) is essential characteristics of a river and its management is a key in river management aiming flood mitigation, water resource utilization and ecosystem conservation.

In Fig. 3.6 is mechanics of sediment transport and represented by sediment

transport formula; 2 is represented by continuity equation of sediment; and 3 is boundary condition of flow. They were previously investigated as fluvial system without vegetation. If we take vegetation into account, invasion or growing condition in riparian are 4, resistance of vegetation (form drag in particular) 5; and destruction or deformation of vegetation by flood flow 6 should be properly investigated (Tsujimoto, 1999).

In general, the horizontal scales in river flow are more dominated than the vertical scale, 2D depth-averaged analysis is effective for understanding processes in a river, and recently 2D depth-averaged numerical analysis becomes popular and it provides much information in river management.

The conventional model give the solutions on spatial variations of depth h , flow direction and depth averaged velocity (U, V). Then by applying the resistance law, We can evaluate shear velocity(u_*), diffusivity, transverse mixing and we can discuss the bed load and suspended sediment transport according to fluvial process, however, improper treatments for flow in vegetated area often brings inaccurate conclusion of the analysis because in conventional method, the 2D depth-averaged analysis consider just spatially averaged drag due to vegetation. It is comparatively well described the flow behavior, but lack of bed roughness resistance law in vegetated area must bring inaccurate description of fluvial processes. In this study, fist we proposed concept of the bed roughness boundary layer in vegetated area. The proposed concept will a little affect on spatial variations of depth h , flow direction and depth averaged velocity(U, V). However, It has a significant impact on shear velocity(u_*). In the newly developed numerical model, the shear velocity to govern sediment transport is evaluated by using bed roughness boundary layer concept proposal with vegetated area and the newly calculated shear velocity(u_*) will significant affect several issues (such as velocity distribution and bed shear stress in flow with vegetation, transverse mixing of flow with vegetation, bed load sediment transport in vegetated area, suspended sediment concentration profile in vegetated area, secondary flow in vegetation) along the scheme of 2D depth-averaged analysis.

The several issues are focused on and the proposed concept will affect other many kinds aspects in fluvial processes (as shown in Fig 3.7), which will be clarified successively.

Reasonable alternatives are proposed by chapter 3-6 and it will be discussed.

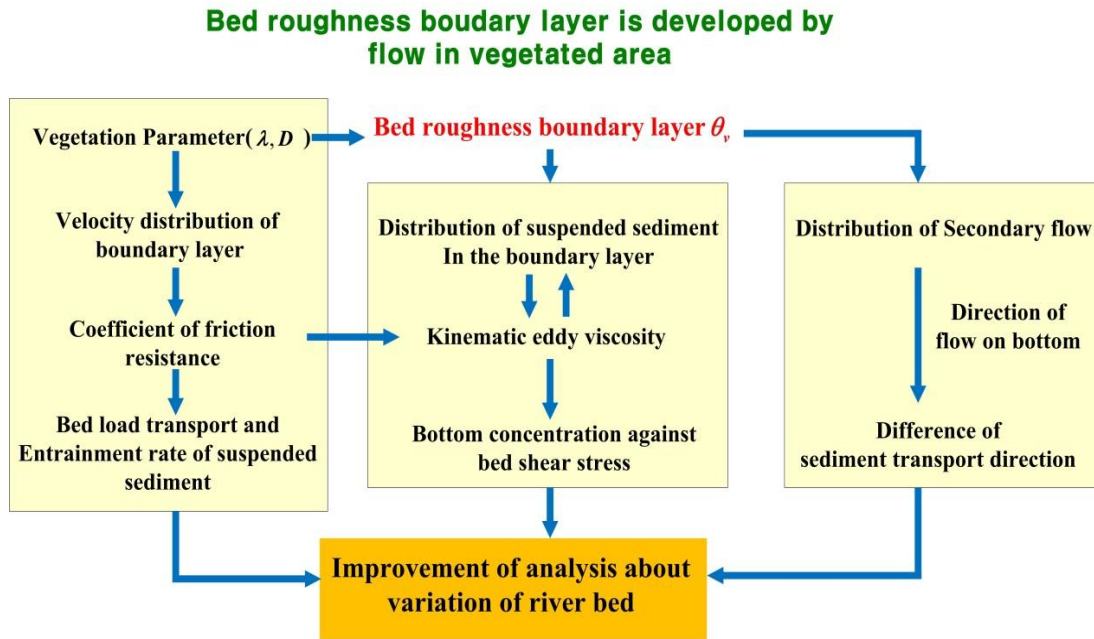


Fig. 3.7 Improvement of analysis about flow and sediment transport in vegetated area

3.4 Concluding Remarks

To analyze hydrodynamic and sediment transport in vegetated area, 2D depth-averaged model was newly developed. The developed numerical model can be described as follow.

1. The numerical scheme adopted suspended sediment equations for analysis of suspended sediment, based on existing numerical model (NHSED2D; Goto et al., (2002)).
2. 2-Dimensional numerical model, which is able to simulate flow fields-vegetation-bed variation interaction directly, is used to investigate fluvial process and mechanics of sediment transport in vegetated area.
3. Applications of 2D depth-averaged analysis have become very familiar and it provides much information in river management, however, improper treatments for flow in vegetated area often brings inaccurate conclusion of the analysis because in conventional method, the 2D depth-averaged analysis consider just spatially averaged drag due to vegetation. It is comparatively well described the flow behavior, but lack of bed roughness resistance law in

vegetated area must bring inaccurate description of fluvial processes.

4. In the newly developed numerical model, the shear velocity to govern sediment transport is evaluated by using bed roughness boundary layer concept proposal with vegetated area and the newly calculated shear velocity(u_*) will significant affect several issues along the scheme of 2D depth-averaged analysis. It will affect other aspects in fluvial processes, which will be clarified successively.

References

1. Ashida, K., Michiue, M. (1972) Studies on bed load transation for nonuniform sediment and river bed variation. *Disaster prevention research institute annuals* 14B, pp. 259–273.
2. Chow, W., Rhie, C. (1982) A numerical study of the turbulent flow past an isolated airfoil with trailing edge separation.
3. C.A. Vionnet, P.A. Tassi, M.J.P. Vide. (2004) Estimates of flow resistance and eddy viscosity coefficients for 2D modelling on vegetated floodplains, *Hydrol. Proc.* 18 pp. 2907–2926.
4. C.M. David, M.S. Horritt. (2003) Floodplain friction parameterization in two-dimensional river flood models using vegetation heights derived from airborne scanning laser altimetry, *Hydrol. Proc.* 17 pp. 1711–1732.
5. Darby, S. E. (1999) Effect of riparian vegetation on flow resistance and flood potential, *J. Hydraul. Eng.*, 125(5), pp. 443– 454.
6. Einstein, HA. (1950) “The bed-load function for sedimentation in open channel flows”. Sedimentation, edited by Shen HW, Colorado State University, Fort Collins, Colorado, USA.
7. Fang, H.W. and G.Q. Wang (2000) “Three-dimensional mathematical model of suspended-sediment transport”. *Journal of Hydraulic Engineering* 126, p. 578.
8. Ferziger, J. H., Peric, M. (1997) Computational methods for fluid dynamics. Vol. 3. Springer Berlin.
9. F. López, M.H. García. (2001) Mean flow and turbulence structure of open-channel flow through non-emergent vegetation, *ASCE J. Hydraul. Eng.* 127 (5) pp. 392–402.

10. Goto, T., T. Tsujimoto and T. Kitamura. (2002) Numerical model for simulating channelization and its validation, *Advances in Fluid Modeling & Turbulence Measurements*, Edited by H. Ninokata et al., World Scientific, pp.127-134.
11. Hu, C. and Q. Guo. (2010) “Near-Bed Sediment Concentration Distribution and Basic Probability of Sediment Movement”. *Journal of Hydraulic Engineering* 1, pp. 207.
12. H. Yoshida, A. Dittrich. (2002) 1D unsteady-state flow simulation of a section of the upper Rhine, *J. Hydrol.* 269 pp. 79–88.
13. K. Nadaoka, H. Yagi. (1998) Shallow-water turbulence modelling and horizontal large-eddy computation of river flow, *ASCE J. Hydraul. Eng.* 124 pp. 493–500.
14. Lane, EW and AA Kalinske. (1941) “Engineering calculations of suspended sediment”. *Trans. AGU* 22, pp. 603–607.
15. Lopez, F., and M. Garcia. (2001) Mean flow and turbulence structure of open-channel flow through non-emergent vegetation, *J. Hydraul. Eng.*, 127(5), pp. 392– 402.
16. Nakagawa, H., T. T., Murakami, S. (1986) Non-equilibrium bed load along side bank. *Proc.3rd Int.Sym. River Sedimentation.*, Jackson, Mississippi, USA.
17. Neary, V. S. (2003) Numerical simulation of fully-developed flow with vegetative resistance, *J. Eng. Mech.*, 129, pp. 558– 563.
18. Nikora, V.I. and D.G. Goring. (2002) “Fluctuations of suspended sediment concentration and turbulent sediment fluxes in an open-channel flow”. *Journal of Hydraulic Engineering* 128, p. 214.
19. Rhie, C. M. and W. L. Chow. (1983) A numerical study of the turbulent flow past an isolated airfoil with trailing edge separation, *AIAA J.*, 21, pp.1525-1532.
20. Rouse, H. (1937) “Modern conceptions of the mechanics of fluid turbulence”. *Trans. ASCE* 102, pp. 463–543.
21. Shimizu, Y., and T. Tsujimoto. (1994) Numerical analysis of turbulent open-channel flow over a vegetation layer using a k-e turbulence model, *J. Hydrosci. Hydraul. Eng.*, 11(2), pp. 57– 67.
22. Simon, A., S. J. Bennett, and V. S. Neary. (2004) Riparian vegetation and fluvial geomorphology: Problems and opportunities, in *Riparian Vegetation and Fluvial Geomorphology*, *Water Sci. Appl. Ser.*, vol. 8, edited by S. J. Bennett and A. Simon, pp. 1 – 10, AGU, Washington D. C.
23. Tsujimoto, T., Yamamoto, T. (1986) Stochastic model for determining suspended sediment concentration distribution with particular reference to comparison

- with diffusion theory. "Memoirs, Faculty of Technology, Kanazawa University" , 19(2) pp. 33-42
24. Tsujimoto, T. (1998) Development of sand island with vegetation in fluvial fan river under degradation, *Water Resources Engineering* '98, edited by S. R. Abt et al., vol. 1, pp. 574–579, Am. Soc. Civ. Eng., Reston, Va.
25. T.Tsujimoto. (1999) Morphological dynamics around vegetated area in sand rivers , "Proc.IAHR Sym. River, Coastal and Estuarine Morphodynamics, Genovea, Italy"
26. Tsujimoto, T. (2008) River management for ecosystem conservation: policy making support though mathematical modeling. *Proc. JST Presto Symposium.*, No.136, pp. 32-41.
27. Van de Wiel, M. J., and S. E. Darby. (2004) Numerical modeling of bed topography and bank erosion along tree-lined meandering rivers, in Riparian Vegetation and Fluvial Geomorphology, *Water Sci. Appl. Ser.*, vol. 8, edited by S. J. Bennett and A. Simon, pp. 267 – 282, AGU, Washington, D. C.
28. Van Rijn (2007). "Unified view of sediment transport by currents and waves. II: Suspended transport". *Journal of Hydraulic Engineering* 133, p. 668.
29. W. Wu, F.D. Shields Jr., S.J. Bennett, S.S.Y. Wang (2005) A depth averaged two-dimensional model for flow, sediment transport, and bed topography in curved channels with riparian vegetation, *Water Resour. Res.* 41 pp. 1–15.

CHAPTER 4

CONCEPT OF BED ROUGHNESS BOUNDARY LAYER IN VEGETATED AREA

4.1 General

Recently 2D depth averaged analysis is familiar even in a stream with vegetation by taking account of form drag due to vegetation (Shimizu and Tsujimoto, 1994; Lopez and Garcia, 1998; Tsujimoto and kitamura, 1998; Neary 2000). Because the resistance law due to bed roughness is not reasonably modified in vegetated area, it is comparatively well described the flow behavior, but lack of bed roughness resistance law in vegetated area must bring inaccurate description of fluvial processes. Better understanding flow processes provided by vegetation in the stream requires detailed flow structure. The drag coefficient is the key in determining the drag related with vegetation and also to understand the vertical distribution of the velocity. Many researches about the drag related with various vegetation configurations were carried out and focus on determining drag coefficients and empirical formulas (Li and Shen, 1973; Nepf, 1999; Stone and Shen, 2002; Garcia et al., 2004). Other researchers attempt to describe physical processes using velocity and turbulence intensity profiles with (Tsujimoto et al., 1992; Ikeda and Kanazawa, 1996; Nepf, 1999; Liu et al., 2008). While it is important to develop many kinds of solution to vegetation resistance, it is also important to understand the detailed characteristics of the flow through vegetation. The aim of the proposed chapter is describe detailed characteristics of flow unsubmerged vegetation.

In this chapter, bed roughness boundary layer is focused on, and its thickness, velocity distribution in that layer and then the resistance law due to bed roughness in vegetated area are investigated.

4.2. Concept and formulation of Boundary layer thickness

In depth averaged model, the resistance law to relate the depth averaged velocity (U) to the shear velocity (u_*) for uniform flow is introduced. If the logarithmic law is applied as velocity profile $u(z)$, Keulegan's equation obtained by integration the velocity profile along the depth is employed.

$$\frac{u(z)}{u_*} = \frac{1}{\kappa} \ln \left(\frac{z}{k_s} \right) + B_s(Re_*) \quad (4.1a)$$

$$\frac{U}{u_*} = \frac{1}{\kappa} \ln \left(\frac{h}{k_s} \right) + B_s(Re_*) - \frac{1}{\kappa} \quad (4.1b)$$

where z =vertical distance from the bed; κ =Karman's constant; h =depth; k_s =equivalent sand roughness, $B_s(Re_*)$ =function of roughness Reynolds number $Re_* = u_* k_s / \nu$; h =depth; and ν =kinematic viscosity. In vegetated area, form drag is predominant and velocity profile is uniform (U_v) along the depth only except the thin layer near the bed where the boundary layer is developed to bring a shear flow (see Fig. 4.1), and such a boundary layer is considerably thin in general. In Fig. 4.1, the roughness boundary layer thickness is suggested by θ_v .

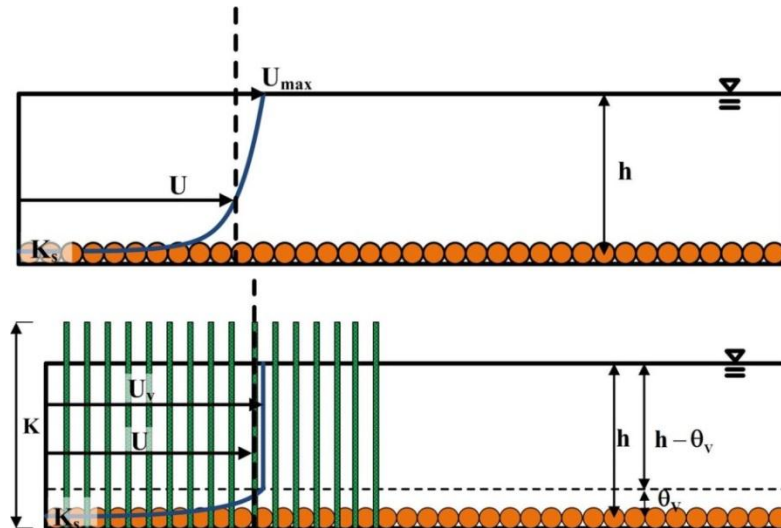


Fig. 4.1 Vertical distribution of velocity in vegetated area

The characteristic velocity in vegetated area called U_v is expressed as follows.

$$U_v = \sqrt{\frac{2gI_e}{C_D\lambda D}} \quad (4.2)$$

where g =gravitational acceleration; I_e =energy gradient of flow, D =diameter; λ =number density of piles; and C_D =drag coefficient. In the conventional depth-averaged analysis for flow with vegetation, the form drag for vegetation is introduced in addition to the bed friction in the vegetated area, but the resistance law due to bed roughness is treated by employing the same equation with that in non-vegetated area (Equation 4.1b). However, depending on the velocity profile as shown in Fig. 4.1, a proper resistance law should be applied in vegetated area. As mentioned later, though the resistance law is not necessarily sensitive for calculation of depth and depth-averaged flow, it brings underestimation of the shear velocity and subsequently sediment transport rate, and it may not bring a reasonable analysis of sediment transport and subsequent fluvial process. In this chapter, we discuss the bed roughness boundary layer in flow with non-submerged vegetation and deduce a reasonable relation between U and u_* in vegetated area to proceed the analysis of sediment transport.

4.2.1 Experiment data of Liu

The experiments were conducted at the laboratory flume with vegetation simulated by acrylic dowels. The flume was 4.3m long by 0.3m wide and kept at a constant slope of 0.003. The acrylic dowels were 76mm tall and diameter is 6.35mm. They were attached to a 13mm thick sheet of smooth Plexiglas bolted to the bottom of the flume. The flow became fully developed from the start of the dowels section. The simulated vegetation area was 3.0m long by 0.3m wide and it placed 1.3m from the entrance of the flume. The dowels were arranged either in staggered or linear pattern under emergent conditions as shown Fig. 4.1. Velocity measurements were taken at six locations using rotating the scope of the LDV 90°. Velocity readings were taken at 14-18 measurement points along the vertical direction at each location. We specify the most of steady flow. As you can see, In case of Exp1.1, Exp1.3 and Exp 2.1, data of location 5 was used. In case of Exp1.2, data of location 4 was used.

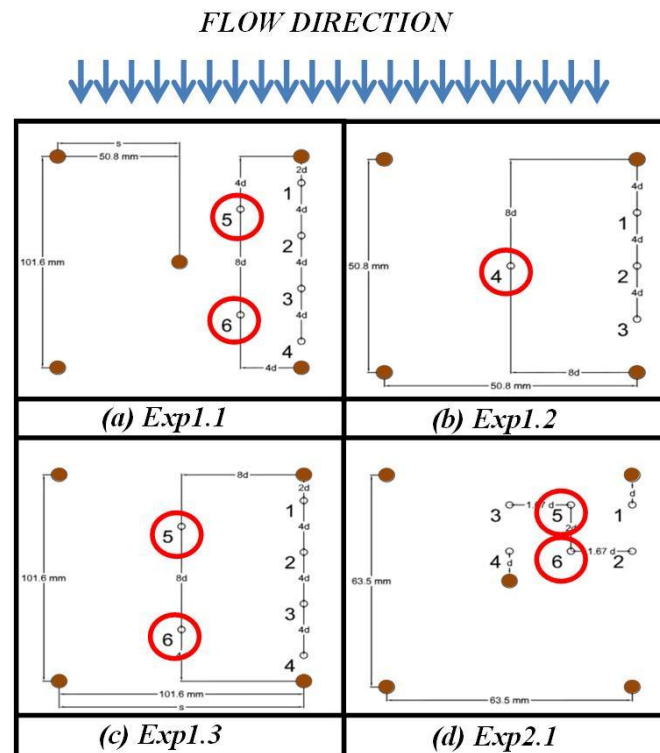


Fig. 4.2 Measurement location for Exp1.1, Exp1.2, Exp1.3 and Exp2.1

For each case dowel's diameter is same but density of vegetation is different. In case of Exp2.1, The value of vegetation density is largest. The detailed conditions for each experiment are summarized in Table 4.1

Table 4.1 Detail of each experimental condition

	λ	$D(\text{mm})$	Submergence condition	Flow Rate (m^3/s)
Exp 1.1	0.000193	6.35	Emergent	0.0057
Exp 1.2	0.000387	6.35	Emergent	0.0057
Exp 1.3	0.000096	6.35	Emergent	0.0057
Exp 1.4	0.000496	6.35	Emergent	0.0044

4.2.2 Interaction formula

Fig. 4.3 shows elaborate measurement of vertical distribution in flow with non-submerged vegetation conducted by Liu et al (2008), where a group of piles arranged pattern was utilized as non-submerged vegetation.

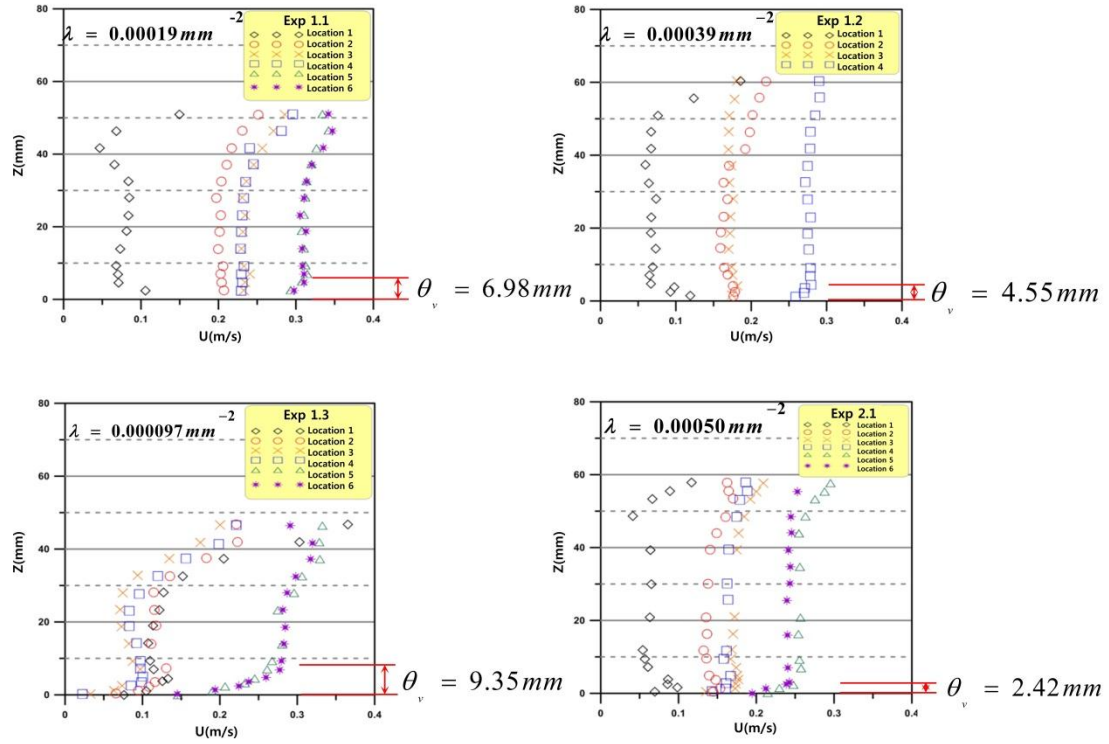


Fig. 4.3 Velocity profile in vegetated area measured by Liu et al

To find the vertical velocity of each point and bed roughness boundary layer thickness, The data has been read using digitizer. Detail of the vertical velocity each point and bed roughness boundary layer thickness shows Table 4.2. The thickness of bed roughness boundary layer (θ_v) was found (see Exp1.1($\theta_v = 6.98\text{mm}$), Exp 1.2($\theta_v = 4.55\text{mm}$), Exp 1.3($\theta_v = 9.35\text{mm}$) and Exp 2.1($\theta_v = 2.42\text{mm}$) in Fig. 4.2), and the local velocity in the boundary layer were obtained.

The bed roughness boundary layer thickness θ_v is subjected to the characteristics of vegetation, and dimensional analysis suggests the relation between θ_v/h and λDh . The data obtained the measurements by Liu *et al.* are plotted in Fig. 4.4. By considering that θ_v may decrease with the vegetation density while it tends to the flow depth with

sufficiently disperse density, the following relation is proposed as a favorable formula(Equation 4.3) to estimate the bed roughness boundary layer thickness.

Table 4.2 Vertical velocity of each point and bed roughness boundary layer thickness

Exp1.1		Exp 1.2		Exp 1.3		Exp 2.1	
Location 6		Location 4		Location 5		Location 5	
u(m/s)	z(mm)	u(m/s)	z(mm)	u(m/s)	z(mm)	u(m/s)	z(mm)
0.297	2.51	0.258	1.19	0.287	0.29	0.214	0.19
0.310	4.75	0.269	2.23	0.313	1.21	0.214	0.19
0.310	6.98	0.271	3.57	0.323	2.51	0.229	1.50
0.308	9.21	0.279	4.55	0.339	3.30	0.229	1.50
0.308	13.98	0.278	6.85	0.346	4.60	0.247	2.42
0.313	18.82	0.278	9.08	0.356	6.93	0.257	6.96
0.305	23.21	0.276	14.15	0.360	9.35	0.257	6.96
0.310	27.90	0.274	18.47	0.367	13.94	0.255	9.30
0.313	32.44	0.278	22.94	0.365	18.60	0.254	16.31
0.320	37.13	0.274	27.85	0.364	23.01	0.256	20.86
0.335	41.75	0.271	32.62	0.376	27.94	0.256	34.75
0.341	46.45	0.274	37.09	0.383	32.22	0.254	43.97
0.346	51.06	0.277	41.86	0.396	41.56	0.254	43.97
		0.278	46.48			0.263	48.65
		0.284	50.94			0.275	53.32
		0.290	55.86			0.287	55.41
		0.290	60.33			0.295	57.75

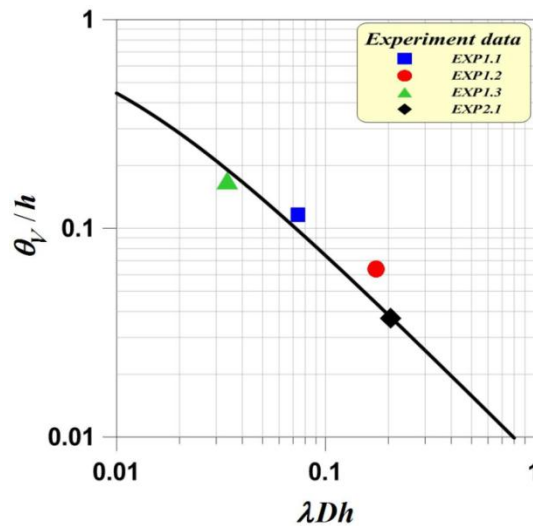


Fig. 4.4 Relation between θ_v/h and λDh

$$\frac{\theta_v}{h} = \frac{0.008}{0.008 + \lambda D h} \quad (4.3)$$

4.2.3 Friction velocity in the vegetation

After decided the boundary layer thickness, Exp 1.1 have just one vertical velocity data below boundary layer thickness. In this case, First we assume that friction velocity in the vegetation from 0.01 to 0.03. After we calculated each value using Equation 4.4

$$\frac{u_v}{u_{*v}} = \frac{1}{\kappa} \ln \left(\frac{9.0 * \theta_v * u_{*v}}{\nu} \right) \quad (4.4)$$

Table 4.3 represents calculation value of friction velocity using Equation 4.4. Fig. 4.5 also depicts calculation value of friction velocity. Black line indicate that calculation value of left equation and red line indicate that calculation value of right equation. Intersection point of two graphs are represents the friction velocity in the vegetation.

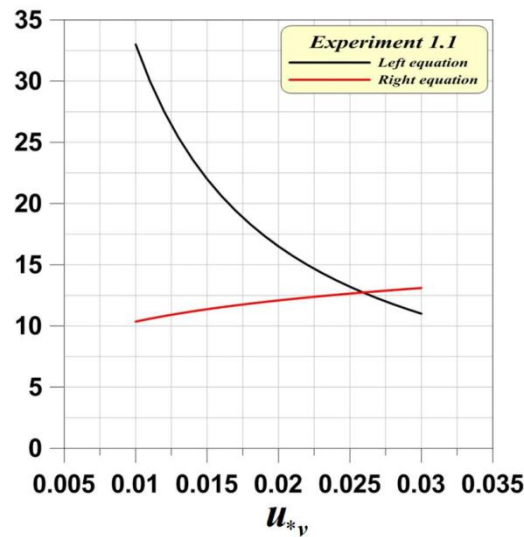


Fig. 4.5 Friction velocity (In case of Exp 1.1)

Table 4.3 Friction velocity (In case of Exp 1.1)

Exp1.1		
u_{*v}	u_v / u_{*v}	$2.5 \ln(9.0 * \theta_v * u_{*v} / \nu)$
0.010	33.0	10.35
0.011	30.0	10.59
0.012	27.5	10.80
0.013	25.4	11.00
0.014	23.6	11.19
0.015	22.0	11.36
0.016	20.6	11.52
0.017	19.4	11.67
0.018	18.3	11.82
0.019	17.4	11.95
0.020	16.5	12.08
0.021	15.7	12.20
0.022	15.0	12.32
0.023	14.3	12.43
0.024	13.8	12.54
0.025	13.2	12.64
0.026	12.7	12.74
0.027	12.2	12.83
0.028	11.8	12.92
0.029	11.4	13.01
0.030	11.0	13.09

Exp 1.2, 1.3, 2.1 have two or more vertical velocity data below boundary layer thickness. In this case, first we read the z , u , u_v , θ_v from the experiment data. Second we calculated z / θ_v . After then, Equation 4.4 change to approximate equation of exponential function. It can be expressed Equation 4.5.

$$z = ae^{bu} \quad (4.5)$$

Assuming that Equation 4.4 is equal to Equation 4.5, we can get Equation 4.6

$$b = 0.4 / u_{*v} \quad (4.6)$$

Position from the bottom surface(z) and vertical velocity on that point(u) under the boundary layer thickness shows a semi-log graph in Fig. 4.6. The approximate equation can be calculated, and obtained value of the slope b . Finally, the friction velocity using Equation 4.6 can be determined.

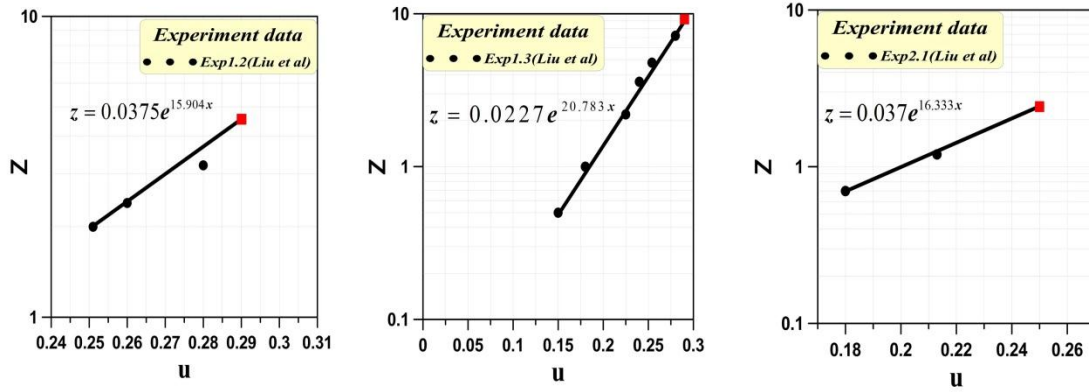


Fig. 4.6 Semi-log graph (In case of Exp 1.2, Exp 1.3, Exp 1.4)

4.2.4 Velocity Distribution in bed roughness boundary layer in vegetated area

Velocity distribution in bed roughness boundary layer in the vegetated area is investigated, and logarithmic law is expected to be applied, which is written as Equation 4.1a. Though the number of the data is small for each run, the shear velocity in the vegetated area, u_* , is evaluated by fitting the logarithmic law for each run, then the data of the all runs are plotted and depicted in the defect law expression in Fig. 4.7 and Table 4.4. Defect law expression is written as follows.

$$\frac{U_v - u(z)}{u_*} = -\frac{1}{\kappa} \ln \left(\frac{z}{\theta_v} \right) \quad (z < \theta_v) \quad (4.7)$$

Table 4.4 Defect law expression of velocity distribution in bed roughness boundary layer

	$\theta_v(\text{mm})$	$z(\text{mm})$	z/θ_v	Slope b	u_{*v}	u_v	u	$(u_{*v}-u)/u_{*v}$
Exp1.3	9.35	0.5	0.053	21.0	0.019	0.29	0.15	7.33
	9.35	1.0	0.107	21.0	0.019	0.29	0.18	5.76
	9.35	2.2	0.235	21.0	0.019	0.29	0.23	3.40
	9.35	3.6	0.385	21.0	0.019	0.29	0.24	2.62
	9.35	4.8	0.513	21.0	0.019	0.29	0.25	1.89
	9.35	7.2	0.770	21.0	0.019	0.29	0.28	0.52
Exp2.1	2.42	0.7	0.289	16.3	0.024	0.25	0.18	2.82
	2.42	1.2	0.496	16.3	0.024	0.25	0.21	1.47
Exp1.2	4.55	2.0	0.440	15.9	0.022	0.29	0.25	1.80
	4.55	2.4	0.527	15.9	0.022	0.29	0.26	1.39
	4.55	3.2	0.703	15.9	0.022	0.29	0.28	0.46
Exp1.1	6.98	3.2	0.458	14.3	0.026	0.33	0.29	1.54

According to this figure, it is recognized that velocity profile follows the logarithmic law though the number of the measured data for each run is very few. We can estimate velocity profile in the bed roughness layer thickness through this figure.

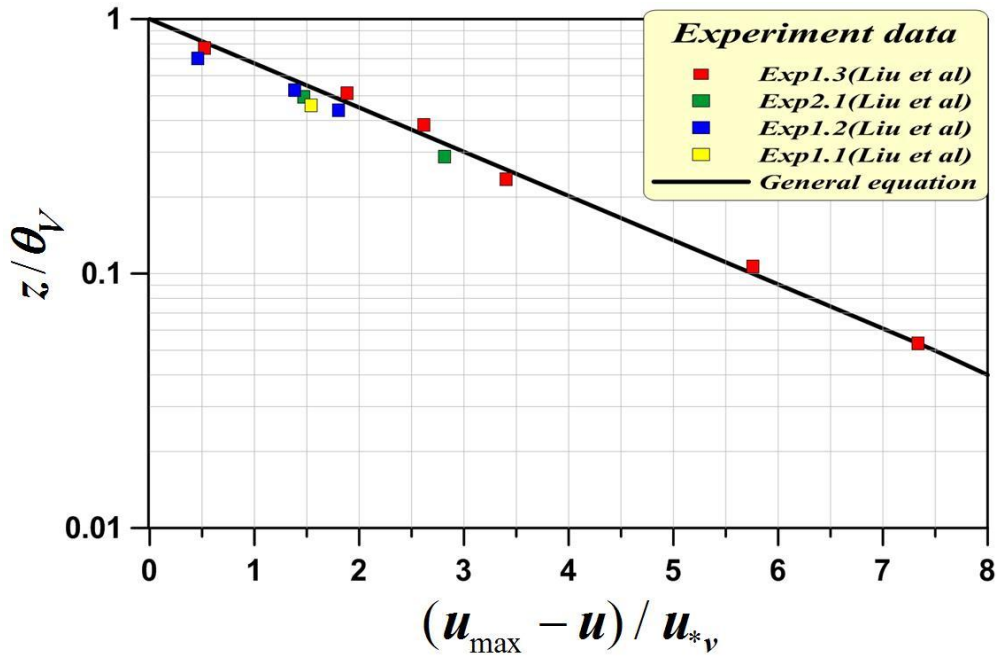


Fig. 4.7 Defect law expression of velocity distribution in bed roughness boundary layer

4.2.5 Resistance law in vegetated area

4.2.5.1 Velocity distribution and kinematic eddy viscosity in bed roughness boundary layer in vegetated area

Flow without vegetation can be described by the logarithmic law, and the vertical distribution of velocity $u(z)$ and the frictional resistance law known as “Keulegan’s equation” is written as Equation 4.1a, b. While, the vertical distribution of velocity of flow in the area with non-submerged vegetation is written as follows according to the recent study by (Jeon et al. 2014).

$$\frac{u(z)}{u_{*v}} = \frac{1}{\kappa} \ln \left(\frac{z}{k_s} \right) + B_s(R_{e*}) \quad (z < \theta_v); \quad U_v = \sqrt{\frac{2gI_e}{C_D \lambda D}} \quad (\theta_v < z < h) \quad (4.8)$$

where vegetation is represented by a group of piles D =diameter of a pile; λ =number density of piles; θ_v =bed roughness boundary layer thickness; g =gravitational acceleration; I_e =energy gradient, and C_D =drag coefficient. θ_v is related to the vegetation characteristics, and Jeon et al formulates according to the measured data by (Liu et al. 2008) in the Equation 4.3.

And, subsequently the following frictional resistance law is proposed (Jeon et al. 2014):

$$\frac{U}{u_*} = \frac{(h - \theta_v)}{h} \frac{U_v}{u_*} + \frac{\theta_v}{h} \left[\frac{1}{\kappa} \ln \left(\frac{\theta_v}{k_s} \right) + B_s(R_{e*}) - \frac{1}{\kappa} \right] \quad (4.9)$$

Applying this law can bring a reasonable evaluation of the shear velocity in the vegetated area and subsequently bed load sediment transport in the vegetated area.

Based on the above velocity distributions, the kinematic eddy viscosity is discussed. For flow without vegetation, it distributes along the depth and its depth-averaged value ν_t is as follows:

$$\nu_t = \frac{\kappa}{6} u_* h \quad (4.10)$$

In the vegetated area, the turbulence diffusivity exists only in the bed roughness boundary layer, and the kinematic eddy viscosity will be formulated as follows:

$$\nu_t = \frac{\kappa}{6} u_* \theta_v \quad (0 < z < \theta_v); \quad \nu_t = 0 \quad (\theta_v < h) \quad (4.11)$$

The apparent depth-averaged value of the kinematic eddy viscosity is written as follows:

$$\nu_t = \frac{\kappa u_* \theta_v^2}{6h} \quad (4.12)$$

Fig. 4.8 shows the conceptual sketch of velocity distribution and kinematic eddy viscosity in non vegetated zone and vegetated zone. As we know from the Fig. 4.8, velocity distribution and kinematic eddy viscosity is a little different in the vegetated zone. The kinematic eddy viscosity is distributed throughout the depth in case of non vegetated zone but it is existed only within the bed roughness layer in case of vegetated zone.

Nevertheless, ordinary Equation 4.10 is applied even in the vegetation zone. In this chapter, the numerical simulation model was added on new Equation 4.12 in the vegetation zone for better accuracy velocity distribution and kinematic eddy viscosity.

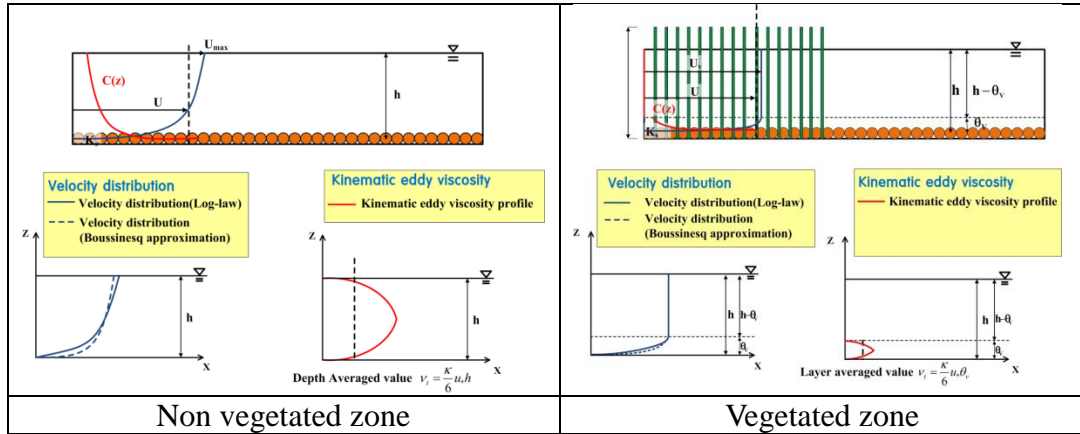


Fig. 4.8 Conceptual sketch of velocity distribution and kinematic eddy viscosity in the non vegetated zone and vegetated zone

4.2.5.2 Lateral mixing of momentum and lateral distribution of depth averaged velocity

The governing equations of flow in depth-averaged 2D scheme are written as

Equation (3.1~3.5). There are some programs based on the above governing equations, but in conventional approaches, the friction resistance law for flow without vegetation is applied even in the vegetated area though the form drag is taken into account for the vegetated area. The authors have derived a reasonable equation of frictional resistance law based on the concept of bed roughness boundary layer in the area with non-submerged vegetation. Applying this law can bring a reasonable evaluation of the shear velocity in the vegetated area and subsequently equilibrium bottom concentration of suspended sediment (entrainment rate is $C_{Be}w_0$).

In lateral mixing, the horizontal diffusion written in Equation 4.13 is subjected to the eddy kinematic viscosity. Conventionally, the vertical diffusion coefficient ν_t which is related to the vertical velocity distribution is applied by simply multiplying a constant even in horizontal mixing as ν_{th} , and furthermore, the value given for flow on the area without vegetation, as follows:

$$\nu_{th} = \alpha u_* h \quad (4.13)$$

where α is empirically determined in the range 0.1~0.5.

Depth-averaged kinematic eddy viscosity is modified as expressed by Equation 4.12, and thus the following equation is reasonably employed for flow with vegetation instead of Equation 4.13.

$$\nu_{th} = \alpha u_* \theta_v^2 / h \quad (4.14)$$

4.3 Discussion on resistance law in vegetated area

In conventional method, in order to obtain the resistance law to be applied to the non vegetated area and vegetated area, velocity distribution is integrated from the bottom to the free surface. It is comparatively well described the flow behavior but lack of bed roughness resistance law in vegetated area must bring inaccurate description of fluvial processes. The authors have derived a reasonable equation of frictional resistance law based on the concept of bed roughness boundary layer in the area with non-submerged vegetation. Applying this law can bring a reasonable evaluation of the shear velocity in the vegetated area. it is applied to bed load

transport rate, entrainment flux of suspended sediment and so on for more accurate evaluation as shown in figure.

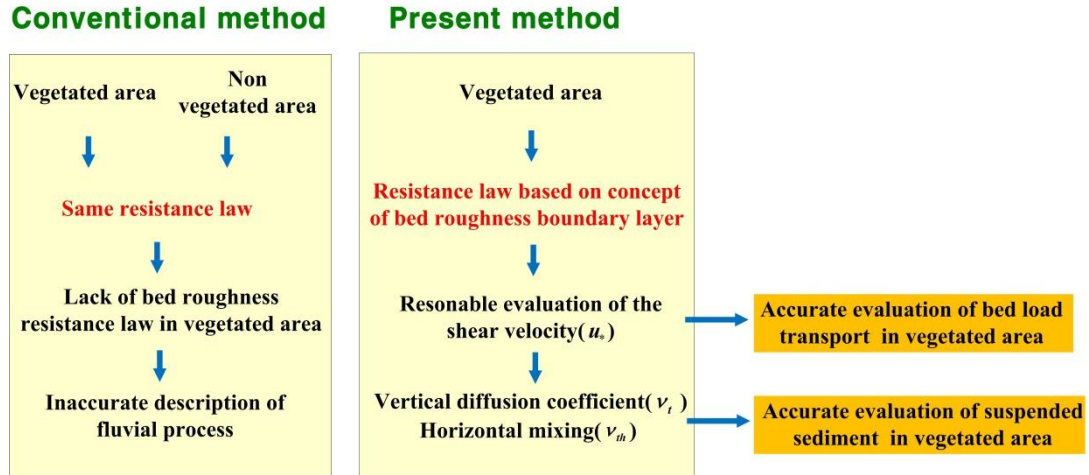


Fig. 4.9 Discussion on resistance law and its application in vegetated area

4.4 Concluding Remarks

Recently, 2D horizontal depth averaged flow model becomes familiar to be recognized as powerful means of stream with vegetation by adding the form drag of vegetation. Though it is expected to apply fluvial process of streams with vegetation, the shear stress may be underestimated and fluvial process may not be properly described. In this chapter, we focused on the bed roughness boundary layer in the vegetated area (non-submerged vegetation) to deduce the resistance law in the vegetated area. Based on the concept of bed roughness boundary layer, fluvial process with full vegetation can be discussed as below:

1. The bed roughness boundary layer is focused on, and its thickness, velocity distribution in that layer and then the resistance law due to bed roughness in vegetated area are investigated.
2. The bed roughness boundary layer thickness θ_v is subjected to the characteristics of vegetation, and dimensional analysis suggests the relation between θ_v/h and λDh . The data obtained the measurements by Liu *et al.*
3. Velocity distribution in bed roughness boundary layer in the vegetated area is

investigated, and logarithmic law is expected to be applied. Though the number of the data is small for each run, the shear velocity in the vegetated area, u_* , is evaluated by fitting the logarithmic law for each run, then the data of the all runs are plotted and depicted in the defect law expression. The velocity profile follows the logarithmic law though the number of the measured data for each run is very few.

4. In conventional method, in order to obtain the resistance law to be applied to the non vegetated area and vegetated area. It is comparatively well described the flow behavior but lack of bed roughness resistance law in vegetated area must bring inaccurate description of fluvial processes. The authors have derived a reasonable equation of frictional resistance law based on the concept of bed roughness boundary layer in the area with non-submerged vegetation. Applying this law can bring a reasonable evaluation of the shear velocity in the vegetated area. it is applied to bed load transport rate, entrainment flux of suspended sediment and so on for more accurate evaluation.

References

1. Garcia, M. H., Lopez, F., Dunn, C., Alonso, C. V. (2004) Flow, turbulence, and resistance in a flume with simulated vegetation. *Riparian vegetation and fluvial geomorphology*, pp. 11-27.
2. Ikeda, S., Kamazawa, M. (1996) Three-dimensional organized vortices above flexible water plants. *Journal of Hydraulic Engineering* 122(11), pp. 634-640.
3. Jeon, H.S., Obana, M. and Tsujimoto, T. (2014) Concept of bed roughness boundary layer and its application to bed load transport in flow with non-submerged vegetation, *Jour. Water Resource and Protection, Scientific Research*.
4. Li, R.-M., Shen, H. W. (1973) Effect of tall vegetations on flow and sediment. *Journal of the Hydraulics Division* 99(5), pp. 793-814.
5. Liu, D., Diplas, P., Fairbanks, J., Hodges, C. (2008) An experimental study of flow through rigid vegetation. *Jouranl of Geophysical Research: Earth Surface*(2003-2012) 113(F4).

6. Lopez F. and Garcia M. (1997) Open-Channel Flow Through Simulated Vegetation: Turbulence Modeling and Sediment Transport, *US Army of Engineers Waterway Experiment Station Wetlands Research Program Technical Report WRP-CP-10*
7. Neary V.S. (2000) Numerical model for open-channel flow with vegetative resistance, *IAHR's 4th International Conference on Hydroinformatics*, July 23-27, Cedar Rapids, Iowa, USA
8. Nepf, H. (1999) Drag, turbulence, and diffusion in flow through emergent vegetation. *Water resources research* 35(2), pp. 479-489.
9. Shimizu Y. and Tsujimoto T. (1994) Numerical analysis of turbulent open-channel flow over a vegetation layer using a k- ϵ model, *Journal of Hydroscience and Hydraulic Engineering*, 11(2), pp.57-67
10. Stone, B. M., Shen, H. T. (2002) Hydraulic resistance of flow in channels with cylindrical roughness. *Journal of Hydraulic Engineering* 128(5), pp. 500-506.
11. Tsujimoto T., and Kitamura T. (1990) Velocity profile of flow in vegetated-bed channels, KHL Progressive Report, Hydraulic Laboratory, Kanazawa University
12. Tsujimoto, T., Shimizu, Y., Kitamura, T., Okada, T. (1992) Turbulent open-channel flow over bed covered by rigid vegetation. *Journal of Hydroscience and Hydraulic Engineering* 10(2), pp. 13-25.

CHAPTER 5

APPLICATION OF BED ROUGHNESS BOUNDARY LAYER CONCEPT

5.1 General

When the value of the friction velocity just exceeds the critical value for beginning of motion, the sediment will start rolling and sliding in continuous contact with the river bed. For increasing values of the bed shear stress the sediment transport is inevitably accompanied with sorting of the bed surface. When the value of the bed shear velocity exceeds the Sedimentation velocity, the suspended sediment particles can be lifted to a level at which the upward turbulent forces will be comparable to or higher than the submerged particle weight and as a result of the particle with the bed in the suspension mode is occasional and random. The Sediment particle velocity in longitudinal direction is almost equal to the fluid velocity. Usually, the behavior of suspended sediment particles is described in terms of the sediment concentration, which is the solid volume per unit fluid volume or the solid mas per unit fluid volume. The most common method to approach the suspended sediment transport is based on the integration of the advection/diffusion equation of suspended load in steady uniform flow conditions (Lane and Kalinske 1941; Rouse 1937; Van Rijn 2007). Some researchers attempts to simulate flow and suspended sediment transport and deposition on natural flood plains have been conducted predominantly using two dimensional depth averaged models (Nicholas and Walling, 1997; Stewart et al, 1998). Also investigations on suspended load through rigid plants are present in bibliography, and they are generally base on the integration of the diffusion/advection equations by using more or less sophicticated models (Furukawa, Wolanski, and Mueller 1997) and often k- ϵ model(Lopez and Garcia 1998; Nakagawa, Tsujimoto, and Shimizu 1992) Such approaches are flexible, rigid, and provide distributed information quantifying

depths, velocities, sediment concentrations and sedimentation rates. Such approaches have also been extended to more accurate analysis (Tsujiimoto et al., 1994). And also many kinds of numerical model and equation have been proposed for relating the rate of bed load sediment transport to flow characteristics with vegetation.

However, these models incorporate simplified treatments of flood plain roughness and turbulence, and are unable to represent the mechanics of sediment deposition fully because, being depth-averaged, they do not resolve the vertical profile of flow or sedimentological conditions.

In this chapter, first, as for flow with non-submerged vegetation, several points necessary to be modified are theoretically discussed. In flow with vegetation, taking account for drag term due to vegetation is a principal key but it is not necessary sufficient by it alone.

Numerical verification supports the accuracy of both the model predicted bed load sediment and suspended sediment transport rate and the model predicted sediment yield using concept of bed roughness boundary layer. The capability of the numerical model for simulating bed load sediment and suspended sediment transport in vegetated area will also tested in this chapter. Finally the improvement of description bed load sediment and suspended sediment transport by introducing the concept of bed roughness boundary layer is certificated.

5.2 Flow and sediment transport with non submerged vegetation in 1D scheme

From the check along the 2D modeling, the friction resistance law should be reasonably considered and the concept of bed roughness boundary layer has been proposed and formulated against the vegetation density. Based on this concept, the shear flow structure in this layer has been discussed and formulated. It has brought the reasonable evaluation of the shear stress and subsequently the kinematic eddy viscosity as important parameter for discussion of sediment transport. In addition, vertical profile of suspended sediment concentration has been discussed to relate the depth-averaged concentration to the bottom concentration of suspended sediment which is a key when fluvial process is discussed. When the bed deformation due to bed load motion, the direction of bed load motion affected by secondary flow should be evaluated. Thus, the primarily mechanism of secondary motion has been formulated to estimate its change due to vegetation.

In this chapter, formulas to modify parameters necessary for flow with vegetation have been analytically derived which are presented as functions of the vegetation density. Resultantly we are able to apply the 2D depth-averaged analysis reasonably to flow and fluvial process in a stream with various density of vegetation.

5.2.1 Uniform flow in a stream with Non submerged vegetation

The governing equations of uniform flow under equilibrium in a straight wide channel is described as follows.

$$q = Uh \quad (5.1)$$

$$\rho ghI_e = \tau_b + F = \rho c_f U^2 + \frac{1}{2} C_D \lambda D \rho U^2 h \quad (5.2)$$

where q =discharge in unit width; $\tau_b = \rho u_*'^2$ =bed shear stress; ρ =mass density of water; F =form drag due to vegetation per unit area. Then, the relation between q and h is written as follows:

$$q = h\sqrt{gI_e} \left(c_f + \frac{1}{2} C_D \lambda D h \right) = h\sqrt{gI_e} (c_f + c_d) \quad (5.3)$$

When flow with vegetation is treated, c_f and c_d depending on the vegetation parameter. In the previous studies, c_d is taken into account depending on the vegetation parameter ($\lambda D h$), but c_f is often identified with c_{f0} (based on Keulegan's equation for flow without vegetation). $h \sim q$ relation is significantly degenerated depending on the vegetation parameters, where calculated results by employing Equation (5.3) with Equation (4.9) and Keulegan's equation (c_{f0}) are compared with each other. Calculation were conducted under several sets of (I_e , k_s): (1/100, 5mm), (1/200, 2mm), (1/500, 1mm) and (1/1000, 0.3mm); under the following conditions of vegetation (λ , D): (m^{-2} , m).

Table 5.1 Condition of vegetation

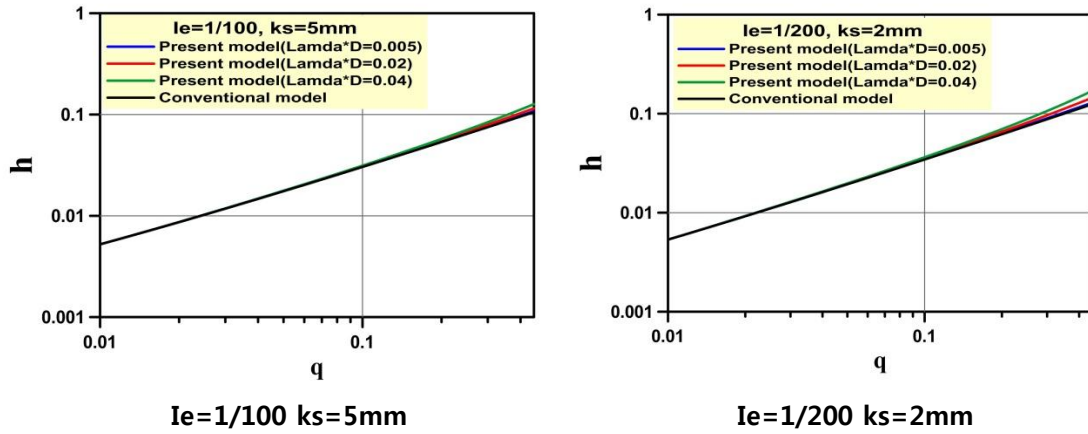
	Case1	Case2	Case3	Case4
$\lambda * D$	0.005	0.02	0.04	Conventional method

The results demonstrate that the taking account of the form drag is more effective in accuracy of the depth (and resultantly of the depth-averaged velocity) against the discharge and the application of c_f instead of shows a secondary effect.

In order to evaluate the sediment transport, it is necessary to estimate the shear velocity u_* as follow:

$$u_* = \sqrt{c_f} U = \frac{q}{h \left(1 - \frac{\theta_v}{h} \right) \left[\frac{1}{\kappa} \ln \frac{\theta_v}{k_s} + B_s(Re_s) \right] + \frac{\theta_v}{h} \left[\frac{1}{\kappa} \ln \left(\frac{\theta_v}{k_s} \right) + B_s(Re_s) - \frac{1}{\kappa} \right]} \quad (5.4)$$

Fig. 5.1 shows the relation $h \sim q$. The black solid line in the figure indicate the conventional model, blue solid line indicate the present model ($\lambda D = 0.005$), red solid line indicate the present model ($\lambda D = 0.02$) and blue solid line represents the present model ($\lambda D = 0.04$), respectively. The results of sensitivity analysis shows that if the rate of flow is small, water depth variation was almost same between conventional model and present model. However, the rate of flow increases, the water depth also increases in the present model. The increase rate of water depth is largest in case of present model ($\lambda D = 0.04$). The results of sensitivity analysis also shows that if the energy slope is small, the water depth was increased.



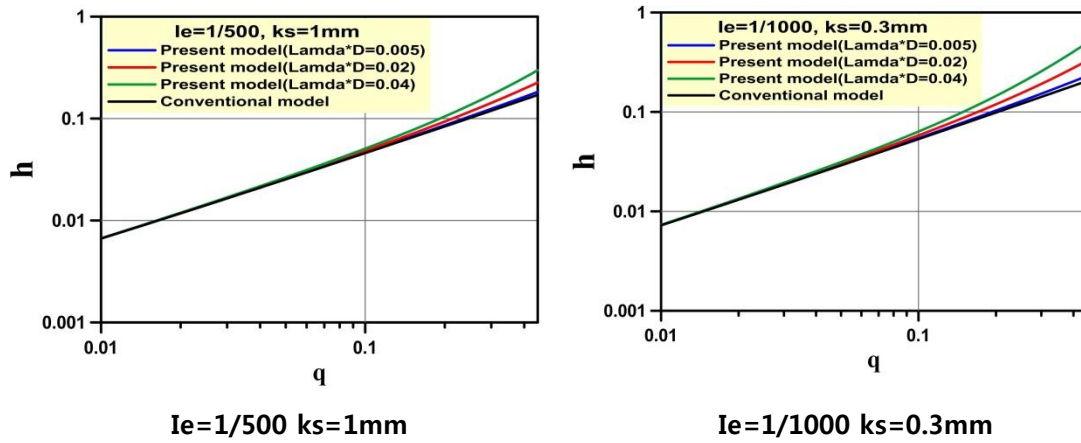
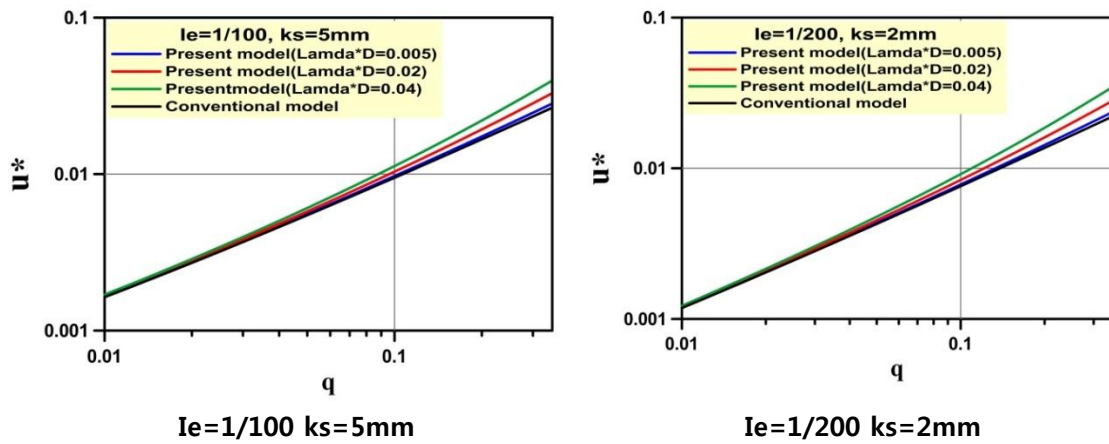


Fig. 5.1 Result of sensibility analysis($h \sim q$)

Fig. 5.2 shows the relation $u^* \sim q$. It depicts the relation $u^* \sim q$, which is more sensitive than $h \sim q$ or $U \sim q$. And, it suggests that the concept of bed roughness boundary layer should be inevitably taken into account in description of sediment transport and fluvial process in streams with vegetation.



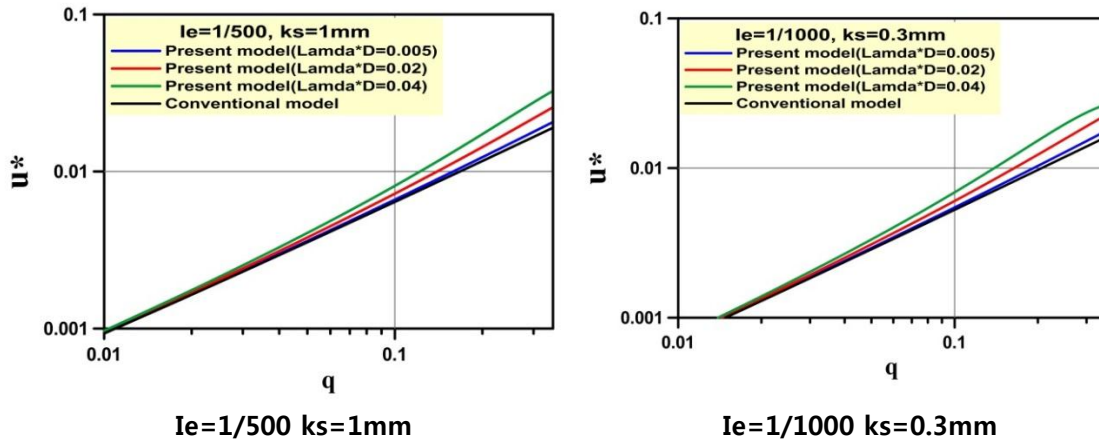
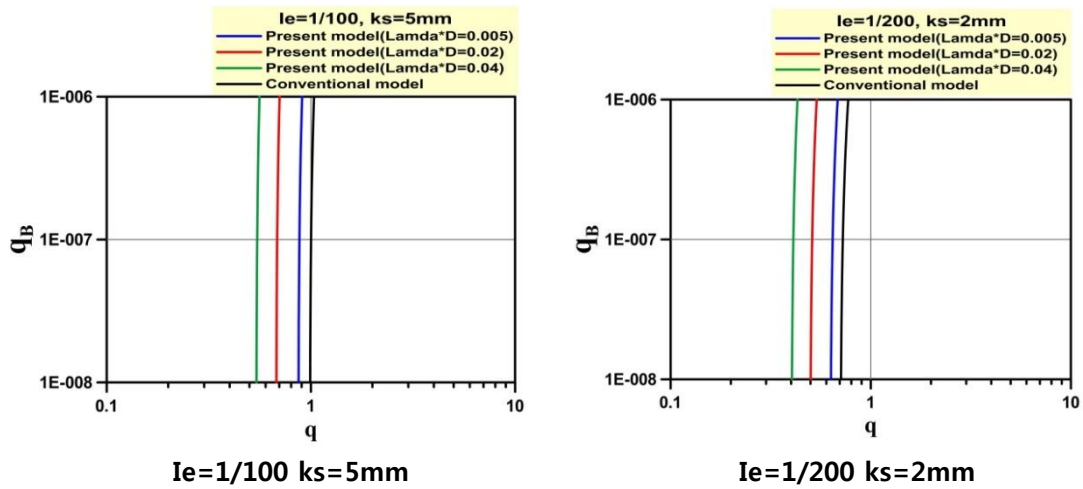


Fig. 5.2 Result of sensibility analysis($u^*\sim q$)

5.2.2 Description of sediment transport in vegetated stream

Bed load transport rate and the bottom concentration of suspended sediment are closely related to the shear stress as shown in the following formulas (Ashida & Michiue, 1972 (Equation 3.15); and Tsujimoto 1992 (Equation 3.29)). Fig. 5.3 and 5.4 depict the relation $q_B \sim q$ and $c_{be} \sim q$.



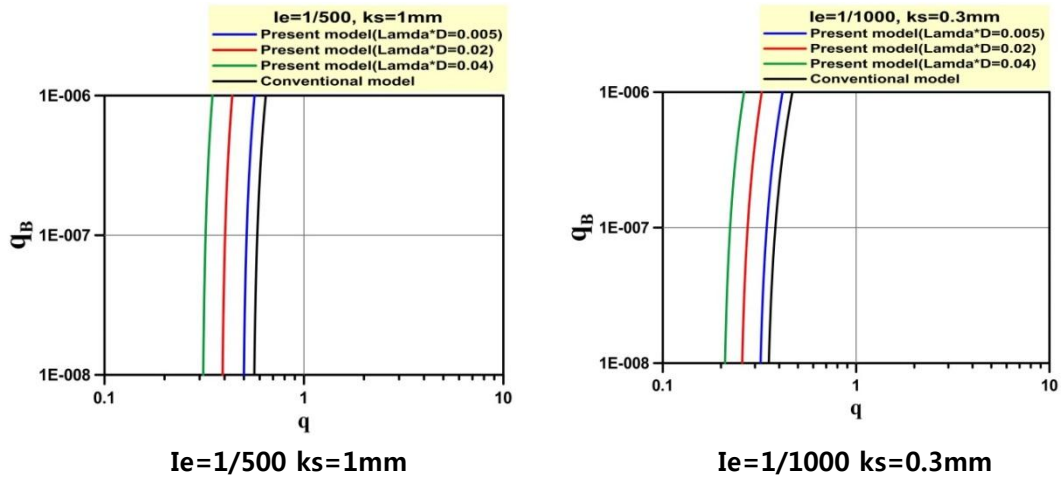


Fig. 5.3 Result of sensibility analysis($q_B \sim q$)

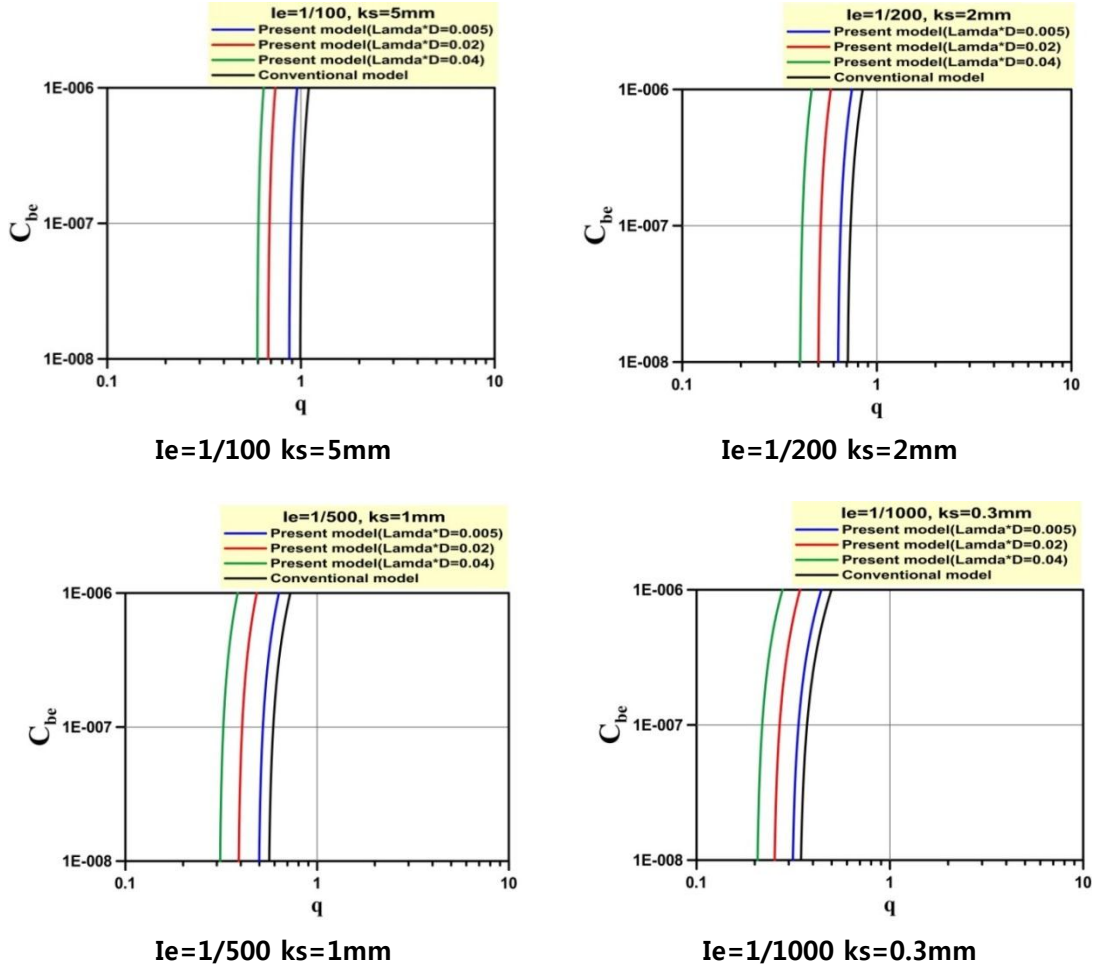


Fig. 5.4 Result of sensibility analysis($C_{be} \sim q$)

We can recognize the accurate and reasonable evaluation of shear stress based on the bed roughness boundary layer. Since the turbulent shear flow appears only in the bed roughness boundary layer, the suspended sediment concentration distributes there by showing the Equation 5.14.

As for the turbulent Schmidt number, Tsujimoto (1984) deduced the Equation 3.26 by comparing the diffusion theory with the stochastic modeling of suspended particle. Then the equation to relate the depth-averaged concentration to the bottom one is derived as Equation 5.15:

5.2.3 Secondary flow and dynamic equilibrium bed profile at a bend in vegetated stream

In a river bend, secondary motion appears because of the centrifugal force. When a stream is accompanied with the lateral bed slope and the secondary flow due to the centrifugal force by the curvature of stream which brings the shift of bottom flow angle from the main flow, γ , the direction of bed load motion deflects from the main flow direction as $\tan\phi$, as follows (Nakagawa, Tsujimoto & Murakami, 1984):

$$\tan \phi = \sqrt{\frac{1}{\mu_d \mu_f} \frac{\tau_{*c}}{\tau_*} \frac{\partial z_b}{\partial n}} + \tan \gamma \quad (5.5)$$

where μ_d , μ_f =dynamic and static friction coefficients of sand; and n =normal direction to the main flow. As for the secondary effect, the following equation is conventionally employed according to study on fully-developed flow at river bend by Engelund (1979):

$$\tan \gamma_0 = \frac{v_b}{u_b} = -N_{*0} \frac{h}{r} \quad (5.6)$$

where (u_b, v_b) =bottom velocity of the main flow and secondary flow component at the bottom; N_{*0} =constant (around 7.0 according to Engelund); and the subscript 0 means the value for flow without vegetation. The authors investigated the secondary flow effect in vegetated channel where the centrifugal force balances the form drag in the outer layer and the Reynolds stress described by Boussinesq model in the bed roughness boundary layer, and the following distribution of the secondary flow was deduced (Jeon, Obana & Tsujimoto, 2014):

$$\frac{v(z)}{u_*} = \frac{v(z)}{u_*} = \frac{6}{\kappa c_f} \frac{h}{R} \frac{\theta_v}{h} \left(1 - \frac{z}{2\theta_v}\right) + \frac{v_b}{u_*} \quad (0 < z < \theta_v); \quad \frac{v(z)}{u_*} = \sqrt{\frac{2}{C_D \lambda D h}} \cdot \frac{h}{R} \cdot \frac{U_v}{u_*} \quad (\theta_v < z < h) \quad (5.7)$$

Since the integration of $v(z)$ along the depth should be zero, v_b is expressed as follows:

$$\frac{v_b}{u_*} = \left(1 - \frac{\theta_v}{h}\right) \sqrt{\frac{2}{C_D \lambda D h}} \cdot \frac{h}{r} \left[\frac{1}{\kappa} \ln \left(\frac{h}{k_s} \cdot \frac{\theta_v}{h} \right) + B_s(\text{Re}_*) \right] - \frac{2}{\kappa c_f} \left(\frac{\theta}{h} \right)^2 \frac{h}{r} \quad (5.8)$$

Then the angle of bottom flow γ is expressed as follows:

$$\tan \gamma = \frac{v_b}{u_b} = \frac{-\frac{2}{\kappa c_f} \left(\frac{\theta_v}{h} \right)^2 \frac{h}{r} + \left(1 - \frac{\theta_v}{h}\right) \sqrt{\frac{2}{C_D \lambda D h}} \left[\frac{1}{\kappa} \ln \left(\frac{h}{k_s} \cdot \frac{\theta_v}{h} \right) + B_s(\text{Re}_*) \right] \sqrt{\frac{h}{r}}}{\frac{1}{\kappa} \ln \left(\frac{h}{k_s} \cdot \frac{\theta_v}{h} \right) + B_s(\text{Re}_*) - \frac{3}{\kappa}} \quad (5.9)$$

When the vegetation density is small enough ($\lambda D h$ tends to 0), θ_v approaches zero and Equation (5.9) tends to Equation (5.6) for flow without vegetation,

Since the gravity effect is independent of the vegetation, Equation (5.5) is revised for flow with vegetation as follows:

$$\tan \phi = \sqrt{\frac{1}{\mu_d \mu_f} \frac{\tau_{*c}}{\tau_*} \frac{\partial z_b}{\partial n} - \Gamma N_{*0}} \frac{h}{r} \quad (5.10)$$

where $\Gamma = N_*/N_{*0}$ is expressed as follows:

$$\Gamma(\theta_v) \equiv \frac{N_*}{N_{*0}} = \frac{\left(\frac{1}{\sqrt{c_{f0}}} - \frac{2}{\kappa} \right) \left\{ \frac{2}{\kappa c_f} \left(\frac{\theta_v}{h} \right)^2 - \left(1 - \frac{\theta_v}{h}\right) \left[\frac{1}{\kappa} \ln \left(\frac{h}{k_s} \cdot \frac{\theta_v}{h} \right) + B_s(\text{Re}_*) \right] \sqrt{\frac{2}{C_D \lambda D h}} \sqrt{\frac{R}{h}} \right\}}{\left[\frac{1}{\kappa} \ln \left(\frac{h}{k_s} \cdot \frac{\theta_v}{h} \right) + B_s(\text{Re}_*) - \frac{3}{\kappa} \right] \frac{2}{\kappa c_{f0}}} \quad (5.11)$$

where $N_{*0} = 7.0$ according to Engelund (1974).

When the channel width B is smaller enough than the curvature of the bend R , a dynamic equilibrium lateral slope of the cross section is given by setting $\varphi = 0$ that means no lateral sediment transport as follows.

$$\tan \phi = \sqrt{\frac{1}{\mu_d \mu_f} \frac{\tau_{*c}}{\tau_*} \frac{\partial z_b}{\partial n}} - \Gamma N_{*0} \frac{h}{r} \quad (5.12)$$

As shown by the above equation, the lateral bed slope with vegetation density by expressed by a parameter Γ governed by the vegetation density

5.3 Comparison with bed load deposition in decelerated area in vegetation

5.3.1 Laboratory experiment (full width vegetation)

In the laboratory experiment, a model vegetation was prepared by a group of cylinders made of bamboo arranged in staggered pattern ($D=0.25\text{m}$, $\lambda=0.25/\text{cm}^2$) being set in the interval of 5.0m in a flume of 20m long and 0.5m wide with the constant slope. The bed was rigid. Firstly, the flow measurements (U and h) were conducted along the centerline of the flume (Obana *et al.*(2012)). Then, sand ($d=0.5\text{cm}$, $\sigma/\rho=2.65$; d =diameter, σ , ρ =mass density of sand and water) was fed at 1.0m upstream of the vegetated area with constant volume along the width. The supplied sediment rate was calculated as $0.047\text{cm}^2/\text{s}$. The profile of bed load deposition in the vegetation area was measured along the centerline in the vegetated zone after 4min, 12min. and 20min.

5.3.2 Simulation of depth-averaged flow and comparison with flume experiment (full width vegetation)

To understand the hydraulic and topographical characteristics in vegetated area, this chapter consider interaction among depth average velocity - shear velocity - sediment transport through 2-dimensional numerical analysis approach and the numerical model can consider effect of vegetation was base on modeling of drag force of vegetation. The numerical model(NHSED2D) is verified firstly by comparisons with the laboratory experimental results. The grid size is $0.05\text{m} \times 0.01\text{m}$. The time step is 0.01s. The grids and the time step are sufficiently small to obtain grid convergent results. Numerical tank partially covered by all width vegetation and 5m length from 6m lower of upstream. The vegetation model is emergent rigid vegetation with same density. Flow discharge of $0.00694\text{m}^3/\text{s}$, flow depth of 0.033m were set as the hydraulic condition of the experiment. Detailed numerical setup conditions used

for verification are summarized in Table 5.2

Table 5.2 Numerical setup condition used for verification

Inflow	0.00694m ³ /s	
Length	20m	
Width	0.5m	
Slope	1/150	
Grain size	Sand	CPOM
	0.00025m	0.0015m
Specific gravity	2.65	1.26
Vegetation density	0.25cm ⁻²	

The measured data of depth and depth-averaged velocity, U and h , are plotted in Fig. 5.5 to be compared with the results of 2D-depth averaged model.

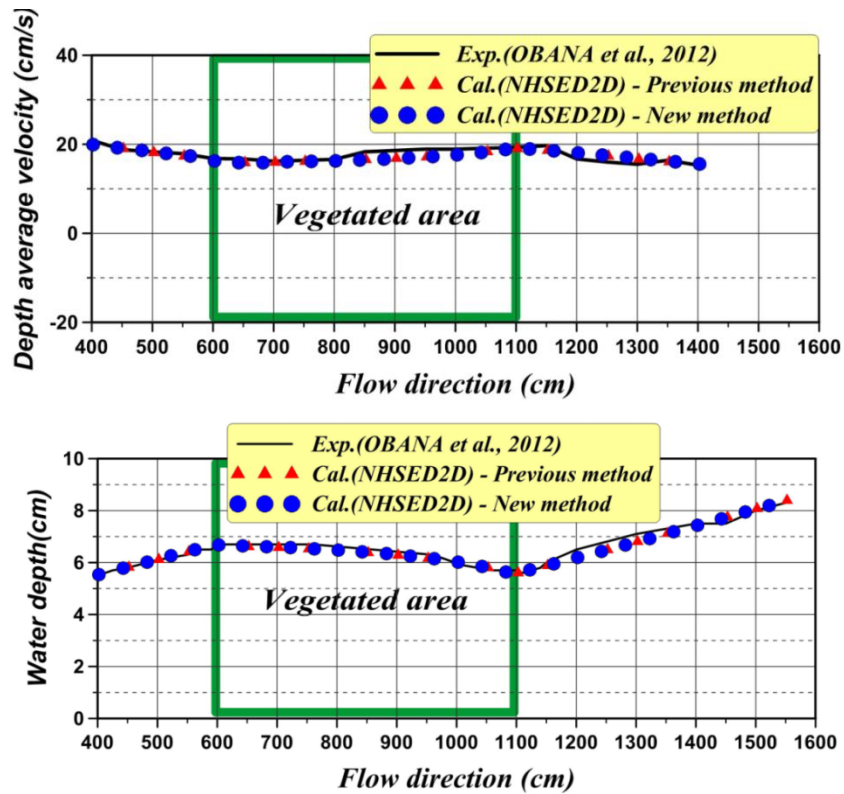


Fig. 5.5 Comparison between measured and calculated results of depth and depth-averaged velocity(full vegetation)

The calculation was conducted by using a program developed for horizontal 2D depth-averaged flow where the bed friction and the form drag due to vegetation are taken into account.

In the conventional way, Keulegan's equation Equation (4.1a, b) is employed for Equation (3.4, 3.5) to both non-vegetated and vegetated areas. While, when the present method is applied, Equation (4.7), which is presently proposed for flow with non-submerged vegetation, is employed in the vegetated area. The vegetation density ($\lambda=0.25\text{cm}^{-2}$) was verified using experiment data where floodplains were not inundated. Vegetation density of Liu's experiment 2.1 is similar to that conducted by this experiment. Boundary layer thickness of experiment 2.1 is measured 0.002m. Therefore, boundary layer thickness of new method was simulated 0.002m.

Fig. 5.5 shows comparison between the experimental data and the numerical results about depth average velocity and water depth. The solid line in the figure indicate the experimental results, red triangle indicate the conventional method and blue circle represents present method, respectively. Vegetation reduced longitudinal depth averaged velocity. As we can see, two kinds of method give good agreements between experimental data and calculated depth average velocity and water depth. The numerical model can accurately simulate the reduction of depth averaged velocity and increase of water depth with impact of vegetation.

Fig. 5.6 shows comparison of shear velocity between conventional method and present method in numerical results. As for the shear velocity, which has not directly measured in the experiment, the calculated one by the conventional model may be appreciably underestimated as shown in Fig. 5.6. The numerical results conducted by new method appear as if the vegetation density was to have a high value, shear velocity will become more faster.

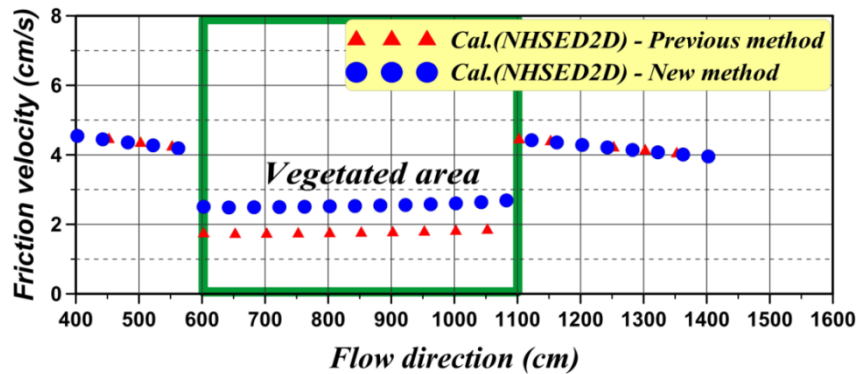


Fig. 5.6 Calculated results on shear velocity (full vegetation)

5.3.3 Bed load transport and deposition in vegetated area (full vegetation)

Fig. 5.7 displays comparison of the bed deformation in the vegetated area between the experimental data and the numerical results during time. The sediment mean diameter is 0.00025m. Sediment were provided at 2m upper part from vegetated area with equilibrium state during 20 minutes.

Bed load transport can be described by the Equation(3.15) proposed by (Ashida and Michiue, 1972). If bed load transport formula by Ashida & Michiue(1972) is applied to evaluating the equilibrium transport rate, the supplied sediment in the present experiment ($0.047\text{cm}^2/\text{s}$) is less than the equilibrium one ($0.062\text{cm}^2/\text{s}$) in the non-vegetated area but excessive than the equilibrium one ($0.036\text{cm}^2/\text{s}$) in the vegetated zone. Thus, bed load sediment deposits just upstream of the vegetated area and the upstream part of the vegetated area.

In Fig. 5.7, longitudinal profile of bed load deposition with time is depicted with the measured profile in the vegetated area at 4min, 12min and 20min after sediment supply. As for the deposition of bed load in the upstream of the vegetated zone, we did not conduct the measurement in the flume experiments. In the vegetated area, the solid line indicate the experimental bed deformation results and red solid line indicate the conventional method and blue solid line represent present method, respectively. Zero point of X-axis indicated that beginning of vegetated zone. Bed deformation changes around the vegetated area were simulated 20 minutes after introducing water to an initially flattened acrylic bed. Clearly, deposition occurs in front of the vegetated area, as well as inside and behind it. Fig. 5.7 gave similar areas where deposition happen between experimental data and numerical results. Numerical analysis conducted this study showed that a relationship exists between boundary layer thickness and vegetation density, which depends on the horizontal orbital velocity.

The calculated results, where we employed the conventional resistance law and the presently proposed one for the vegetated area, are compared with the measured data. The present model can describe the deposition profile with the steeper downstream slope with the faster migration because of the higher value of the shear stress, and it shows better conformity with the experimental result compared with the conventional model. Thus, it is concluded that introduction of the present proposal of the resistance law based on the concept of bed roughness boundary layer in vegetated area can bring accurate description of fluvial process in vegetated area.

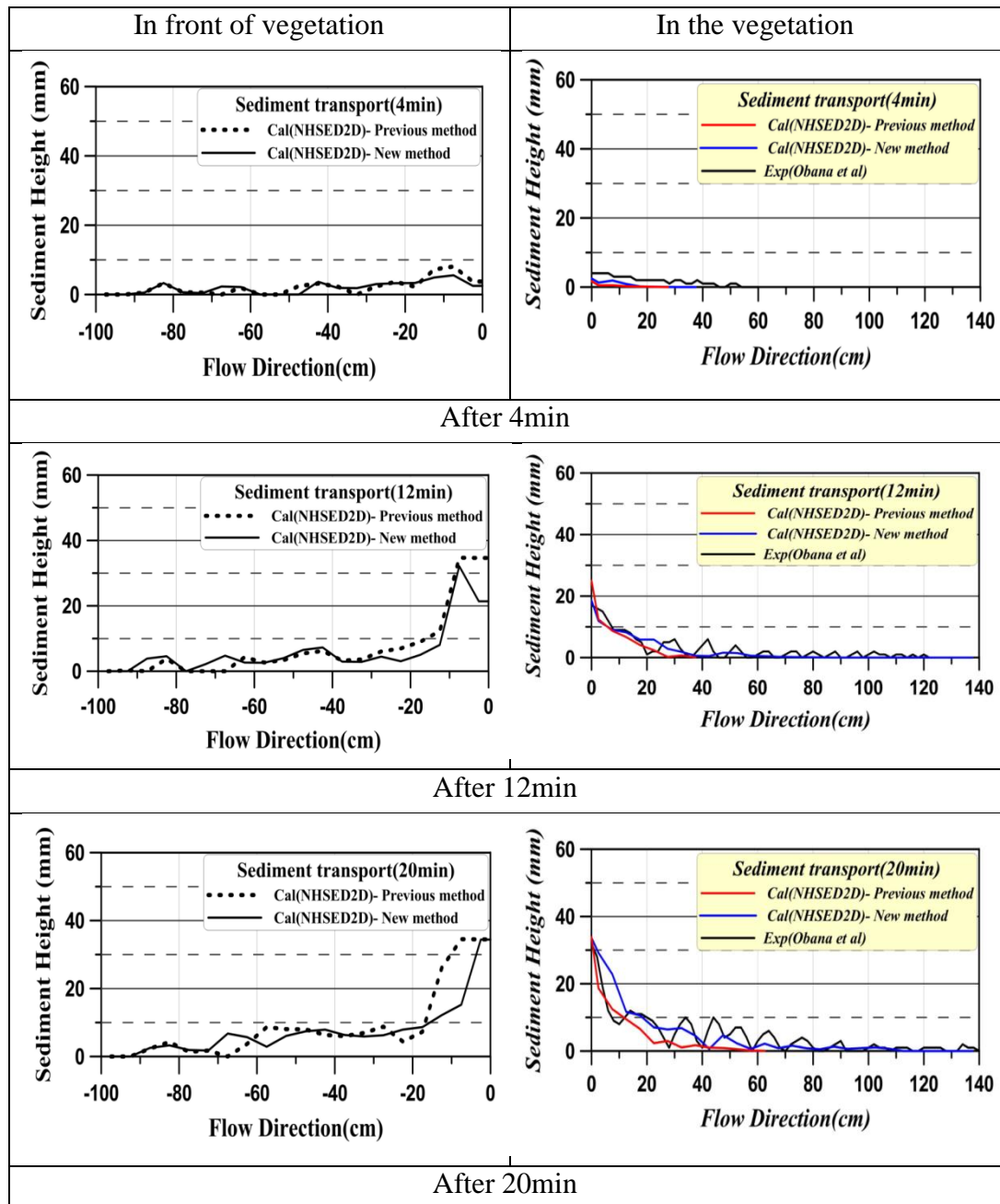


Fig. 5.7 Deposition profile of bed load sediment

Numerical analysis simulate about CPOM to better understand behavior of CPOM. Mean diameter of CPOM is 0.0015m and specific gravity is 1.26.

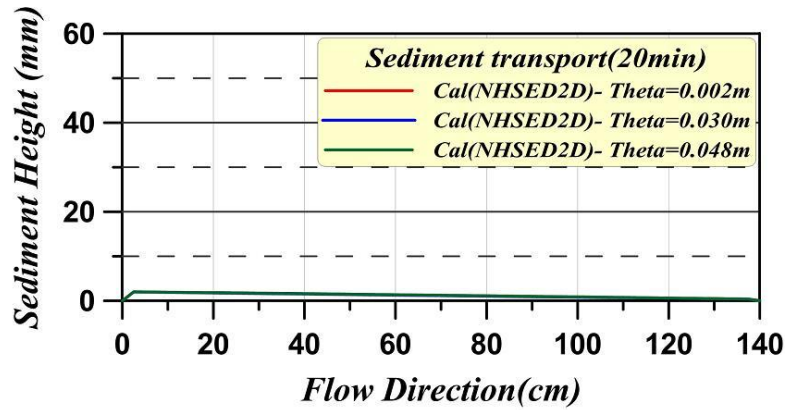


Fig. 5.8 Comparison of the CPOM behavior according to boundary layer thickness

Comparison of the CPOM behavior according to boundary layer thickness shows in Fig. 5.8. Three kinds of boundary layer thickness ($\theta_v=0.002, 0.030, 0.048m$) was conducted in numerical simulation. According to the observation on the experiment, If only CPOM particle was supplied to the vegetation area, CPOM never deposited itself. Such as this tendency also appear that CPOM is transported and flushed away in each case of numerical analysis. For successful application to understand about complicated processes including behaviors of sand and CPOM, It need a further consideration to create a ripple formation.

5.3.4 Laboratory experiment (half width vegetation)

To observe each mechanism of invasion and deposition of sediment into the vegetated zone by transverse dispersion by neighboring faster flow with slow flow in vegetated area along a bank. The experiment was carried out by installing the vegetation model on one side bank. The vegetation model was laying on 7m length and 0.25m width from 6m lower of the upstream of channel. Measurement section is determined at 5.3m point from the beginning of vegetation area by confirming equilibrium condition. In the experiment, two kinds of sand: coarse sand ($d=1.25mm, \sigma/\rho=2.65$); fine sand ($d=0.25mm, \sigma/\rho=2.65$) and two kinds of POM: CPOM model ($d=1.50mm, \sigma/\rho=1.26$); FPOM model ($d=0.15mm, \sigma/\rho=1.26$): were employed.

5.3.5 Simulation of depth-averaged flow and comparison with flume experiment (half width vegetation)

The numerical simulation were carried out to simulate same condition of laboratory

experiment. The grid size is $0.05\text{m} \times 0.01\text{m}$. The time step is 0.01s . The grids and the time step are sufficiently small to obtain grid convergent results. Numerical tank partially covered by half width vegetation and 7m length from 6m lower of upstream.

The vegetation model is emergent rigid vegetation with same density and it was installed on one side bank. Flow discharge of $0.00694\text{m}^3/\text{s}$, flow depth of 0.034m were set as the hydraulic condition of the experiment. Measurement section is determined at 5.3m point from the beginning of vegetation area by confirming equilibrium condition.

The numerical simulation was conducted as two kinds of method. Fig. 5.9 shows comparison between the experimental data and the numerical results about depth average velocity and water depth. The solid line indicate the experimental results, red triangle indicate the conventional method and blue circle represents present method, respectively.

Vegetation reduced longitudinal depth averaged velocity. As we can see, Two kinds of method give good agreements between experimental data and calculated depth average velocity and water depth. The numerical model can accurately simulate the reduction of depth averaged velocity and increase of water depth with impact of vegetation.

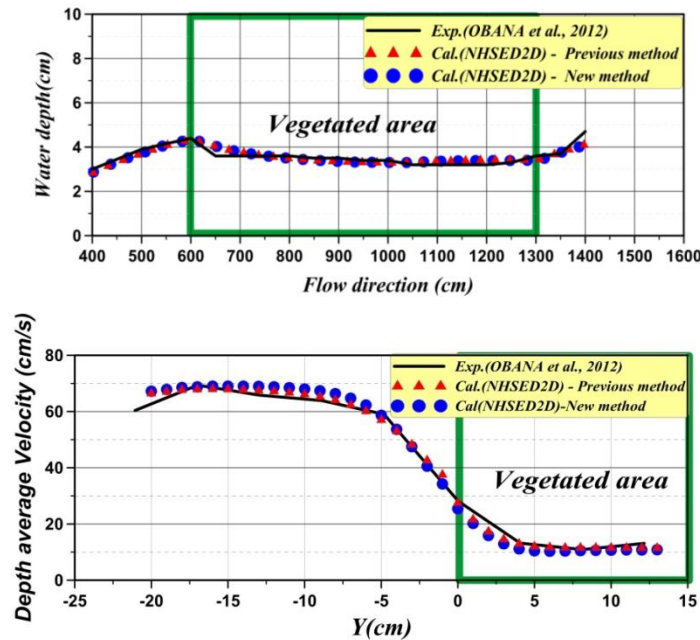


Fig. 5.9 Comparison between measured and calculated results of depth and depth-averaged velocity (half vegetation)

Fig. 5.10 shows comparison of shear velocity between conventional method and present method in numerical results. As for the shear velocity, which has not directly measured in the experiment. The shear velocity in the non-vegetated reach, $u_{*0}=6.5\text{cm/s}$ was obtained by applying the equation $u_{*0}=\sqrt{gh_0I_f}$, while in vegetated reach, $u_{*v}=1.2\text{cm/s}$ as obtained by using the local velocity near the bed there and the ratio of the near bed velocity to the shear stress in non-vegetated area. the calculated one by the conventional model may be appreciably underestimated as shown in Fig. 5.10.

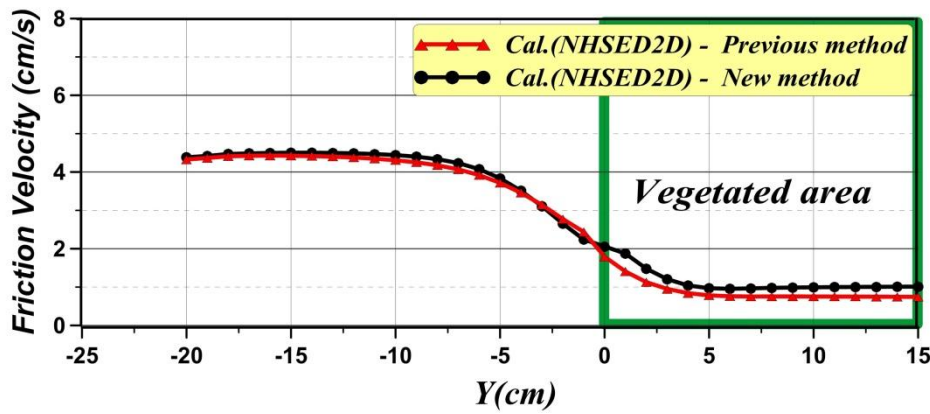


Fig. 5.10 Calculated results on shear velocity (half vegetation)

5.3.6 Bed load transport deposition in vegetated area(half vegetation)

In order to satisfy bed load motion, coarse sand ($d = 1.25\text{mm}$, $\sigma/\rho = 2.65$) is employed. Sediment were provided at 1m upper part from vegetated area with equilibrium state during 16 minutes.

Bed load transport can be described by the Equation (3.15) proposed by (Ashida and Michiue, 1972). Fig. 5.11 indicate a comparison between conventional method and new method of sediment thickness. Half vegetation was installed on one side bank from 6m to 13m. Bed deformation changes around the vegetated area were simulated 16 minutes after introducing water to an initially flattened acrylic bed. Bed load deposition appears on the outside of vegetation boundary. As time goes on, very small amount of sand came into inside of vegetation boundary.

In Fig. 5.12, transverse profile of bed load deposition with time is depicted with the measured profile in the vegetated area at 4min, 8min, 12min and 16min after

sediment supply. Measurement section is determined at 5.3m point from the beginning of vegetation area. The calculated results, where we employed the conventional resistance law and the presently proposed one for the vegetated area, are compared with the measured data.

Zero point of X-axis indicated that vegetation boundary. Inside of vegetation zone represent from 0cm to 8cm. In the case of laboratory experiments, deposition occurs inside of the vegetated area. In other hand, in case of numerical model, sediment which has been deposited on the outside of vegetation came into the vegetation zone a little. The present model can describe the deposition transverse profile with more migration because of the higher value of the shear stress better than conventional model.

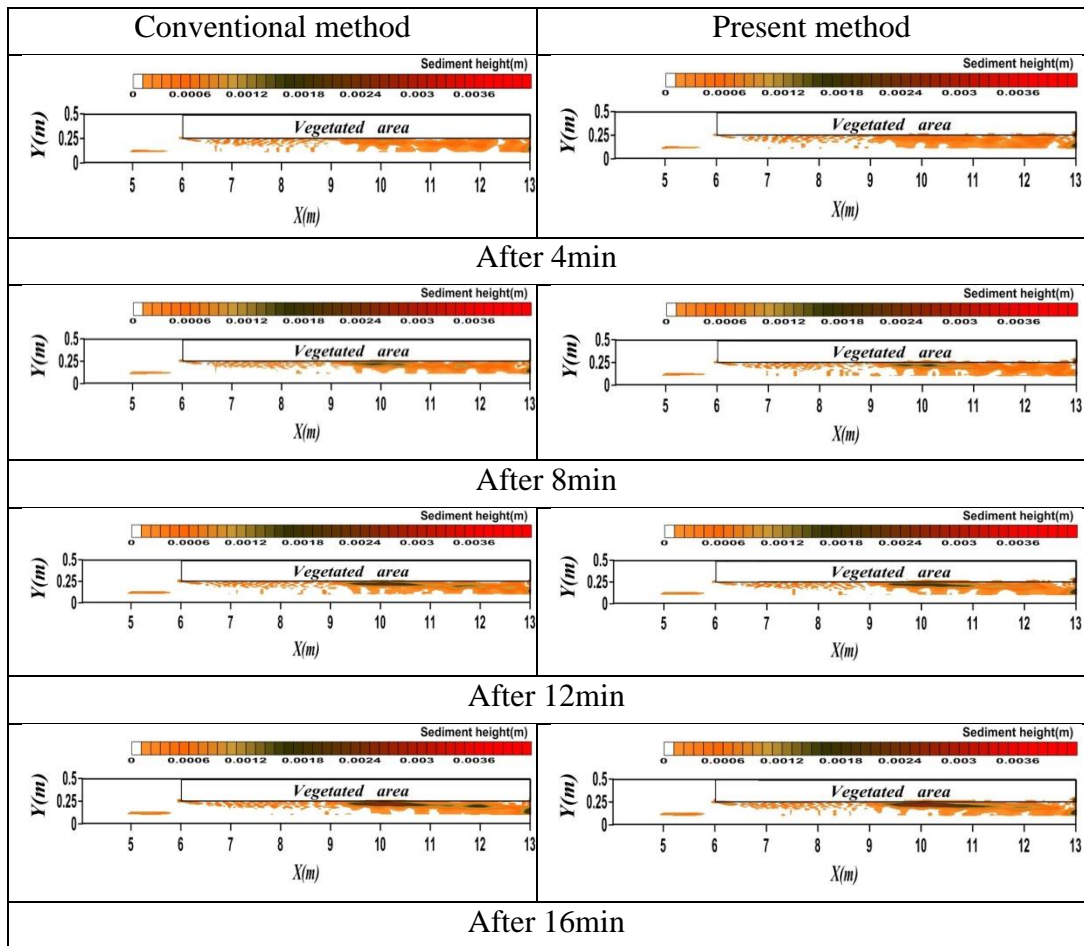


Fig. 5.11 Comparison between conventional method and present method of sediment thickness (half vegetation)

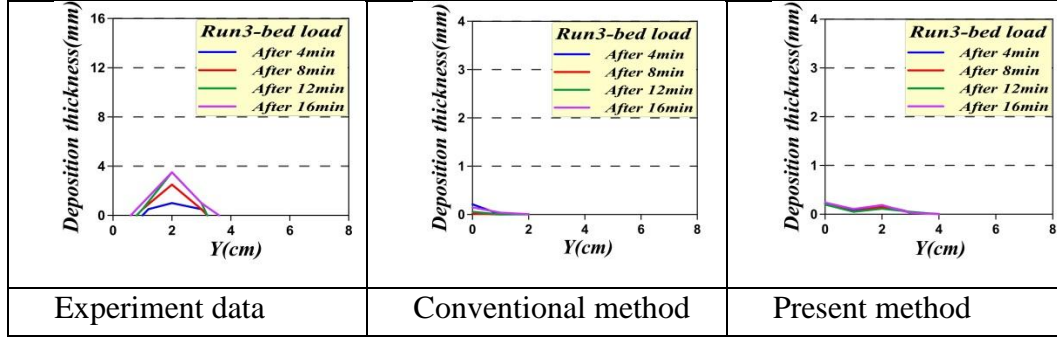


Fig. 5.12 Comparison between measured and calculated results of sediment thickness

5.4 Suspended sediment concentration in bed roughness boundary layer

When the diffusion coefficient of suspended sediment ε_s is expressed as βv_t , the equilibrium suspended sediment concentration distributes along the depth in the area without vegetation and the profile $c(z)$ is written as Equation 3.27 (Lane & Kalinske 1941) by substituting Equation 4.10. The Equation 3.26 is evaluated by (Tsujiimoto 1984) as follows by comparing the diffusion theory with the stochastic model.

Then, the depth averaged suspended sediment concentration C is written by Equation 3.28. On the other hand, suspended sediment distributes only in the bed roughness boundary layer ($0 < z < \theta_v$) because the turbulent diffusivity never exist in the upper layer ($\theta_v < z < h$) as follows:

$$\frac{c(z)}{C_B} = \exp\left(-\frac{6w_0}{\beta\kappa u_*} \frac{z}{\theta_v}\right) \quad (0 < z < \theta_v); \quad \frac{c(z)}{C_B} = 0 \quad (\theta < z) \quad (5.13)$$

And, the layer-averaged concentrations, C_θ for roughness boundary layer and $C_{h-\theta}$ for the upper layer, are written as follows.

$$\frac{C_\theta}{C_B} \equiv \frac{6w_0\theta_v}{\beta\kappa u_*} \left[1 - \exp\left(-\frac{6w_0\theta_v}{\beta\kappa u_*}\right)\right] \quad (0 < z < \theta_v); \quad \frac{C_{h-\theta}}{C_B} = 0 \quad (\theta < z) \quad (5.14)$$

The depth-averaged concentration in the vegetated area is written as follow:

$$\frac{C}{C_B} \equiv \frac{6w_0\theta_v^2}{\beta\kappa u_* h} \left[1 - \exp\left(-\frac{6w_0\theta_v}{\beta\kappa u_*}\right) \right] \quad (5.15)$$

The equilibrium bottom concentration, C_{Be} , is related to the shear velocity.

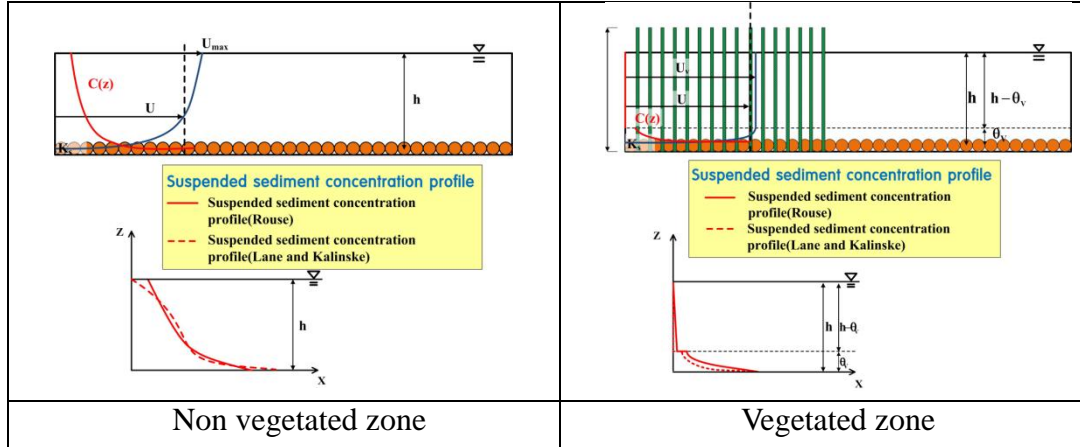


Fig. 5.13 Conceptual sketch of suspended sediment concentration profile in the non vegetated zone and vegetated zone

Fig. 5.13 shows the conceptual sketch of suspended sediment concentration profile in non vegetated zone and vegetated zone. As we know from the Fig. 5.13, suspended sediment concentration profile is a little different in the vegetated zone. The suspended sediment concentration profile is distributed throughout the depth in case of non vegetated zone but it is existed only within the bed roughness layer in case of vegetated zone.

Nevertheless, ordinary Equation 3.28 is applied even in the vegetation zone. In this chapter, the numerical simulation model was added on new Equation 5.15 in the vegetation zone for better accuracy suspended sediment concentration profile.

5.4.1 Ratio of depth averaged concentration and bottom concentration

To observe each mechanism of invasion and deposition of suspended sediment into the vegetated zone by transverse dispersion by neighboring faster flow with slow flow in vegetated area along a bank. The experiment was carried out by installing the vegetation model on one side bank. The vegetation model was laying on 7m length

and 0.25m width from 6m lower of the upstream of channel. Measurement section is determined at 5.3m point from the beginning of vegetation area by confirming equilibrium condition. In the experiment, Suspended sediment ($d=0.25\text{mm}$, $\sigma/\rho=2.65$) was fed at 1m upstream of the vegetated area with constant volume along the half width.

The numerical simulation were carried out to simulate same condition of laboratory experiment. The grid size is $0.05\text{m} \times 0.01\text{m}$. The time step is 0.01s. The grids and the time step are sufficiently small to obtain grid convergent results. Numerical tank partially covered by half width vegetation and 7m length from 6m lower of upstream. The vegetation model is emergent rigid vegetation with same density and it was installed on one side bank. Flow discharge of $0.00694\text{m}^3/\text{s}$, flow depth of 0.034m were set as the hydraulic condition of the experiment. Measurement section is determined at 5.3m point from the beginning of vegetation area by confirming equilibrium condition. In order to satisfy suspended sediment motion, Fine sand was provided at 1m upper part from vegetated area with equilibrium state during 16 minutes.

In the numerical model, Suspended sediment transport can be consider by the Equation (3.19). Entrainment of suspended sediment at bottom Ξ_{θ} (Equation (3.21)) is applicable to numerical model. The depth averaged suspended sediment concentration C is considered by Equation (3.28).

The numerical simulation was conducted as two kinds of new model. First, ordinary equation 4.10 about kinematic eddy viscosity change into new equation 4.12 based on bed roughness boundary layer concept for better accuracy suspended sediment concentration and kinematic eddy viscosity. Second, ordinary Equation 3.28 about depth averaged concentration change into new Equation 5.15 based on bed roughness boundary layer concept for better accuracy suspended sediment concentration. Two kinds of present model is compared with the conventional model.

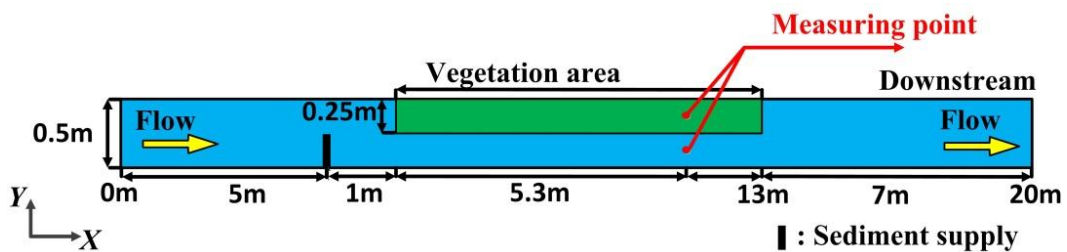


Fig. 5.14 Measuring point of suspended sediment concentration

Fig. 5.14 indicated that measuring point of suspended sediment concentration. The suspended sediment concentration and hydraulic characteristics was measured in middle of each vegetation and non vegetation. Fig. 5.15 shows condition of numerical condition. For calculating suspended sediment, two kinds of present method was conducted. In case of kinematic eddy viscosity of flow with vegetation by considering BRBL concept. It was calculated only changing the kinematic eddy viscosity in vegetated area. In other case is depth averaged suspended sediment concentration based on BRBL concept. It was calculated changing the ratio of depth averaged concentration to the bottom concentration and kinematic eddy viscosity.

● **Conventional method**

$$\frac{C}{C_B} \equiv \frac{6w_0h}{\beta\kappa u_*} \left[1 - \exp\left(-\frac{6w_0h}{\beta\kappa u_*}\right) \right] \quad \oplus \quad \nu_t = \frac{\kappa}{6} u_* h$$

● **Kinematic eddy viscosity based on BRBL concept**

$$\nu_t = \frac{\kappa}{6} u_* \theta_v \quad (0 < z < \theta_v); \quad \nu_t = 0 \quad (\theta_v < h)$$

$$\frac{C}{C_B} \equiv \frac{6w_0h}{\beta\kappa u_*} \left[1 - \exp\left(-\frac{6w_0h}{\beta\kappa u_*}\right) \right] \quad \oplus \quad \nu_t = \frac{\kappa u_* \theta_v^2}{6h}$$

● **Depth averaged suspended sediment concentration based on BRBL concept**

$$\frac{C_\theta}{C_B} \equiv \frac{6w_0\theta_v}{\beta\kappa u_*} \left[1 - \exp\left(-\frac{6w_0\theta_v}{\beta\kappa u_*}\right) \right] \quad (0 < z < \theta_v);$$

$$\frac{C_{h-\theta}}{C_B} = 0 \quad (\theta_v < z)$$

$$\nu_t = \frac{\kappa}{6} u_* \theta_v \quad (0 < z < \theta_v); \quad \nu_t = 0 \quad (\theta_v < h)$$

$$\frac{C}{C_B} \equiv \frac{6w_0\theta_v^2}{\beta\kappa u_* h} \left[1 - \exp\left(-\frac{6w_0\theta_v}{\beta\kappa u_*}\right) \right] \quad \oplus \quad \nu_t = \frac{\kappa u_* \theta_v^2}{6h}$$

Fig. 5.15 Condition of numerical simulation

Table 5.3 Numerical result of hydraulic characteristics

	X=11.3m					
	Non vegetation			Vegetation		
	Conventional	Kinematic eddy viscosity (BRBL)	Depth averaged concentration (BRBL)	Conventional	Kinematic eddy viscosity (BRBL)	Depth averaged concentration (BRBL)
h	0.03518	0.03504	0.03525	0.03518	0.03504	0.03525
u_*	0.04220	0.04223	0.04222	0.00797	0.00984	0.00988
θ_v	0	0	0	0	0.00380	0.00380

h: water depth, u_* : shear velocity, θ_v : boundary layer thickness

Table 5.3 shows comparison of water depth, shear velocity and boundary layer thickness between conventional model and two kinds of present model in numerical results. As for the water depth, there was no significant difference calculation results in a non vegetation and vegetation.

As for the shear velocity, which has not directly measured in the experiment. The shear velocity in the non-vegetated reach, $u_{*0}=0.042\text{m/s}$ was obtained by numerical calculation. There was no significant difference calculation results between conventional method and two kinds of present method, while in vegetated reach, $u_{*v}=0.0079\text{cm/s}$ as obtained by using conventional method. The calculated one by the conventional model may be appreciably underestimated as shown in Table 5.3.

Table 5.4 Numerical result of depth averaged concentration and bottom concentration

	X=11.3m					
	Non vegetation			Vegetation		
	Conventional	Kinematic eddy viscosity (BRBL)	Depth averaged concentration (BRBL)	Conventional	Kinematic eddy viscosity (BRBL)	Depth averaged concentration (BRBL)
C	0.01638	0.01630	0.01598	0.00289	0.00126	0.00036
C_b	0.09922	0.09877	0.09680	0.00724	0.00367	0.00998

C: depth averaged concentration, C_b : bottom concentration

Table 5.4 shows comparison between conventional model and two kinds of present model about depth averaged concentration and bottom concentration. The depth

averaged concentration of conventional model in a non vegetation is largest of all and depth averaged concentration of present model was found to be slightly decrease. The same tendency was appearing in bottom concentration.

In vegetated area, difference of depth averaged concentration between conventional model and two kinds of present model was larger than non vegetation. Depth averaged concentration of conventional model is also largest of all. In case of bottom concentration, Present model by using the kinematic eddy viscosity based on bed roughness boundary layer concept was smaller than conventional model. On the other hand, Present model by using the ratio of the depth average and bottom concentrations based on bed roughness boundary layer concept is larger than conventional model.

5.4.2 Comparison of suspended sediment concentration profile

Vertical suspended sediment concentration profile, obtained by vertically integrating the product of mean velocity and local sediment concentration. The vertical distribution of suspended sediment concentration in a 2D numerical model is an important subject in the mechanics of sediment transport. Results of vertical concentration profiles were compared between conventional model and two kinds of present model. Fig. 5.12 shows computed vertical suspended sediment concentration profile. The black solid line in the figure indicate conventional model, red solid line indicate present model by using the kinematic eddy viscosity based on bed roughness boundary layer concept (BRBL concept), respectively. The transverse diffusion coefficient of both method were used 0.3.

In the non vegetation area, the vertical distribution of suspended sediment concentration is almost same. However, In the vegetated area it was found that, due to the present model by using the kinematic eddy viscosity based on BRBL concept, simulated relative distributions of suspended sediment concentration differ slightly from conventional model. Distribution of suspended sediment concentration using present model is smaller than conventional model.

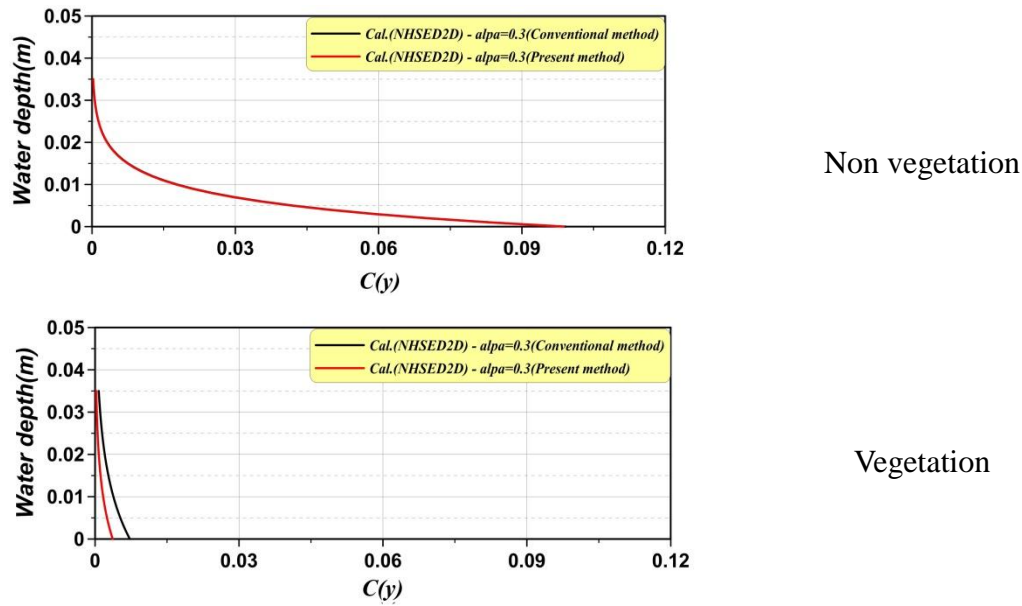
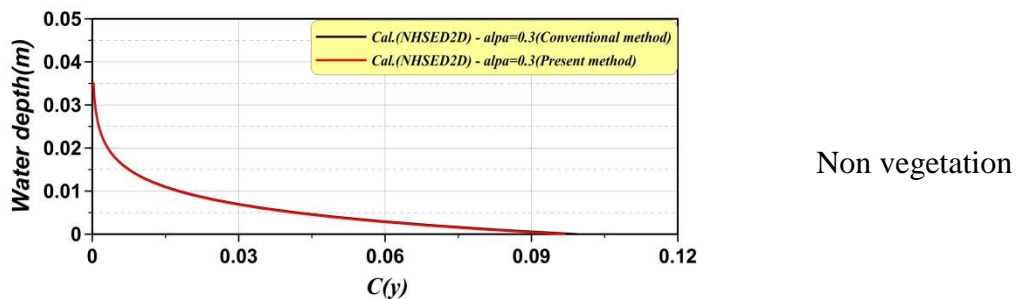


Fig. 5.15 Comparison of suspended sediment concentration profile between conventional model and present model by using the kinematic eddy viscosity based on BRBL concept

Fig. 5.13 also shows computed vertical suspended sediment concentration profile. The black solid line in the figure indicate conventional model, red solid line indicate present model by using the ratio of the depth average and bottom concentrations based on BRBL concept, respectively. The vertical distribution of suspended sediment concentration is almost same in non vegetated area. In the vegetated area, present model by using the ratio of the depth average and bottom concentrations based on BRBL concept distributes only in the bed roughness boundary layer because the turbulent diffusivity never exist in the upper layer. And distribution of suspended sediment concentration using present model is smaller than conventional model.



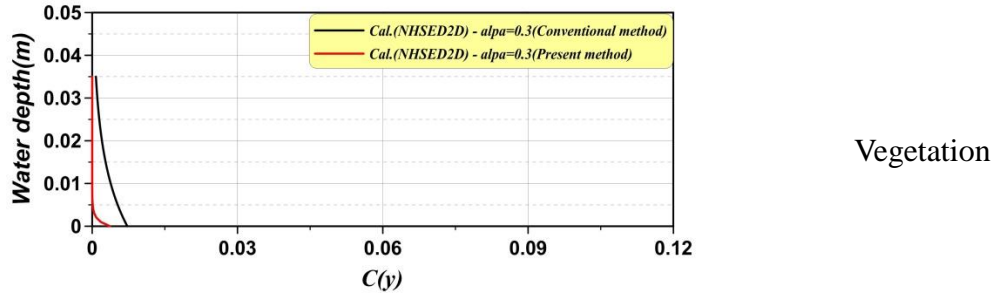


Fig. 5.16 Comparison between conventional model and present model by using the ratio of the depth average and bottom concentrations based on BRBL concept

5.5 Concluding Remarks

Recently 2D depth-averaged analysis has become popular and powerful, and one expects its applicability to a stream with vegetation. However, there must be some restriction for application in 2D analysis for flow with vegetation. In this paper, as for flow with non-submerged vegetation, several points necessary to be modified are theoretically discussed. In flow with vegetation, taking account for drag term due to vegetation is a principal key but it is not necessary sufficient by it alone.

From the check along the 2D modeling, the friction resistance law should be reasonably considered and the concept of “bed roughness boundary layer” has been proposed and formulated against the vegetation density. Based on this concept, the shear flow structure in this layer has been discussed and formulated. It has brought the reasonable evaluation of the shear stress and subsequently the kinematic eddy viscosity as important parameter for discussion of sediment transport. In addition, vertical profile of suspended sediment concentration has been discussed to relate the depth-averaged concentration to the bottom concentration of suspended sediment which is a key when fluvial process is discussed.

In this chapter formulas to modify parameters necessary for flow with vegetation have been analytically derived which are presented as functions of the vegetation density and some of them are depicted in figure.

Based on the concept of bed roughness boundary layer, fluvial process with full vegetation can be discussed as below:

1. The calculation was conducted by using a program developed for horizontal 2D depth-averaged flow where the bed friction and the form drag due to

vegetation are taken into account.

2. In the conventional way, Keulegan's equation is employed for to both non-vegetated and vegetated areas. While, when the present method is applied, Equation (4.7), which is presently proposed for flow with non-submerged vegetation
3. Two kinds of method give good agreements between experimental data and calculated depth average velocity and water depth. The numerical model can accurately simulate the reduction of depth averaged velocity and increase of water depth with impact of vegetation.
4. As for the shear velocity, which has not directly measured in the experiment, the calculated one by the conventional model may be appreciably underestimated. The numerical results conducted by new method appear as if the vegetation density was to have a high value, shear velocity will become more faster.
5. The results of sensitivity analysis shows that if the rate of flow is small, water depth variation was almost same between conventional model and present model. However, the rate of flow increases, the water depth also increases in the present model. The increase rate of water depth is largest in case of present model ($\lambda D=0.04$). The results of sensitivity analysis also shows that if the energy slope is small, the water depth was increased.
6. Sensitivity analysis depicts the relation $u^* \sim q$, which is more sensitive than $h \sim q$ or $U \sim q$. And, it suggests that the concept of bed roughness boundary layer should be inevitably taken into account in description of sediment transport and fluvial process in streams with vegetation.

Comparison of the bed deformation in the full vegetated area between the experimental data and the numerical results during time can be described as below:

1. The calculated results, where we employed the conventional resistance law and the presently proposed one for the vegetated area, are compared with the measured data. The present model can describe the deposition profile with the steeper downstream slope with the faster migration because of the higher value of the shear stress, and it shows better conformity with the experimental result compared with the conventional model. Thus, it is concluded that introduction of the present proposal of the resistance law based on the concept of bed roughness boundary layer in vegetated area can bring accurate

description of fluvial process in vegetated area.

2. According to the observation on the experiment, If only CPOM particle was supplied to the vegetation area, CPOM never deposited itself. Such as this tendency also appear that CPOM is transported and flushed away in each case of numerical analysis.

Based on the concept of bed roughness boundary layer, fluvial process with half vegetation can be discussed as below:

1. Vegetation reduced longitudinal depth averaged velocity. As we can see, Two kinds of method give good agreements between experimental data and calculated depth average velocity and water depth. The numerical model can accurately simulate the reduction of depth averaged velocity and increase of water depth with impact of vegetation.
2. The shear velocity in the non-vegetated reach, $u_{*0}=6.5\text{cm/s}$ was obtained by applying the equation $u_{*0}=\sqrt{gh_0I_f}$, while in vegetated reach, $u_{*v}=1.2\text{cm/s}$ as obtained by using the local velocity near the bed there and the ratio of the near bed velocity to the shear stress in non-vegetated area. the calculated one by the conventional model may be appreciably underestimated.

Comparison of the bed deformation in the half vegetated area between the experimental data and the numerical results during time can be described as below:

1. Transverse profile of bed load deposition with time is depicted with the measured profile in the vegetated area at 4min, 8min, 12min and 16min after sediment supply. Measurement section is determined at 5.3m point from the beginning of vegetation area. The calculated results, where we employed the conventional resistance law and the presently proposed one for the vegetated area, are compared with the measured data.
2. Zero point of X-axis indicate that vegetation boundary. Inside of vegetation zone represent from 0cm to 8cm. In the case of laboratory experiments, deposition occurs inside of the vegetated area. In order hand, in case of numerical model, Bed load deposition appears on the outside of vegetation boundary. As time goes on, very small amount of sand came into inside of vegetation boundary.

3. The present model can describe the deposition transverse profile with more migration because of the higher value of the shear stress better than conventional model.

Based on the concept of bed roughness boundary layer, suspended sediment concentration with vegetation can be discussed as below:

1. In vegetated area, difference of depth averaged concentration between conventional model and two kinds of present model was larger than non vegetation. Depth averaged concentration of conventional model is also largest of all. In case of bottom concentration, Present model by using the kinematic eddy viscosity based on BRBL concept was smaller than conventional model. On the other hand, Present model by using the ratio of the depth average and bottom concentrations based on BRBL concept is larger than conventional model.
2. In the non vegetation area, the vertical distribution of suspended sediment concentration is almost same. However, In the vegetated area it was found that, due to the present model by using the kinematic eddy viscosity based on BRBL concept, simulated relative distributions of suspended sediment concentration differ slightly from conventional model. present model by using the ratio of the depth average and bottom concentrations based on BRBL concept distributes only in the bed roughness boundary layer because the turbulent diffusivity never exist in the upper layer. Distribution of suspended sediment concentration using present model is smaller than conventional model.

References

1. Ashida, K. & M. Michiue. (1972) Hydraulic resistance of flow in an alluvia bed and bed load transport rate. *Proc. JSCE*, No.206, pp.59-69 (in Japanese).
2. Furukawa, K., E. Wolanski, and H. Mueller. (1997) "Currents and sediment transport in mangrove forests". *Esruarine, Coastal and Shelf Science* 44.3, pp. 301-310.
3. Lane, EW and AA Kalinske. (1941) "Engineering calculations of suspended sediment". *Trans. AGU* 22, pp. 603-607.
4. Liu, D., Diplas, P., Fairbanks, J., Hodges, C. (2008) An experimental study of flow through rigid vegetation. *Jouranl of Geophysical Research: Earth Surface*(2003-2012) 113(F4).
5. Lopez, F. and M. Garcia. (1998) "Open-channel flow through simulated vegetation: Suspended sediment transport modeling". *Water resources research* 34.9, pp.2341-2352.
6. Middlekoop , H. & Van der Perk , M. (1998) Modelling spatial patterns of overbank sedimentation on embanked flood plains. *Geografiska Annaler* 80A, pp. 95-109 .
7. Nakagawa, H., T. Tsujimoto, and Y. Shimizu. (1992) "Sediment transport in vegetated bed channel". *Conference Proceedings of the 5th International Symposium on River Sedimentation*, Karlsruhe.
8. Nicholas , A.P. & D.E . Walling. (1997) Modelling flood hydraulics and overbank deposition on river floodplains. *Earth Surface. Processes and Landforms*. 22, pp. 59-77 .
9. Obana, M, T. Uchida & T. Tsujimoto. (2012) Deposition of Sand and particulate organic matter in riparian vegetation, *Advances in River Eng.*, JSCE, pp.47-52 (in Japanese).
10. Rouse, H. (1937) "Modern conceptions of the mechanics of fluid turbulence". *Trans. ASCE* 102, pp. 463-543.
11. Stewart , M . D. , Bates, P . D . & Price . A . P. (1998) Modelling the spatial variability in flood plain soil contamination during flood events to improve chemical mass balance estimates. *In: High Resolution Flow Modelling in Hydrology and Geomorphology* (ed . by P . D. Bates & S. N . Lane) , pp. 239-261 . John Wiley & Sons , Chichester , UK .
12. Tsujimoto, T., Shimizu, Y., Kitamura, T. & Izumi, N. (1994) Flow and suspended sediment transport in compound open-channel with vegetation. KHL

Progressive Report, Hydraulics Laboratory, Kanazawa University.

13. Van Rijn, L.C. (2007) “Unified view of sediment transport by currents and waves. II: Suspended transport”. *Journal of Hydraulic Engineering* 133, p. 668.

CHAPTER 6

TRANVERSE MIXING IN FLOW AND SUSPENDED SEDIMENT IN STREAM WITH VEGETATION ZONE

6.1 General

The transverse interaction between vegetated and non-vegetated zones is a turbulence phenomenon, and (unlike phenomena which are dominated by geometry rather than turbulence) predictions are therefore extremely sensitive to the specification of eddy viscosity. Many research has been conducted into the spreading of materials in open channel. in term of lateral or transverse spreading there is a general custom to assume that the transverse dispersion coefficient is proportional to the product of shear velocity and average depth.

The transverse transfer of sediment from an unvegetated channel to adjacent vegetated zones is more complex, and requires description of the transverse distribution of velocity and the transverse eddy viscosity. Tsujimoto and Shimizu (1994) used a similar approach to that of Lopez and Garcia (1998; 2001) to simulate the vertical and transverse distributions of suspended sediment concentration in simple and compound channels with vegetation zones in the cross-sections. Nepf (1999) used measurements of dye dispersion to determine transverse diffusivities in flows through arrays of cylindrical rods. She found transverse diffusivities to vary with stem characteristics and flow velocity.

Though experiments, Tsujimoto and kitamura (1992) pointed out that transverse mixing is caused by rather organized and low-frequency fluctuation of transverse velocity and is associated with the fluctuation of free surface. Another experimental investigations performed in the laboratory provided details of the diffusion processes in the presence of vegetation (Sharpe and James, 2006; Murphy et al., 2007; Nepf et

al., 2007).

The transverse transport situations were investigated and simulated using appropriate formulations of the diffusion-convection model to confirm their applicability and to enable inference of realistic values of sediment diffusivity. And The relation for transverse mixing coefficient was offered and analyzed.

The concept of bed roughness boundary layer apply to the numerical simulation model will provide more accurate results.

6.2 Lateral mixing between flow and suspended sediment between areas without and with non submerged vegetation

6.2.1 Lateral mixing of momentum and lateral distribution of depth-averaged velocity

The governing equations of flow in depth averaged 2D scheme are written as Equation(3.1~3.5), Equation(3.9, 3.10). C_f =friction coefficient given by $(U/u_*)^2$ (Equation 4.1b for area without vegetation and Equation 4.9 for area with vegetation). There are some programs based on the above governing equations, but in conventional approaches, the friction resistance law for flow without vegetation is applied even in the vegetated area though the form drag is taken into account for the vegetated area. The authors have derived a reasonable equation of frictional resistance law based on the concept of bed roughness boundary layer in the area with non-submerged vegetation. Applying this law can bring a reasonable evaluation of the shear velocity in the vegetated area and subsequently equilibrium bottom concentration of suspended sediment (entrainment rate is $C_{Be}W_0$).

In lateral mixing, the horizontal diffusion written in Equation 3.1 is subjected to the eddy kinematic viscosity. Conventionally, the vertical diffusion coefficient ν_t which is related to the vertical velocity distribution is applied by simply multiplying a constant even in horizontal mixing as ν_{th} , and furthermore, the value given for flow on the area without vegetation, as Equation(4.13).

where α is empirically determined in the range 0.1~0.5.

Depth-averaged kinematic eddy viscosity is modified as expressed by Equation 4.12, and thus the Equation 4.14 is reasonably employed for flow with vegetation instead of Equation 4.13.

6.2.2 Lateral mixing of suspended sediment and lateral distribution of depth averaged concentration of suspended sediment

The spatial distribution of depth-averaged concentration is described by the flowing equation:

$$\frac{\partial hC}{\partial t} + \frac{\partial}{\partial x} \left(hCU - \beta v_{th} h \frac{\partial C}{\partial x} \right) + \frac{\partial}{\partial y} \left(hCV - \beta v_{th} h \frac{\partial C}{\partial y} \right) = \Xi_{\ominus} \quad (6.1)$$

where Ξ_{\ominus} =difference between deposition and entrainment from the bed to be expressed by $(C_{Be}-C_B)w_0$ and it represents the bed deformation; and the horizontal diffusion coefficient of suspended sediment is assumed to be βv_{th} .

6.3 Transverse distribution of depth-averaged flow in stream with vegetation

6.3.1 Transverse diffusion coefficient for flow with vegetation

A simplest example of flow to be treated in 2D scheme, the flow in a straight channel with a zone of non-submerged vegetation is investigated. Far from the boundary between the zones with and without vegetation. Without any separation wall to prevent from mixing between two zones, there appears a mixing zone where velocity and suspended sediment concentration changes laterally to connect the characteristic values of respective zones. In the conventional approach, α is assumed to be appreciably larger than $\kappa/6$ (same to the vertical mixing). With the larger value of α , the wider the mixing width becomes as shown in Fig. 6.1. And the experimental data can be described well by larger value of α (around 0.3) as shown in Fig. 6.1. According to the elaborate flow measurement, migration of horizontal components of the flow, and it may cause an increase of horizontal diffusivity.

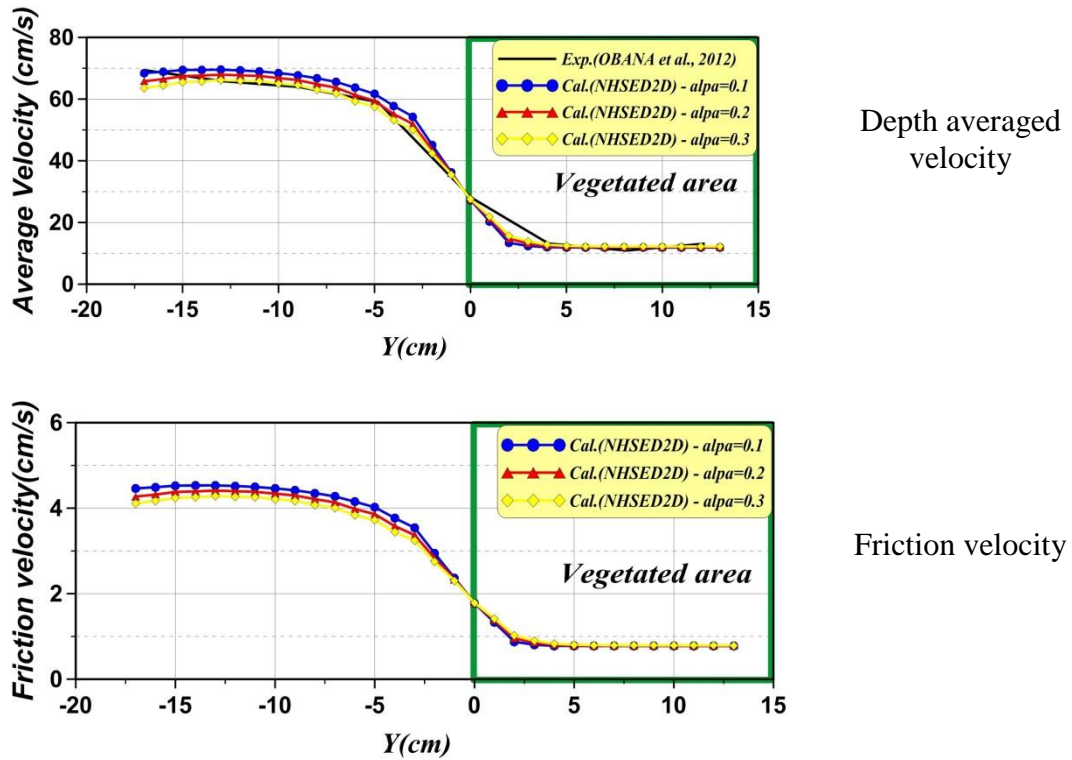


Fig. 6.1 Comparison of depth averaged velocity and friction velocity between measured and calculated results (transverse diffusion coefficient 0.1-0.3)

A Fig 6.2 shows comparison between the experimental data and the numerical results about depth average velocity and shear velocity. Transverse diffusion coefficient was calculated as a constant value(0.3). The solid line in the figure indicate the experimental results, yellow diamond indicate the conventional model and red triangle represents present model by using the kinematic eddy viscosity based on BRBL concept, respectively. Vegetation reduced lateral depth averaged velocity. As we can see, two kinds of method give good agreements between experimental data and calculated depth average velocity. The numerical model can accurately simulate the reduction of depth averaged velocity.

Below figure shows comparison of shear velocity between conventional model and new model by using the kinematic eddy viscosity based on BRBL concept in numerical results. As for the shear velocity, which has not directly measured in the experiment, the calculated one by the conventional model may be appreciably underestimated as shown in Fig. 6.2.

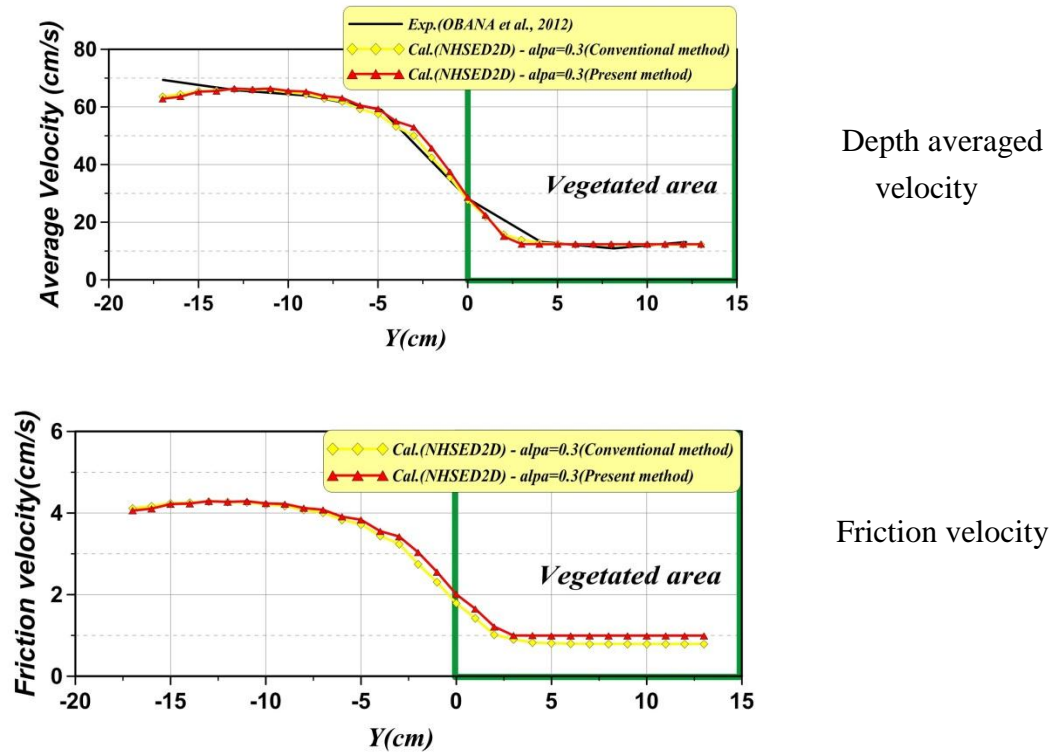


Fig. 6.2 Comparison of depth averaged velocity and friction velocity between conventional model and present model by using the kinematic eddy viscosity based on BRBL concept

A Fig. 6.3 also shows comparison between the experimental data and the numerical results about depth average velocity and shear velocity. The solid line in the figure indicate the experimental results, yellow diamond indicate the conventional method and red triangle represents present method by using the ratio of the depth average and bottom concentrations based on BRBL concept, respectively. As we can see, two kinds of method give good agreements between experimental data and calculated depth average velocity. The numerical model can accurately simulate the reduction of depth averaged velocity.

Below figure shows comparison of shear velocity between conventional model and present model by using the ratio of the depth average and bottom concentrations based on BRBL concept. The calculated one by the conventional model may be appreciably underestimated as shown in Fig. 6.3. The BRBL concept has been applied to 2D depth averaged numerical model has brought the reasonable evaluation of the

shear stress and velocity.

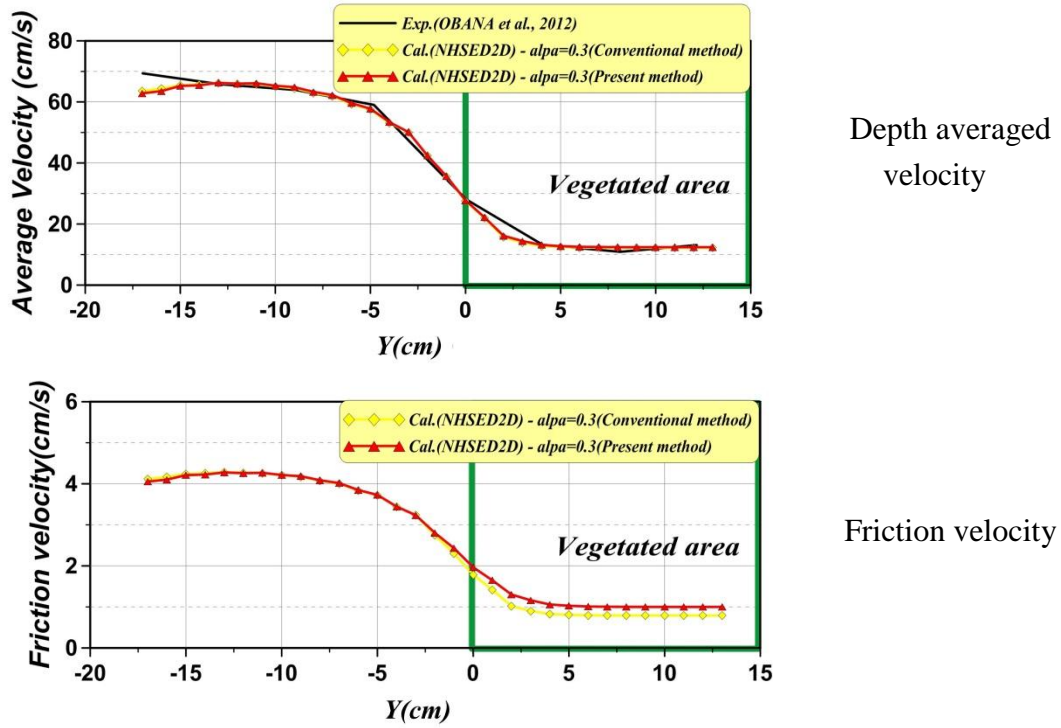
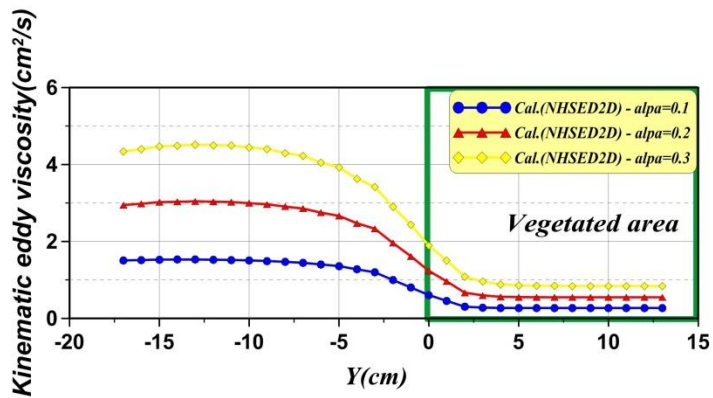


Fig. 6.3 Comparison of depth averaged velocity and friction velocity between conventional model and present model by using the ratio of the depth average and bottom concentrations based on BRBL concept

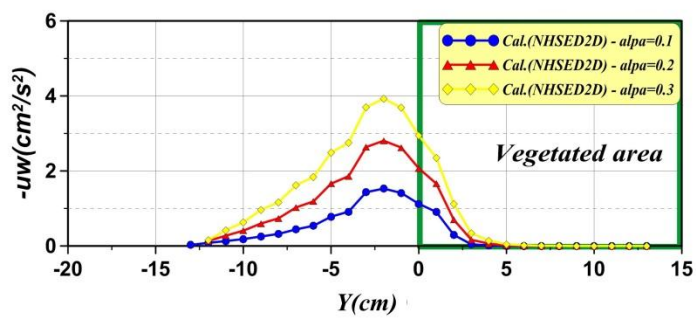
6.3.2 Kinematic eddy viscosity investigated by $k-\epsilon$ model

From the check along the 2D numerical modeling, the friction resistance law should be reasonably considered and the concept of bed roughness boundary layer has proposed and formulated against the vegetation density. Based on this concept, we can confirm that 2D numerical model has brought the reasonable evaluation of the shear stress and velocity. And shear velocity will affect the kinematic eddy viscosity as important parameter for discussion of sediment transport.

Fig. 6.4 shows comparison of kinematic eddy viscosity and Reynolds stress regarding the change to transverse diffusion coefficient. The larger transverse diffusion coefficient tend to increase the kinematic eddy viscosity and Reynolds stress in the vegetated area.

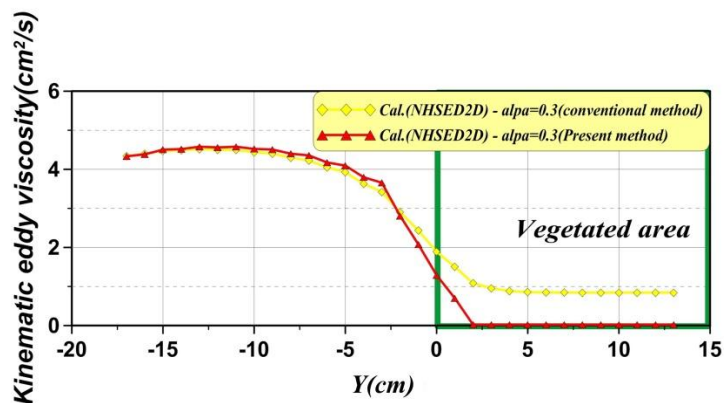


Kinematic eddy viscosity



Reynolds stress

Fig. 6.4 Comparison of kinematic eddy viscosity and Reynolds stress (transverse diffusion coefficient 0.1-0.3)



Kinematic eddy viscosity

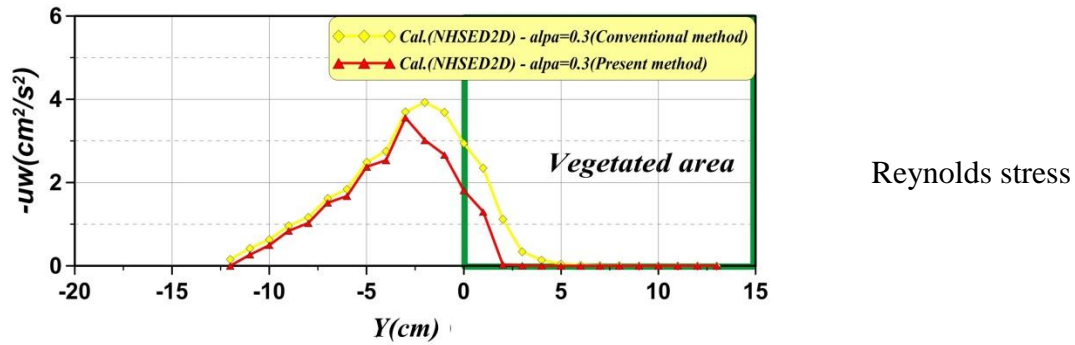


Fig. 6.5 Comparison of kinematic eddy viscosity and Reynolds stress between conventional model and present model by using the kinematic eddy viscosity based on BRBL concept

Fig 6.5 shows Comparison of kinematic eddy viscosity and Reynolds stress between conventional model and present model by using the kinematic eddy viscosity based on BRBL concept. By using the present model we can confirm that kinematic eddy viscosity is smaller than conventional model near the boundary of vegetation zone and within the vegetation area because the turbulence diffusivity exist only in the bed roughness boundary layer with vegetation. Conventional method kinematic eddy viscosity is distributed throughout the depth even in vegetated area. By using the present model, Reynolds stress also appear same tendency. Kinematic eddy viscosity and Reynolds stress is important parameter for discussion of sediment transport. The bed roughness boundary layer concept will affect kinematic eddy viscosity and Reynolds stress reasonably.

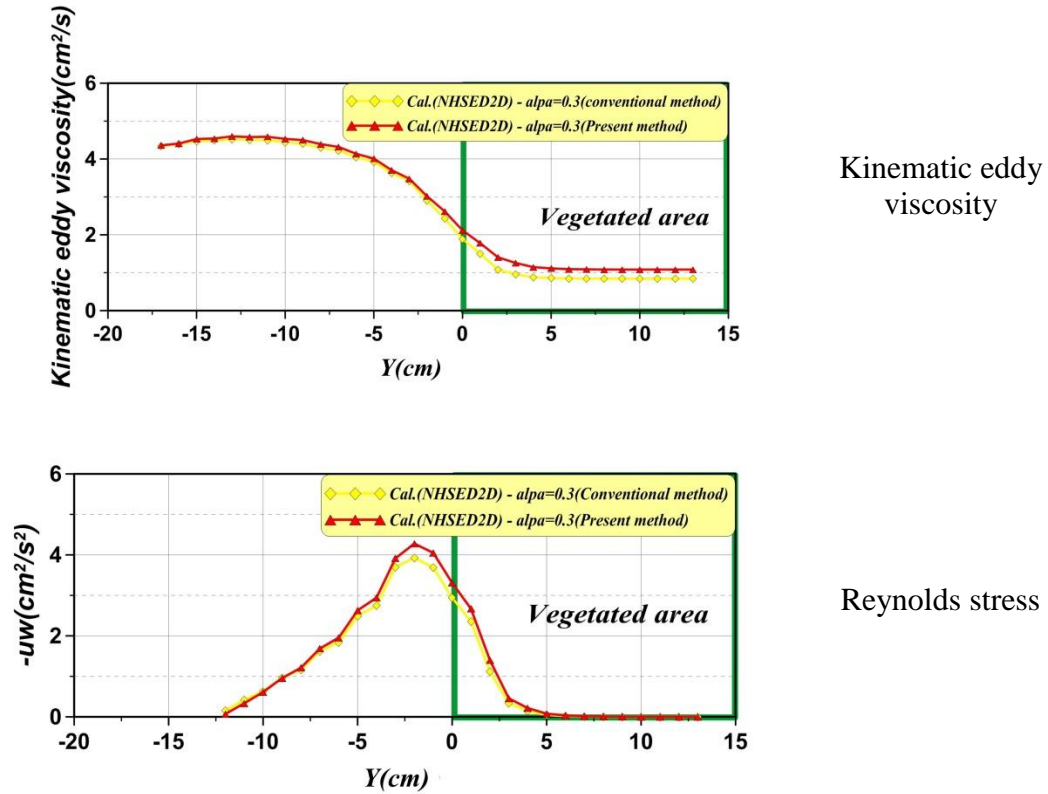
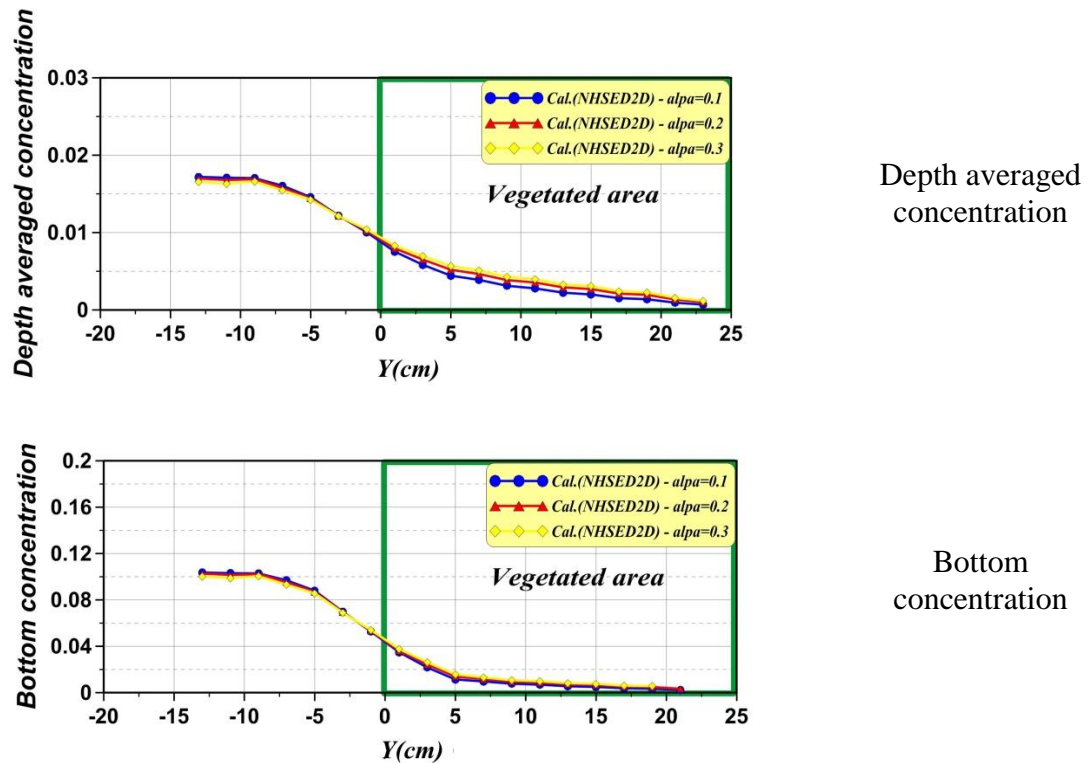


Fig. 6.6 Comparison of depth averaged velocity and friction velocity between conventional model and present model by using the ratio of the depth average and bottom concentrations based on BRBL concept

Fig. 6.6 shows Comparison of depth averaged velocity and friction velocity between conventional model and present model by using the ratio of the depth average and bottom concentrations based on BRBL concept. By using the present model we can confirm that kinematic eddy viscosity is larger than conventional model near the boundary of vegetation zone and within the vegetation area because the shear velocity by using bed roughness boundary layer concept is more faster than conventional model. By using the present model, Reynolds stress also appear same tendency. The present model by using the ration of the depth average and bottom concentrations based on BRBL concept will affect kinematic eddy viscosity and Reynolds stress reasonably.

6.4 Transverse distribution of depth-averaged concentration of suspended sediment in stream with vegetation

The transverse distribution of depth averaged concentration of suspended sediment with vegetation computed numerically. Fig. 6.7 shows Comparison of transverse distribution of depth averaged suspended sediment concentration regarding the change to transverse diffusion coefficient. The larger transverse diffusion coefficient tend to increase the depth averaged concentration, bottom concentration and Bottom concentration under equilibrium in the vegetated area because the larger transverse diffusion coefficient bring more larger kinematic eddy viscosity.



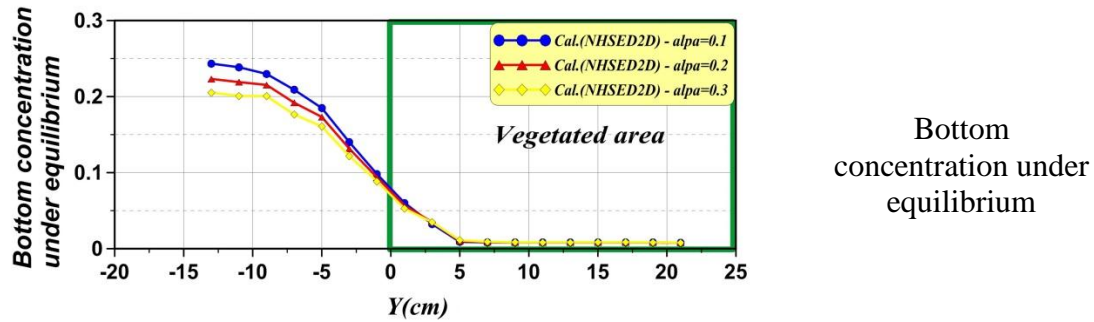
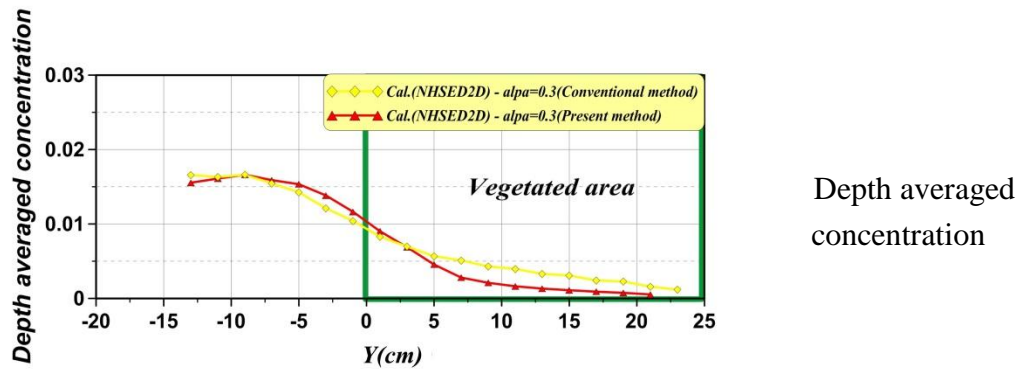


Fig. 6.7 Comparison of transverse distribution of depth averaged suspended sediment concentration (transverse diffusion coefficient 0.1-0.3)

Fig. 6.8 shows Comparison of transverse distribution of depth averaged suspended concentration between conventional model and present model by using the kinematic eddy viscosity based on BRBL concept.

By using the present model we can confirm that depth averaged concentration and bottom concentration is larger than conventional model near the boundary of vegetation zone. After that the present model is smaller than conventional model within the vegetation area. By using the present model, Bottom concentration under equilibrium is larger than conventional model because the shear velocity by using bed roughness boundary layer concept is more faster than conventional model.



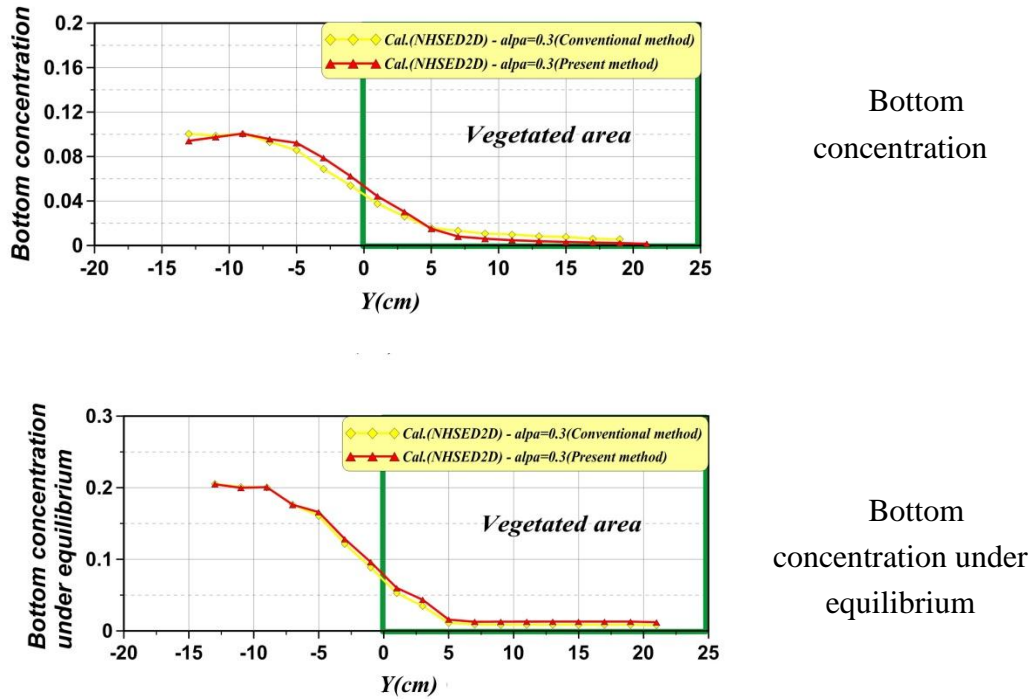


Fig. 6.8 Comparison of transverse distribution of depth averaged suspended concentration between conventional model and present model by using the kinematic eddy viscosity based on BRBL concept

Fig. 6.9 shows Comparison of transverse distribution of depth averaged suspended concentration between conventional model and present model by using the ratio of the depth average and bottom concentrations based on BRBL concept.

By using the present model we can confirm that depth averaged concentration is significantly smaller than conventional model within vegetation zone. By using the present model, bottom concentration is larger than conventional model Bottom concentration implied the lateral distribution of settling flux of suspended particles (C_{BW_o}) to cause the deposition on the bed. On the other hand, from the lateral distribution of shear velocity, the potential upward flux of suspension (C_{beW_o}) is evaluated. It is the maximum re-suspension if deposition on the rigid bed exists. By using the present model, bottom concentration under equilibrium is also larger than conventional model because the shear velocity by using bed roughness boundary layer concept is more faster than conventional model. The bed roughness boundary layer concept will affect reasonable evaluation of the shear velocity in vegetated area, bottom concentration and equilibrium bottom concentration of suspended sediment.

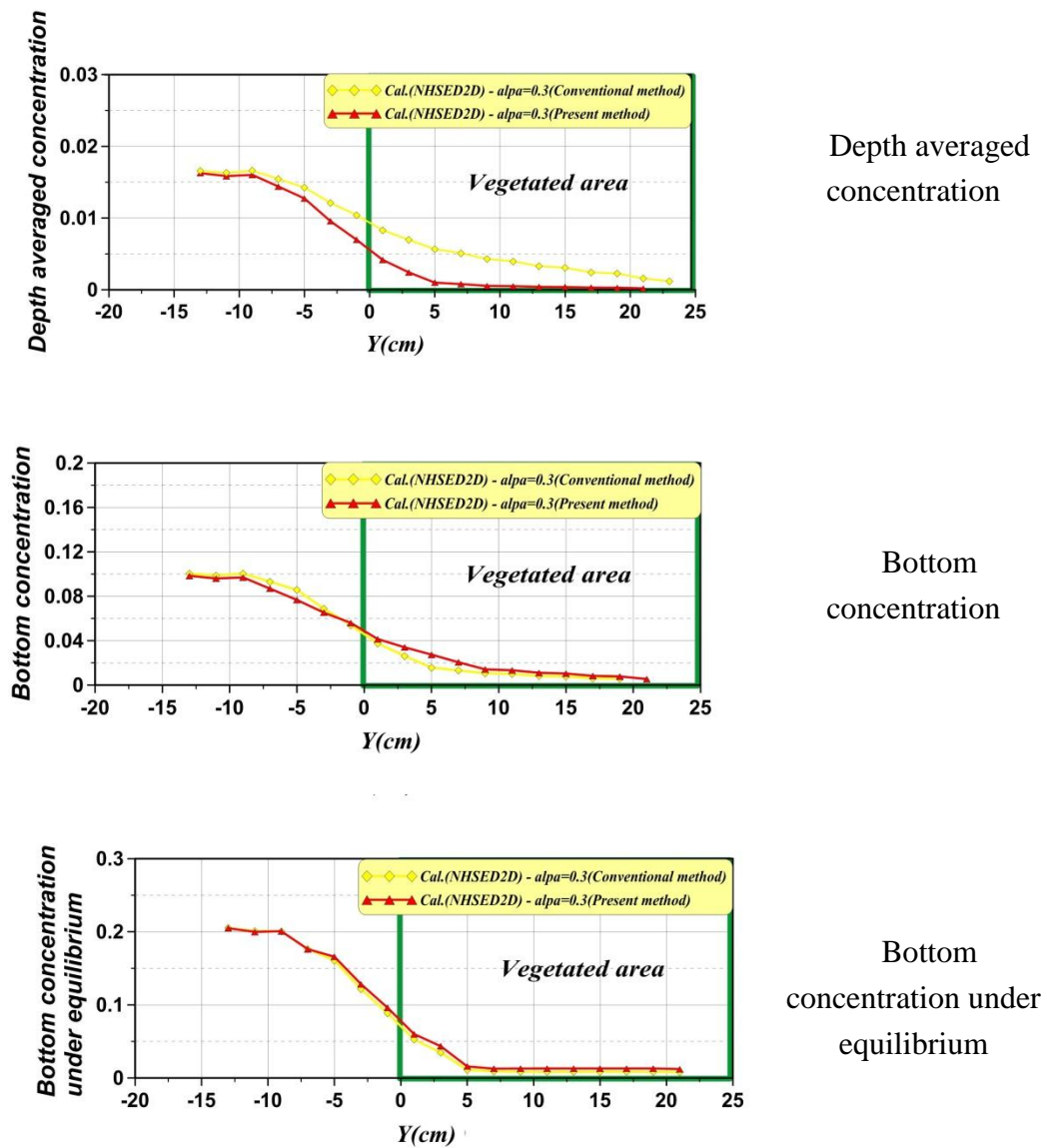


Fig. 6.9 Comparison of transverse distribution of depth averaged suspended concentration between conventional model and present model by using the ratio of the depth average and bottom concentrations based on BRBL concept

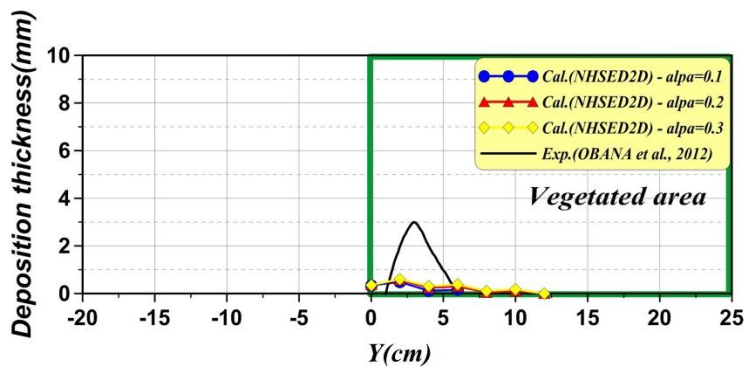
6.5 Suspended sediment transport deposition in vegetated area

In order to satisfy suspended sediment motion, fine sand ($d=0.25\text{mm}$, $\sigma/\rho=2.65$) is employed. Sediment were provided at 1m upper part from vegetated area with equilibrium state during 16 minutes. Suspended sediment transport can be described by the Equation (3.19).

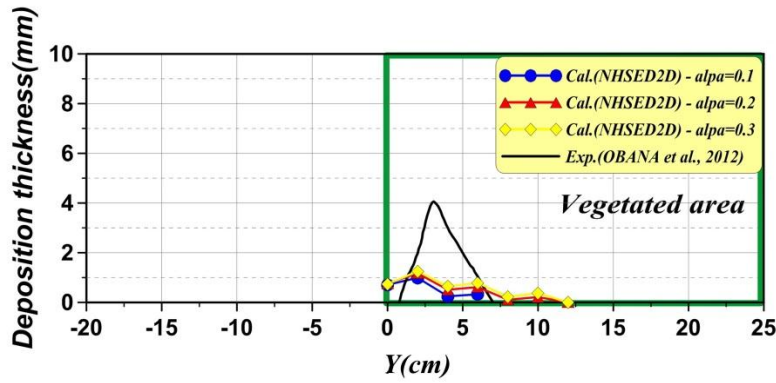
The lateral distribution of net deposition flux is calculated and it can be compared with the measured change of deposition thickness.

In Fig. 6.10, transverse profile of bed load deposition with time is depicted with the measured profile in the vegetated area at 4min, 8min, 12min and 16min after suspended sediment supply. Measurement section is determined at 5.3m point from the beginning of vegetation area. The calculated results, where we employed the conventional resistance law with changing transverse diffusion coefficient are compared with the measured data as shown in Fig. 6.10.

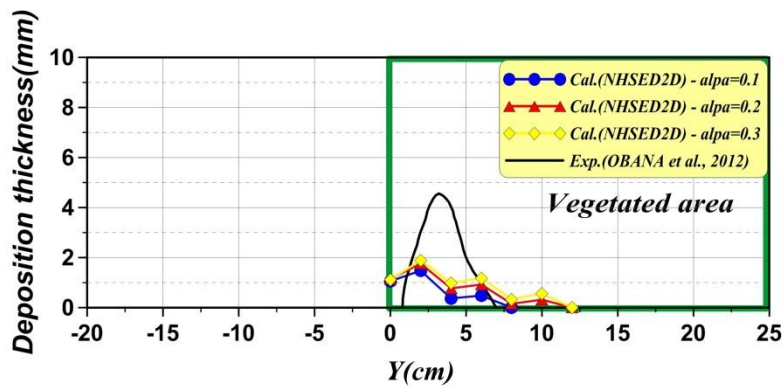
Zero point of X-axis indicate that vegetation boundary. Inside of vegetation zone represent from 0cm to 25cm. In the case of laboratory experiments, deposition occurs inside of the vegetated area. Numerical model also deposited inside vegetation but deposited sediment tend to progress inside a little more. These kinds of tendency is stronger being transverse diffusion coefficient increases.



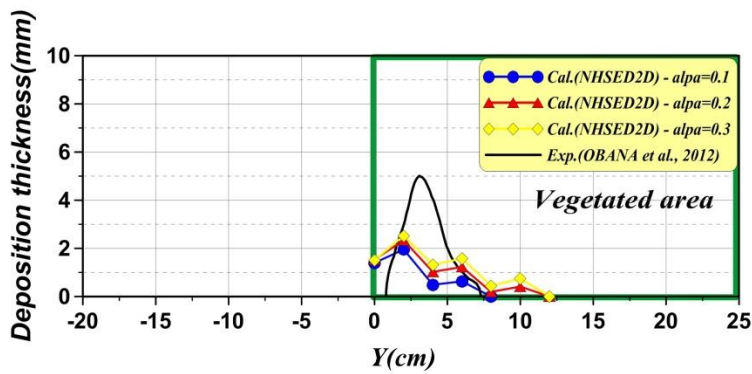
After 4min



After 8min



After 12min



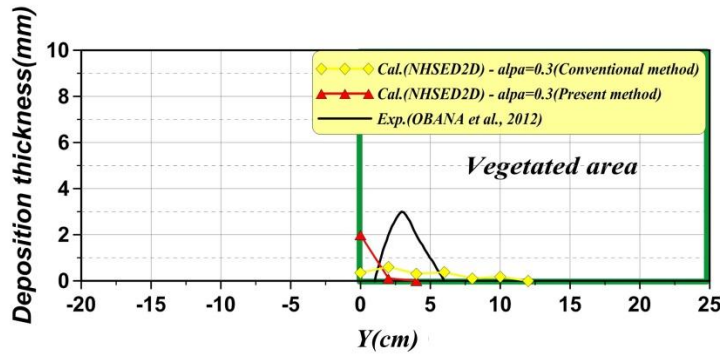
After 16min

Fig. 6.10 Comparison of sediment deposition thickness(transverse diffusion coefficient)

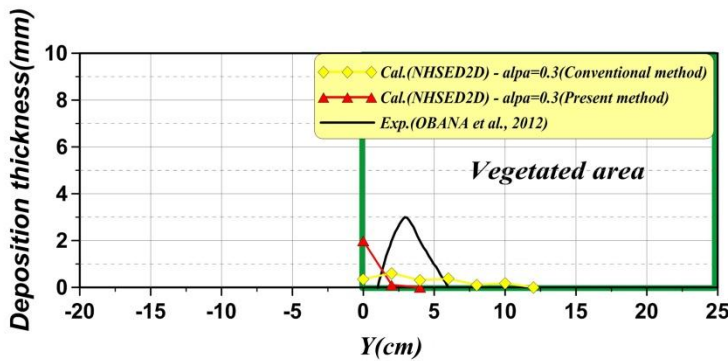
Fig. 6.11 shows comparison of sediment deposition thickness between

conventional model and present model by using the kinematic eddy viscosity based on BRBL concept. The calculated results, where we employed the conventional resistance law and the presently proposed one for the vegetated area, are compared with the measured data.

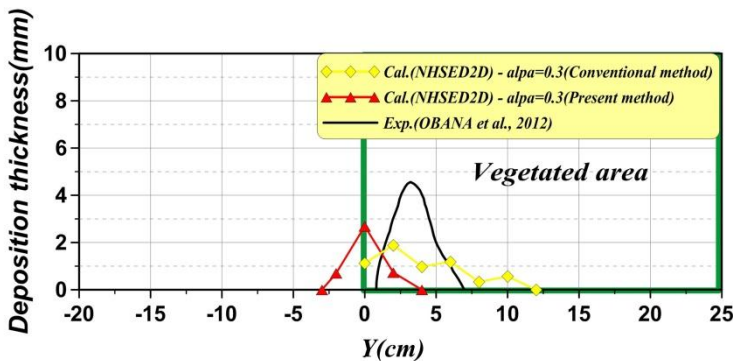
By using present model, the sediment deposition appear near the boundary of vegetation and deposition thickness appear higher than conventional model as time goes on.



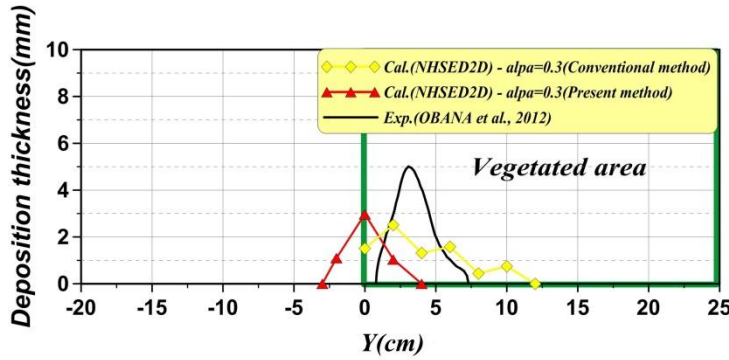
After 4min



After 8min



After 12min

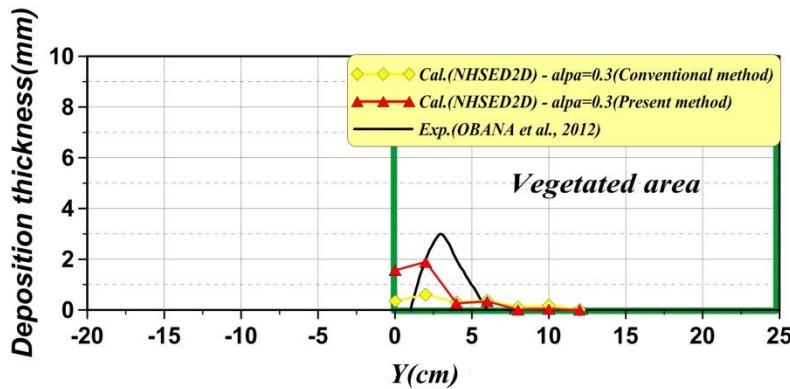


After 16min

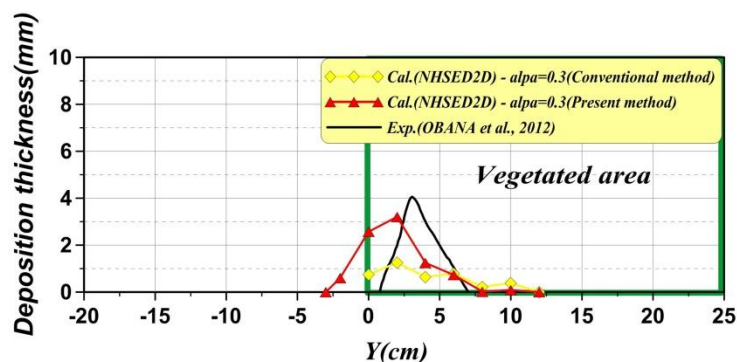
Fig. 6.11 Comparison of sediment deposition thickness between conventional model and present model by using the kinematic eddy viscosity based on BRBL concept

Fig. 6.12 shows Comparison of sediment deposition thickness between conventional model and present model by using the ratio of the depth average and bottom concentrations based on BRBL concept. The calculated results, where we employed the conventional model and the present model one for the vegetated area, are compared with the measured data.

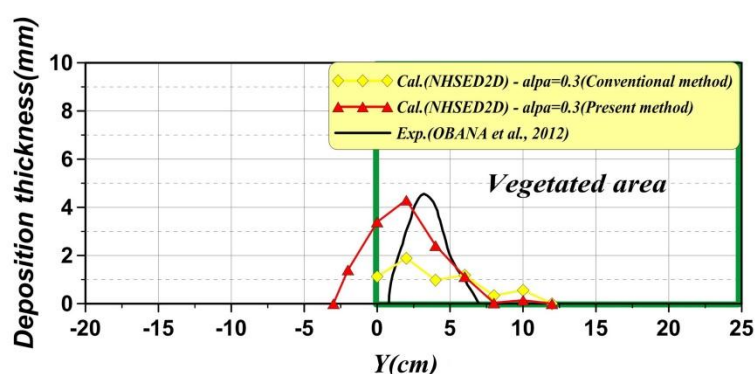
By using present model, deposition thickness appear higher than conventional model as time goes on. It was confirmed that the calculation result of the present model is to obtain a more accurate extend.



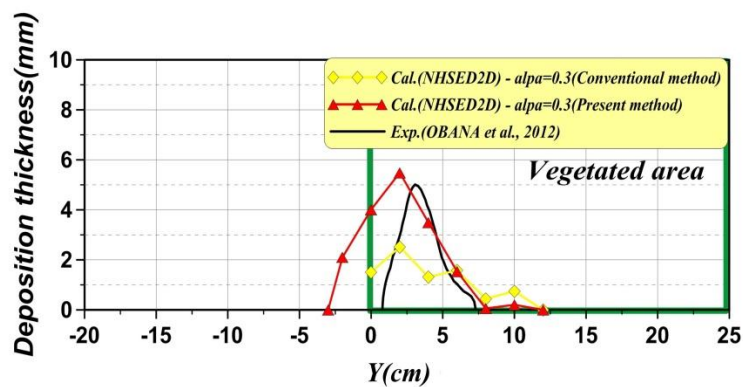
After 4min



After 8min



After 12min



After 16min

Fig. 6.12 Comparison of sediment deposition thickness between conventional model and present model by using the ratio of the depth average and bottom concentrations based on BRBL concept

6.6 Concluding Remarks

Along the 2D depth averaged model, the friction resistance law should be reasonably considered and the concept of “bed roughness boundary layer” has been proposed and formulated against the vegetation density. Based on this concept, the kinematic eddy viscosity and Reynolds stress has been discussed. It has brought the reasonable evaluation of the depth averaged concentration, bottom concentration and Bottom concentration under equilibrium as important parameter for discussion of suspended sediment transport. In addition, transverse profile of suspended sediment concentration has been discussed.

Based on the concept of bed roughness boundary layer, suspended sediment with vegetation can be discussed as below:

1. BRBL concept (bed roughness boundary layer) has been applied to 2D depth averaged analysis of flow with vegetation. Flow with vegetation has shear flow layer near the limited layer determined by vegetation parameter, and it governs the resistance law.
2. BRBL concept is applied to the suspended sediment concentration in vertical direction as similarly as the vertical velocity distribution. It gives the ratio depth averaged concentration and bottom concentration
3. BRBL concept governs bed shear stress and successively the kinematic eddy viscosity, diffusion coefficient of suspended sediment, entrainment rate of suspended sediment. Furthermore, it may governs the transverse mixing.
4. 2D depth averaged flow analysis with BRBL concept has been applied to the flow with vegetation zone, and the followings have been fairly discussed: transverse distributions of depth averaged velocity and depth averaged concentration of suspended sediment, bottom concentration and its equilibrium one, then the deposition rate.

References

1. Lopez F and Garcia M. (1998) Open channel flow through simulated vegetation: Suspended sediment transport modelling. *Water resour. Res.* 34(9) pp. 2341-2352.
2. Lopez F and Garcia M. (2001) Mean flow and turbulence structure of open channel flow through non-emergent vegetation. *J. Hydraul. Eng.* 127 (5) pp. 392-402.
3. Murphy, E., M. Ghisalberti, and H. Nepf. (2007) Model and laboratory study of dispersion in flows with submerged vegetation, *Water Resour. Res.*, 43, W05438
4. Nepf HM. (1999) Drag, turbulence, and diffusion in flow through emergent vegetation. *Water Resour. Res.* 35 (2) pp. 479-489.
5. Nepf, H., M. Ghisalberti, B. White, and E. Murphy. (2007) Retention time and dispersion associated with submerged aquatic canopies, *Water Resour. Res.*, 43, W04422
6. Sharpe, R. G., and C. S. James. (2006) Deposition of sediment from suspension in emergent vegetation, *Water SA*, 32(2), pp. 211-218.
7. Tsujimoto, T. and Kitamura, T. (1992) Appearance of organized fluctuations in open channel flow with vegetated zone. KHL- Commun., Kanazawa Univ., No.3, pp37-45.
8. Tsujimoto T and Shimizu Y. (1994) Flow and suspended sediment in a compound channel with vegetation. *Proc. 1st Int. Symp. on habitat Hydraulics*. Held in Trondheim, Norway, August. pp. 357-370.

CHAPTER 7

TRANSPORT OF POM WITH SEDIMENT

7.1 General

River landscapes are characterized by an interrelating system of flow, sediment transport, morphology and vegetation.

The transport and deposition of particulate organic matter (POM) in river streams has recently received much attention as one of important ecological processes in rivers.

It is known that particulate organic matter (POM) with sand particles in bed load and suspended load transported by flood are captured and deposited on sandbar with riparian vegetation. Capture of POM there must be significant in ecosystem (Vannote *et al.*, Cummins) and it is important to understand how POM drifts are different from sediment behavior in flow over the vegetated area, because it reversely influences the vegetation productivity and supports the diversity through riverine bio-geochemical processes.

We focused on interacted behaviors of sand particles in bed load and POM in vegetated area on sand bars. The purpose of this study is to clarify the characteristics of deposition of POM with bed load on sandbars with the riparian vegetation. A basic experiment on POM transport and deposition with vegetation is conducted in a laboratory flume. It demonstrates that several issues still remain to be future investigated. In particular, the shear due to the bed roughness in the vegetated area and the transport and deposition process of sand particles and POM are required to be described by the proper modeling which will be introduced into a simulation model of various fluvial processes. The purpose of this study is to clarify the deposition mechanism of POM in consideration of the influence of sediment transport in the riparian vegetation, and to develop the model of POM behavior based on the deposition mechanism. Thus, field observation and laboratory experiment were

conducted, and then a modeling necessary in numerical calculation was also conducted.

The main results of this study are that ripples are formed by bed load in riparian vegetation and POM deposition is promoted by ripple behavior. Based on these results, the POM deposition with ripples in vegetated area is described by a conceptual model which will affect various aspects in ecosystem management based on fluvial processes.

7.2 Field observation

7.2.1 Overview of field observation

An investigation was conducted on the Yahagi River (Chubu region, Japan). To evaluate the deposition characteristics of sediments and POM on sandbar with riparian vegetation in a field, we selected a conspicuous island sandbar covered with vegetation which is located in the right angle for the river flow at middle part of the river around 50 km from river mouth, as shown in Fig. 7.1.

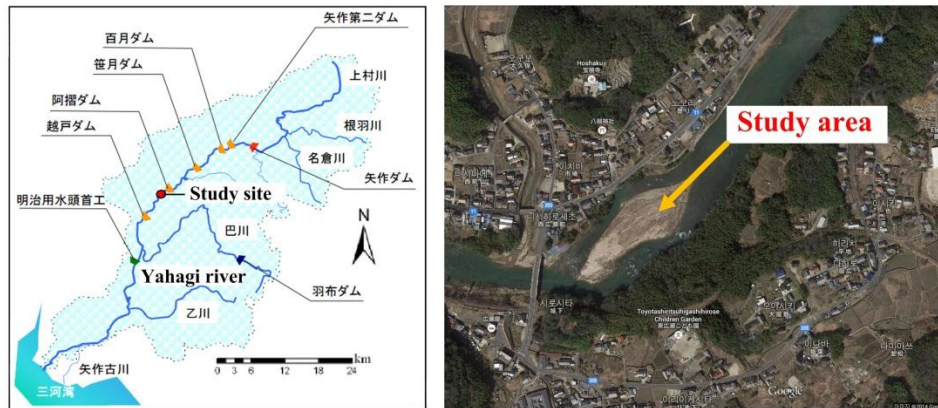


Fig 7.1 Investigation site in yahagi river

The longitudinal length of sandbar was around 300 m, the cross sectional length was around 100 m and the average bed slope was 1/150. The whole sandbar is submerged during flood. The bed was composed mainly cobbles and boulders as basement rock. And coarse sand mixed with fine sand and gravels transported by flood were covered thickly on the basement rock. An herbaceous plant occupied the

whole sandbar. The investigation was conducted for two days on October, 2011 during normal flow stage. Tasks included measuring the topography of sandbar and the thickness of sediment deposition layer, observing the spatial distribution of vegetation, analyzing the grain size distribution of deposited sediments and the quantity of particulate organic matters contained the deposited sediments. As for the observation of vegetation, the height and density of vegetation were measured after extracting representative plant community in whole sandbar. The thickness of deposition layer was measured the height from the top of basement rock to the top of fine sand layer by using a soil auger at 15 locations in the target sandbar (see Fig. 7.2).

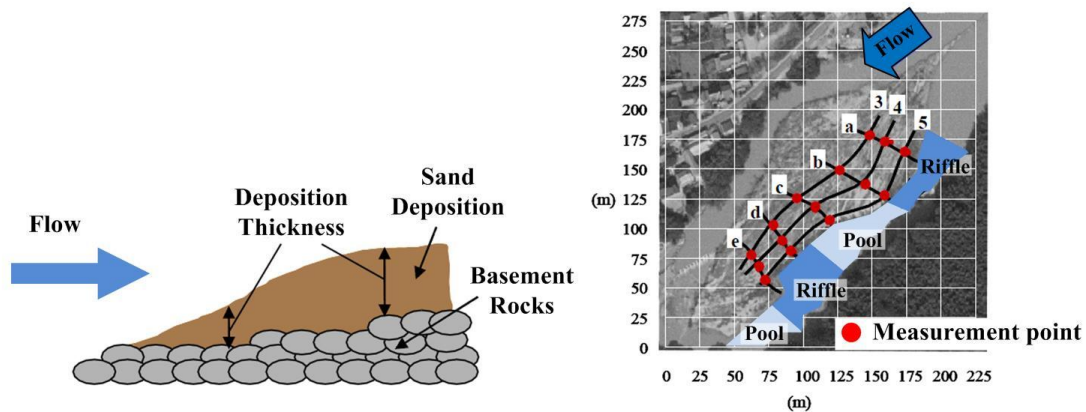


Fig. 7.2 Overview target sandbar

7.2.2 Deposition characteristic in the field

The whole sandbar was covered with 4 kinds of herb plant, especially reed and amur silver-grass were mainly occupied on sandbar. Fig. 7.3 indicate that the elevation difference of sandbar. Elevation difference increase from upstream toward center of sandbar. It is shaped like a mountain which elevation difference appears to become smaller toward downstream. The largest part of elevation difference is slightly below the center of sandbar. Variation of elevation difference appeared gently at the upstream and downstream. However, Variation of elevation difference appeared rapidly at the center of sandbar. The Variation value of elevation difference is from 0m to 2m at the center of sandbar.

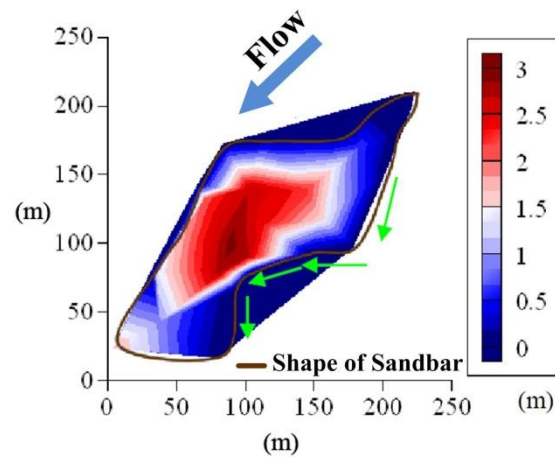


Fig. 7.3 Elevation difference of sandbar

The Fig. 7.4 shows the deposition thickness in sandbar. The deposition thickness is the highest slightly backward from center of sandbar. It is possible to surmise that this deposition phenomenon is caused the deceleration of flow velocity by vegetation worked the resistance of longitudinal water flow. The result of relative height of sandbar showed same tendency to be high at backward from center (4-d point) of sandbar, become slowly low from top to downstream part in sandbar.

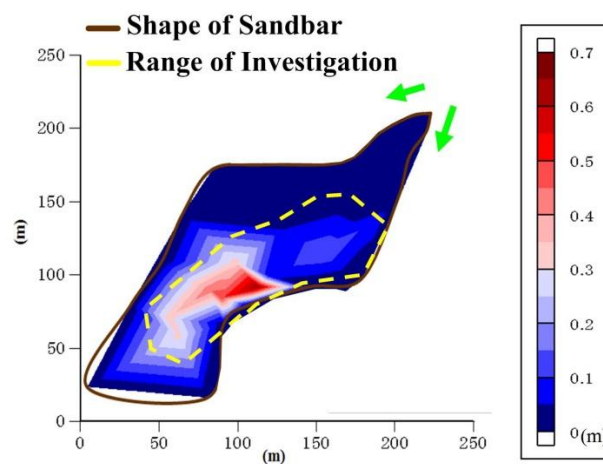


Fig. 7.4 Deposition thickness of sandbar

Fig. 7.5 shows the spatial distribution of grain size (d_{50}) that extracted at 15 locations as shown in Fig. 7.2. The grain size of deposited sediment in longitudinal direction was coarse in upstream part, became finer from up to downstream part of sandbar. Their distribution in transverse direction was coarser in water-line than inland part as same tendency with longitudinal direction.

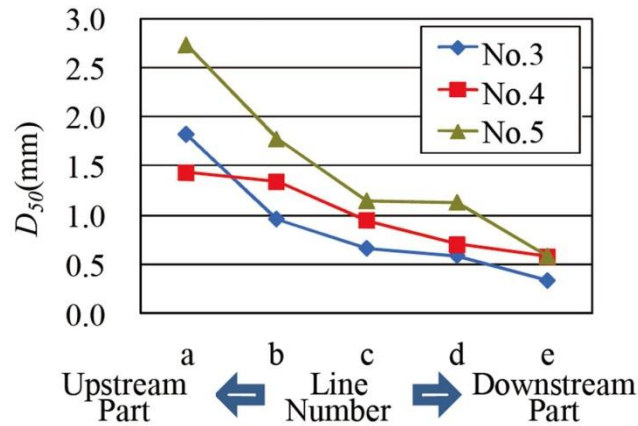


Fig. 7.5 Spatial distribution of grain size in sandbar

Fig. 7.6 shows the spatial distribution of POM content according to grain size as one example. The POM content become increasing from upstream to downstream part.

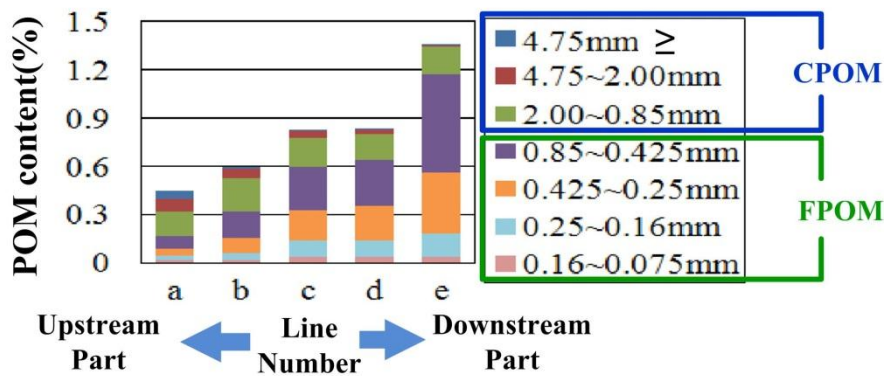


Fig. 7.6 Spatial distribution of POM content according to grain size

Details of POM content shows that upstream part of sandbar are mainly composed of CPOM, on the other hand FPOM is mainly deposited at downstream part. The reason why POM size smaller than 0.16mm did not deposited is that flood transported all of them.

7.2.3 Sedimentation test

We checked the deposition movement and specific weight by conducting the sedimentation test for each sample such as sand and POM. The sample is taken from sediments can be separated particulate organic matters were used. Separated particulate organic matter is mainly piece of wood.(Fig. 7.7)

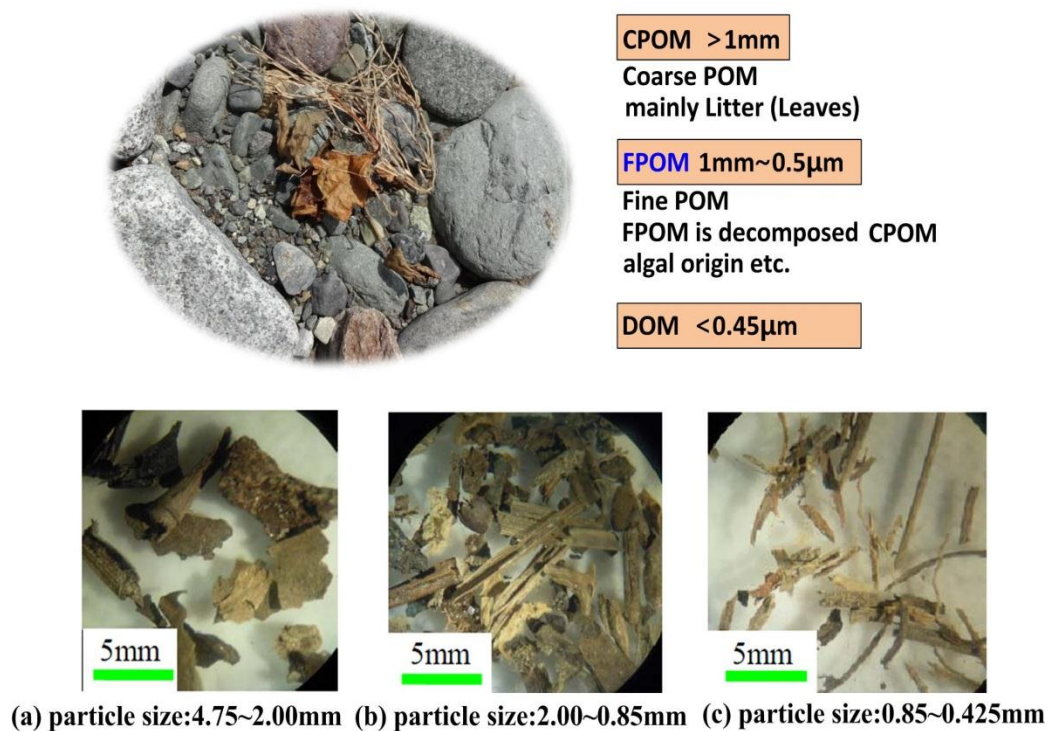


Fig. 7.7 Particulate organic matter by particle size

Overview of the sedimentation test shows Fig. 7.8.

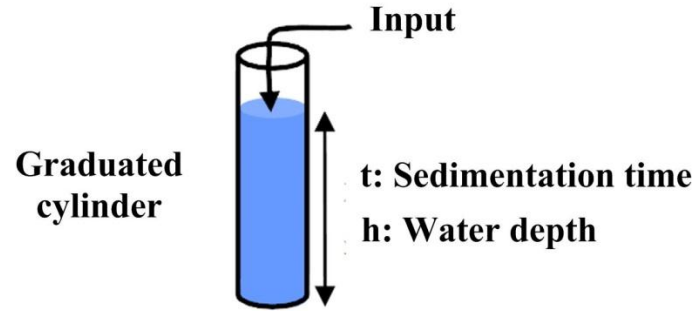


Fig. 7.8 Overview of the sedimentation

First, fill the graduated cylinder with water and then particulate organic matter put into the graduated cylinder. Sedimentation velocity(w_f) was determined by measuring sedimentation time and depth. The density was calculated using the Equation (7.2) has been altered Equation (7.1).

$$\frac{w_f}{\sqrt{sgd}} = \sqrt{\frac{2}{3} + \frac{36v^2}{sgd^3}} - \sqrt{\frac{36v^2}{sgd^3}} \quad (7.1)$$

$$s = \frac{3}{2} \left\{ \left(\frac{w_f}{\sqrt{gd}} = \sqrt{\frac{36v^2}{gd^3}} \right)^2 - \sqrt{\frac{36v^2}{gd^3}} \right\} \quad (7.2)$$

Where, w_f : Sedimentation velocity(cm/s), s : Underwater specific gravity, v : Kinematic eddy viscosity(=0.0114cm²/s, 15°C), d : Particle size, g : gravitational acceleration.

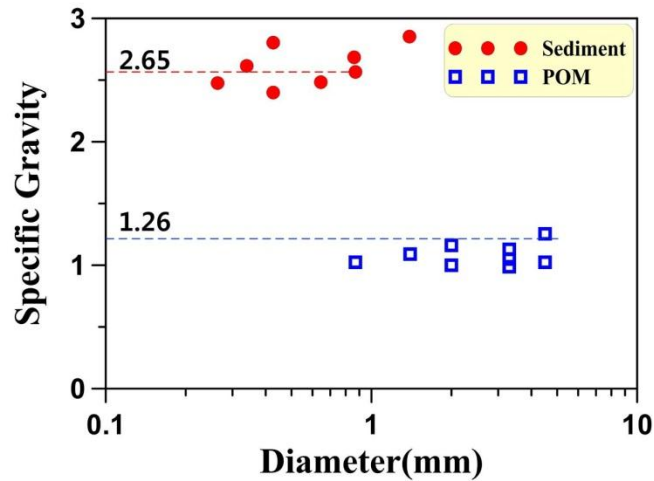


Fig. 7.9 Measurement of specific gravity

Fig. 7.9 shows result of sedimentation test. The experiment seemed to be accurately achieved because specific gravity value appeared around 2.65. Specific gravity of particulate organic matter is distributed from 1.02 to 1.26.

The movement mechanism of POM in sinking process is completely different from sediment. Sediment was sunk rapidly in a group however POM moved flutteringly and sunk slowly from top to the bottom of water. It is clear that the movement mechanism.

As mentioned above, the summary of these results of field survey is that classification of sediment and POM deposition by their size is occurred in longitudinal and transverse direction. In particular, POM deposition has a direct influence of sediment deposition.

7.3 Deposition process of POM transported with sand

7.3.1 Flume experiment

Flume experiment was conducted to understand the deposition mechanism of POM, especially CPOM such as vegetation seeds, litters was selected as our target in this study. In the laboratory, a model vegetation made by a group of cylinders made of bamboo arranged in staggered pattern ($D = 0.25 \text{ mm}$, $\lambda = 0.25 \text{ cm}^2$) was set in the interval of 5 m in a flume 20 m long and 0.5 m wide with the constant slope as shown in Fig. 2.3. The bed was rigid.

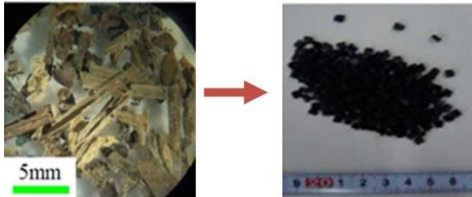
Firstly, the flow measurements (U and h) were conducted along the centerline of the flume (Obana *et al.* 2012). Shear velocity (u_*) is also important factor for an analysis of sediment transport. The form drag is predominant and velocity profile is uniform along the depth in flow with non-submerged vegetations only except the thin layer near the bed where the boundary layer is developed to bring a shear flow. Thus, after measuring the velocity near the bed with and without vegetated area respectively, shear velocity of vegetated area (u_{*v}) was deduced based on the assumption under the assumption of the similarity in the ratio of the velocity near the bed (u_b) to the shear velocity between with and without vegetated area (see Table 7.1). In this table, numerical subscripts 0 and v of shear velocity u_* , velocity near the bed u_b , indicates a value of non-vegetated area and vegetated area respectively. The result of this method is confirmed with the theoretical discussion on bed roughness boundary layer (Jeon *et al.* 2014).

Table 7.1 Experimental condition

$Q(cm^3/s)$	I_b	I_f	$h_0(cm)$	$u_{*0}(cm/s)$	$u_{*v}(cm/s)$	$u_{b0}(cm/s)$	$u_{bv}(cm/s)$
6940	1/150	1/185	3.5	4.3	2.3	14.0	7.4

Then, the condition of sand and coarse POM (CPOM) was selected as shown in Fig. 7.10 where d = diameter, σ , ρ = mass density of sand and water. The presumed amounts of them were fed at 1m upstream of the vegetated area with constant volume along the width.

	$d_{50}(cm)$	σ/ρ	W0(cm/g)
Sand	0.025	2.65	3.13
CPOM (usingPVC)	0.15	1.26	5.5



CPOM
Model CPOM(PVC)

Fig. 7.10 Detail of each experimental sample

As for CPOM model, we selected PVC(polyvinyl chloride) controlled the specific weight ($d = 0.15$ cm, $\sigma/\rho = 1.26$). Each supplied sand and POM rate was 0.047 cm²/s and 0.06 cm². At 20 minutes after sediment supply, water is stopped and then deposition of sand and POM in the vegetation area was measured along the centerline in the vegetated zone. Two kinds of experimental cases were run to observe

respective fluvial processes of sand and POM. In Case-1, only sand was supplied, while in Case-2 both sand and CPOM were supplied. Movement condition of respective sand and CPOM is changed with/without vegetation; however, they were transported as bed load under this hydraulic condition.

7.3.2 Deposition process of POM Transported with Sand

Fig. 7.11 shows comparison of deposition thickness of sand and CPOM between Case-1 and Case-2 at 1200 seconds after the experiment starts. We observed that sand deposition was occurred even upstream of the beginning of vegetation area in both of cases, and sand was deposited into wavelike fashion along to longitudinal direction.

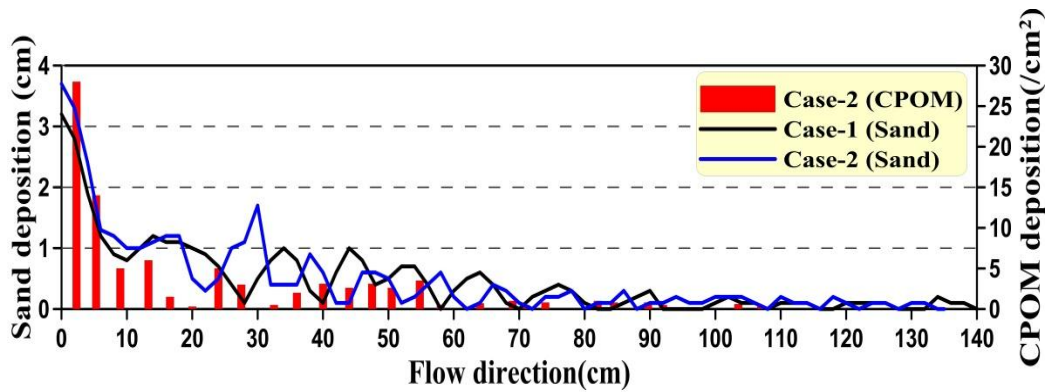


Fig. 7.11 Comparison of deposition state between Case-1(Sand) and Case-2(Sand+CPOM) at 1200 seconds after the experiment starts

It was judged “ripples” by the figure in the book of Yalin (1977) which are prepared by overlaying the formation area of ripples and dunes on Shields diagram. Ripples were formed by sediment transport and propagated to downstream with time progress. In contrast, CPOM had never deposited when it was transported by itself in vegetated area. However it was captured and deposited with the progress of ripples due to the both of interactions. The 77% of all CPOM supply was deposited in vegetated area with sand deposition.

The CPOM deposition mechanism with sand is as follows; 1) firstly fine sand forms ripples; 2) CPOM is deposited behind the crest of ripple, and then, fine sand is deposited and covered on CPOM deposition; 3) finally new CPOM is coming and deposited behind shifted crest of ripple. These steps are then repeated.

In Fig. 7.12, we can confirm that CPOM deposition is increasing and propagating with the development of ripples. CPOM deposition amount was measured at representative point in vegetated area as shown in Table 7.2.

Table 7.2 Measured CPOM deposition amount at representative point(Case-2)

x(cm)	X=40	X=50	X=60
CPOM deposition amount(/cm ²)	14.25	6.50	3.00

By measuring each parameter of ripples at measuring section ($x = 30-60\text{cm}$), the averaged wave length of ripple was about 9-10cm ($L_d = 360-400$), and wave height was 0.45 - 0.65cm. And it was clear that each parameter of Case-2 was decreased because of CPOM which was reduced the development process of ripples by disturbing sand supply from upstream as shown in Table 7.3.

Table 7.3 Comparison of wave length, height and propagation velocity of ripple($x=40-60\text{cm}$)

X=40-60cm	Case-1	Case-2
Wave length: L(cm)	10	9
Wave height: H(cm)	0.65	0.45
Propagation velocity: $U_w(\text{cm/s})$	0.021	0.019

7.4 Modeling of POM deposition with ripple

7.4.1 Model concept

The flume experiment made it clear that CPOM was captured behind the crest of ripple by separation vortex, then they were deposited and buried in ripples with time progress. Bed load transport can be described by the formula proposed by Ashida & Michiue (1972), and written as Equation (3.15).

This equation has a dimensionless form, and it may be applied for the various particles which have each different size and relative density (σ/ρ).

The Equation (3.15) is consisted of two kinds of important factors of bed load motion such as sediment number density v_g and particle velocity u_g as follows Ashida

& Michiue (1972).

$$v_g d^2 = \frac{1}{A_3 \mu_R} (\tau_* - \tau_{*c}) \quad (7.3)$$

$$\frac{u_g}{u_*} = \phi_d \left(1 - \sqrt{\frac{\tau_{*c}}{\tau_*}} \right) \quad (7.4)$$

Bed load transport rate has the following relationship with the above two kinds of factors.

$$q_B = v_g u_g A_3 d^3 \quad (7.5)$$

where A_3 = geometrical coefficient of sand; μ_R = friction coefficient of sand (0.4)
 $\phi_d = 6.8$ (constant); τ_* = dimensionless tractive force; and τ_{*c} = critical tractive force.

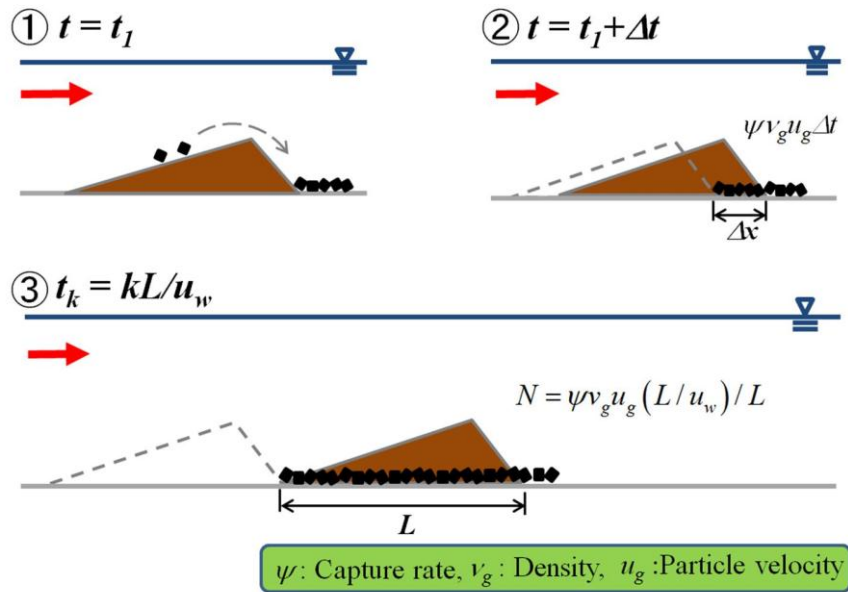


Fig. 7.12 Concept of deposition process of CPOM with ripple.

The CPOM particles transported to the lee side of crest of ripple can be described by using the accumulation of supplied number density v_g , particle velocity u_g and

capture ratio ψ During the 1st step of time progress(Δt), CPOM is captured by the trough of ripple ($\psi v_g u_g \Delta t$), and number of ripple will be increased toward downstream part ($t_k = kL/U_w = k\Delta t$, k : number of ripple) according to the sand deposition.

They are buried and deposited along the longitudinal direction (Δx) while the ripple migrate one wave length. Thus, CPOM is deposited on a straight line which is connected with the trough of ripple (see Fig. 7.12). And then, temporal change of CPOM deposition amount can be calculated at representative point of vegetated area ($x_j = x_0 + jL$ ($j=1 \sim k$)) according to each time step.

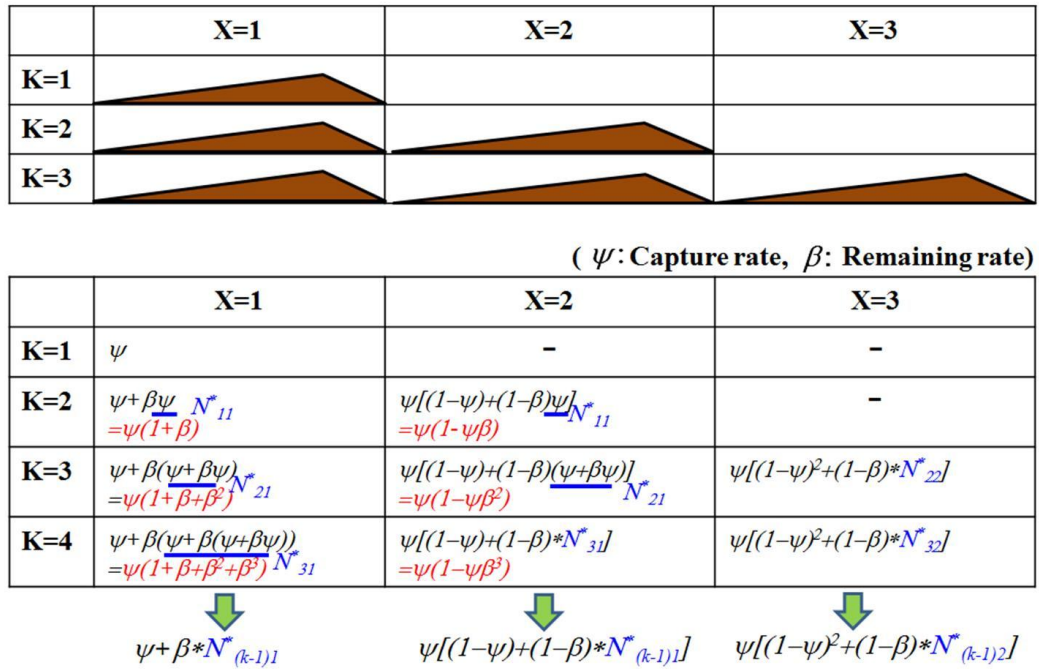


Fig. 7.13 Model concept of CPOM deposition process with ripple.

Accumulated deposition of CPOM (in number) N_{kj} from x_1 to x_j along longitudinal direction according to the temporal change t_k could be calculated as shown in Fig. 7.13. When a first ripple is formed ($t = t_1$), the accumulated amount of CPOM at representative point (x_1) is evaluated by ($N_{11}^* = \psi(N^* = N/[v_g(u_g/U_w)])$). As for the second step ($k = 2$), two ripples are formed. Accumulated amount of CPOM N_{21}^* is described with sand re-entrainment according to ripple migration presented as the capture ratio ψ and the residual rate β written as follows ($N_{21}^* = \psi(1 + \beta)$). At the same

time, N_{22}^* in ripple of downstream part is described as $\psi(1 - \psi\beta)$.

As above mentioned, we can calculate the temporal and spatial distribution of CPOM deposition with interaction of ripple by using the conceptual model.

7.4.2 Simulation of CPOM deposition and comparison with flume experiment

Fig. 7.14 shows the comparison between calculated and evaluated results of CPOM deposition by using the conceptual model we proposed. The temporal and spatial change of CPOM deposition amount was calculated by using the proposed model on the basis of assumption of $\psi = 0.7$, $\beta = 0.4$. Ripples were formed at 500 seconds intervals ($t_k = kL/U_w = k\Delta T$, $L=10\text{cm}$, $U_w = 0.02\text{ cm/s}$) based on our experimental results. Bar graph represents the calculated CPOM deposition amount N^* for every time during 2000 seconds at representative point of vegetated area ($x_j = x_0 + jL$ ($j=1\sim k$), $x_0=30\text{cm}$, $L=10\text{cm}$).

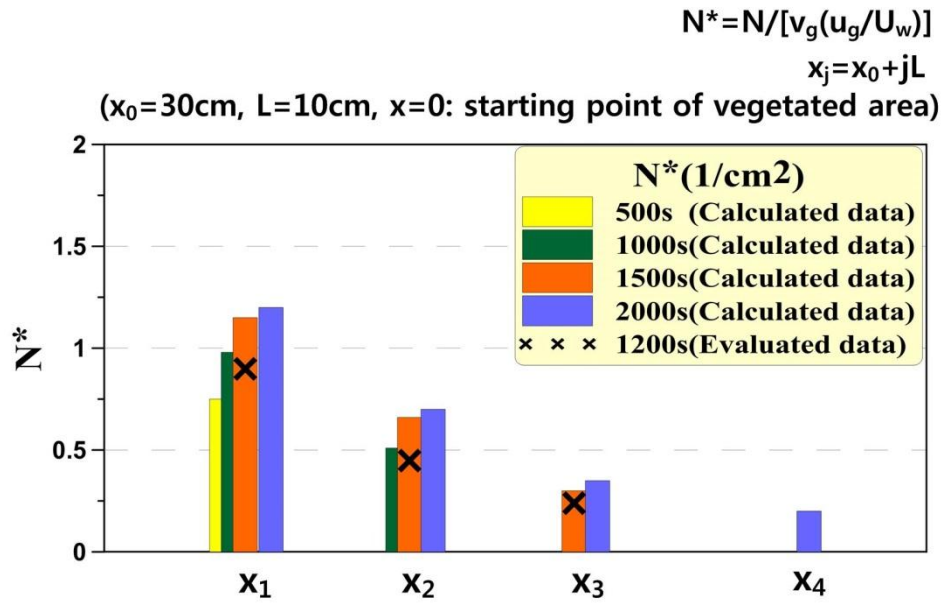


Fig. 7.14 Comparison between calculated and evaluated results of CPOM deposition.

The point of CPOM deposition is propagated in the downstream direction with the migration of ripples according to time progress. And CPOM deposition amount at

each point is increased with the development of ripples, and propagated to the downstream. These characteristics of CPOM deposition were represented well by our calculation as shown in Fig. 7.14.

X marks in the figure represent the evaluated CPOM deposition amount by using the measured experimental data of CPOM deposition amount at 1200 seconds after the flume experiment starts. They are evaluated by using the relationship between several factors of ripple migration and bed load transport rate based on the following equation ($N^* = N[v_g(u_g/U_w)]$) and these each value of $U_w=0.02\text{cm/s}$, $u_g=5\text{cm/s}$ (estimated by Equation (7.3)) $v_g= 0.06\text{cm}^2$ (calculated based on the supplied POM ratio and u_g), N (measured CPOM deposition amount by flume experiment, see Table 7.2). The figure shows the comparison of the evaluated results at 1200 seconds with the calculated results with time progress. The calculated value agrees well with the evaluated value. Therefore, our conceptual model is effective to understand the general tendency of temporal and spatial change of CPOM deposition as shown in Fig. 7.14.

7.5 Concluding Remarks

In this chapter, our efforts have highlighted on evaluation of POM deposition on sandbar which is characterized by vegetated area and fine sand deposition there. We investigated the deposition mechanisms of sediment and POM through a field observation.

First, deposition mechanisms of sediment and POM by the field observation can be described as below.

1. Investigation was conducted on Yahagi river(Chubu region, Japan). We selected a conspicuous island sandbar covered with vegetation. The whole sandbar is submerged during flood. The bed was composed mainly cobbles and boulders as basement rock. Tasks included measuring the topography of sandbar and the thickness of sediment deposition layer, observing the spatial distribution of vegetation, analyzing the grain size distribution of deposited sediments and the quantity of particulate organic matters contained the deposited sediments.
2. Elevation difference increase from upstream toward center of sandbar. It is shaped like a mountain which elevation difference appears to become smaller toward downstream. The largest part of elevation difference is slightly below

the center of sandbar.

3. Variation of elevation difference appeared gently at the upstream and downstream. However, Variation of elevation difference appeared rapidly at the center of sandbar.
4. Deposition thickness and relative height of sandbar is the highest slightly backward from center of sandbar. It is possible to surmise that this deposition phenomenon is caused the deceleration of flow velocity by vegetation worked the resistance of longitudinal water flow.
5. The grain size of deposited sediment in longitudinal direction was coarse in upstream part, became finer from up to downstream part of sandbar. Their distribution in transverse direction was coarser in water-line than inland part as same tendency with longitudinal direction.
6. The POM content become increasing from upstream to downstream part. Details of POM content shows that upstream part of sandbar are mainly composed of CPOM, on the other hand FPOM is mainly deposited at downstream part. The reason why POM size smaller than 0.16mm did not deposited is that flood transported all of them.

After the basic deposition characteristics were extracted by the field observation, We observed the deposition mechanisms by the laboratory experiment. The conclusions are summarized that ripples are formed by the bed load in the riparian vegetation. And CPOM is captured by through of ripples formed by the wave action.

In contrast, their multifunction of movement of both sample were decreased the propagation velocity of wave height and length of ripples. Then, POM behavior with ripples is described by a conceptual model which will affect other aspects in ecosystem management based on fluvial processes.

References

1. Ashida, K. and Michiue, M. (1972) Hydraulic Resistance of Flow in an Alluvia Bed and Bed Load Transport Rate. Proceedings of Japan Society of Civil Engineers,

- No. 206, pp. 59-69(in Japanese).
2. Cummins, K.W. (1974) Structure and Function of Stream Ecosystems. BioScience, 24, pp. 631-641.
 3. Jeon, H.S., Obana, M. and Tsujimoto, T. (2014) Concept of Bed Roughness Boundary Layer and Its Applicationn to Bed Load Transport in Flow with Non-Submerged Vegetation. Journal of Water Resource and Protection, 6, pp. 881-887.
 4. Obana, M., Uchida, T. and Tsujimoto, T. (2012) Deposition of sand and Particulate Organic Matter in Riparian Vegetation. Advances in River Engineering, 18, pp. 47-52(in Japanese)
 5. Vannote, R.L., Minshall, G.W., Cummins, K.W., Sedell, J.R. and Cushing, C.E. (1980) The River Continuum Concept. Canadian Journal of Fishery and Aquatic Science, 37, pp. 130-137.
 6. Yalin, M.S. (1977) Sediment Transport. 2nd Edition, Pergamon Press, New York, Chapter 7, pp. 209-267.

CHAPTER 8

GENERAL SUMMARY AND CONCLUSIONS

8.1 General

In order to manage river from the viewpoints of flood mitigation, water resources utilization and ecosystem conservation, river flow and morphological changes there would be fairly understood and reasonably described.

Especially vegetation plays an important role in fluvial processes, and fluvial processes in streams with vegetation have become hot topics in river hydraulics. Because it significantly affects flow, sediment transport and bed morphology, while morphology governs growth and decay of vegetation with flow regime. Better understanding flow processes provided by vegetation in the stream requires detailed flow structure. So there have been many hydraulic and numerical model tests and field trips to understand the hydrodynamic and morphodynamic characteristics of vegetation zone by many researchers.

To date, many kinds of research have been performed to analyze hydrodynamical and geomorphological characteristics of riparian vegetation zone, but several issues remained. Thus, this research conducted field observation, experimental and numerical studies to understand 2-D hydrodynamic and morphodynamic characteristics of vegetation.

For experimental research, a model vegetation made by a group of cylinders made of bamboo arranged in staggered pattern was set in the interval of 5m in a flume 20m long and 0.5m wide with the constant slope.

For numerical research, 2-Dimensional numerical model made by Nagoya hydraulic, which is able to simulate flow fields vegetation bed variation interaction directly, is used to investigate fluvial process and mechanics of sediment transport in vegetated area.

To verify the newly developed numerical model, existing hydraulic model test

results were compared with experimental results of this research.

In addition transport and deposition of POM(particular organic matters) including plants seeds were studied through experimental research.

8.2 Experimental studies

Flood mitigation and ecosystem conservation are simultaneously required in recent river management, and understanding and analysis of flow and river morphology in a stream with vegetation have become important topics in river hydraulics.

In this study, we investigated the deposition mechanisms of sediment and POM through a laboratory experiment. After we observed the deposition mechanisms by the laboratory experiment focusing on two kinds of empirical hydraulic processes.

Deposition mechanisms of sediment and POM by the laboratory experiment can be described as below:

8.2.1 Longitudinal transition in riparian vegetation

1. Sediment deposition was occurred at the beginning of vegetation area in both of cases. Ripples were formed by fine sand and propagated it with time progress. In contrast, CPOM is not deposited by itself in vegetated area but it deposited with fine sand.
2. Firstly fine sand formed ripples. CPOM is deposited behind mountain of fine sand. Second, fine sand is deposited on CPOM depositions, Finally new CPOM is coming and deposited behind mountain and the steps are then repeated.
3. Temporal change of wave length and height of each case at 40-60cm downstream part from the beginning of vegetation area was compared. The wave length is constant with time progress however the wave height is tend to develop.
4. In particular, the wave height of case 2 is lower than case 1 because the phenomena is caused by multifunction of sand and CPOM deposition. The decrease of wave height are affected by the quantity of fine sand transported into vegetation area whether CPOM exist or not.

5. According to comparison of the progress speed of wave length measured of each case. Case 1 was faster twice than case 2 because of the influence of CPOM deposited in trough of ripple.

8.2.2 Transverse dispersion in riparian vegetation

1. The movement of suspended sediment transport has good followability with fluid motion, hence it predominate in transverse dispersion into vegetation area. This is the reason why the deposition width of suspended sediment became twice as wide as bed load.
2. The wave action that caused the active movement of transverse dispersion could change the quantity of bed load in lateral direction. The proportion of suspended and bed load sediment in mixed sand deposited was 9 to 1. Moreover, the bed load was transported more wide than it was transported by itself.
3. Invasion rate of CPOM into vegetation area was measured. Their range of movement is expanded according to height of sediment deposition. The height and width of sediment deposition is developed with time progress, on the other hand tractive force to transport sediment and CPOM in lateral direction was decreased according to the development of ridge of sediment.
4. Deposition of FPOM is increased with coarser sand. FPOM are captured by porosity in sediment and deposited, in particular FPOM is tend to deposit at backward from the top of ridge of sediment.

8.3 Numerical studies

8.3.1 Development of numerical analysis method

To analyze hydrodynamic and sediment transport in vegetated area, 2D depth-averaged model was newly developed. The developed numerical model can be described as follow.

1. The numerical scheme adopted suspended sediment equations for analysis of

suspended sediment, based on existing numerical model (NHSED2D; Goto et al., (2002)).

2. 2-Dimensional numerical model, which is able to simulate flow fields-vegetation-bed variation interaction directly, is used to investigate fluvial process and mechanics of sediment transport in vegetated area.
3. Applications of 2D depth-averaged analysis have become very familiar, however, improper treatments for flow in vegetated area often brings inaccurate conclusion of the analysis.
4. To numerically consider bed roughness boundary layer in the vegetated area, It will affect other aspects in fluvial processes, which will be clarified successively.

8.3.2 boundary layer thickness

Recently, 2D horizontal depth averaged flow model becomes familiar to be recognized as powerful means of stream with vegetation by adding the form drag of vegetation. Though it is expected to apply fluvial process of streams with vegetation, the shear stress may be underestimated and fluvial process may not be properly described. We focused on the bed roughness boundary layer in the vegetated area(non-submerged vegetation) to deduce the resistance law in the vegetated area. Based on the concept of bed roughness boundary layer, fluvial process with full vegetation can be discussed as below:

1. The bed roughness boundary layer thickness θ_v is subjected to the characteristics of vegetation, and dimensional analysis suggests the relation between θ_v/h and λDh . The data obtained the measurements by Liu *et al.*
2. Velocity distribution in bed roughness boundary layer in the vegetated area is investigated, and logarithmic law is expected to be applied. Though the number of the data is small for each run, the shear velocity in the vegetated area, u_* , is evaluated by fitting the logarithmic law for each run, then the data of the all runs are plotted and depicted in the defect law expression. The velocity profile follows the logarithmic law though the number of the measured data for each run is very few.
3. The result of sensitivity analysis shows that if the rate of flow is small, water depth variation was almost same between conventional model and present model. However, the rate of flow increases, the water depth also increases in

the present model. The increase rate of water depth is largest in case of present model ($\lambda D=0.04$). The result of sensitivity analysis also shows that if the energy slope is small, the water depth was increased.

4. Sensitivity analysis depicts the relation $u^* \sim q$, which is more sensitive than $h \sim q$ or $U=q$. And, it suggests that the concept of bed roughness boundary layer should be inevitably taken into account in description of sediment transport and fluvial process in streams with vegetation.

8.3.3 Comparison with bed load deposition in decelerated area in vegetation

1. The calculation was conducted by using a program developed for horizontal 2D depth-averaged flow where the bed friction and the form drag due to vegetation are taken into account.
2. In the conventional way, Keulegan's equation is employed for both non-vegetated and vegetated areas. While, when the present method is applied, Equation (4.7), which is presently proposed for flow with non-submerged vegetation
3. Two kinds of method give good agreements between experimental data and calculated depth average velocity and water depth. The numerical model can accurately simulate the reduction of depth averaged velocity and increase of water depth with impact of vegetation.
4. As for the shear velocity, which has not directly measured in the experiment, the calculated one by the conventional model may be appreciably underestimated. The numerical results conducted by new method appear as if the vegetation density was to have a high value, shear velocity will become more faster.

Comparison of the bed deformation in the full vegetated area between the experimental data and the numerical results during time can be described as below:

1. The calculated results, where we employed the conventional resistance law and the presently proposed one for the vegetated area, are compared with the measured data. The present model can describe the deposition profile with the steeper downstream slope with the faster migration because of the higher value of the shear stress, and it shows better conformity with the experimental

result compared with the conventional model. Thus, it is concluded that introduction of the present proposal of the resistance law based on the concept of bed roughness boundary layer in vegetated area can bring accurate description of fluvial process in vegetated area.

2. According to the observation on the experiment, If only CPOM particle was supplied to the vegetation area, CPOM never deposited itself. Such as this tendency also appear that CPOM is transported and flushed away in each case of numerical analysis.

Based on the concept of bed roughness boundary layer, fluvial process with half vegetation can be discussed as below:

1. Vegetation reduced longitudinal depth averaged velocity. As we can see, Two kinds of method give good agreements between experimental data and calculated depth average velocity and water depth. The numerical model can accurately simulate the reduction of depth averaged velocity and increase of water depth with impact of vegetation.
2. The shear velocity in the non-vegetated reach, $u_{*0}=6.5\text{cm/s}$ was obtained by applying the equation $u_{*0}=\sqrt{gh_0I_f}$, while in vegetated reach, $u_{*v}=1.2\text{cm/s}$ as obtained by using the local velocity near the bed there and the ratio of the near bed velocity to the shear stress in non-vegetated area. the calculated one by the conventional model may be appreciably underestimated.

Comparison of the bed deformation in the full vegetated area between the experimental data and the numerical results during time can be described as below:

1. Transverse profile of bed load deposition with time is depicted with the measured profile in the vegetated area at 4min, 8min, 12min and 16min after sediment supply. Measurement section is determined at 5.3m point from the beginning of vegetation area. The calculated results, where we employed the conventional resistance law and the presently proposed one for the vegetated area, are compared with the measured data.
2. Zero point of X-axis indicate that vegetation boundary. Inside of vegetation zone represent from 0cm to 8cm. In the case of laboratory experiments, deposition occurs inside of the vegetated area. In order hand, in case of

numerical model, Bed load deposition appears on the outside of vegetation boundary. As time goes on, very small amount of sand came into inside of vegetation boundary.

3. The present model can describe the deposition transverse profile with more migration because of the higher value of the shear stress better than conventional model.

8.3.4 Comparison with transverse distribution in stream with vegetation

1. BRBL concept (bed roughness boundary layer) has been applied to 2D depth averaged analysis of flow with vegetation. Flow with vegetation has shear flow layer near the limited layer determined by vegetation parameter, and it governs the resistance law.
2. BRBL concept is applied to the suspended sediment concentration in vertical direction as similarly as the vertical velocity distribution. It gives the ratio depth averaged concentration and bottom concentration
3. BRBL concept governs bed shear stress and successively the kinematic eddy viscosity, diffusion coefficient of suspended sediment, entrainment rate of suspended sediment. Furthermore, it may governs the transverse mixing.
4. 2D depth averaged flow analysis with BRBL concept has been applied to the flow with vegetation zone, and the followings have been fairly discussed: transverse distributions of depth averaged velocity and depth averaged concentration of suspended sediment, bottom concentration and its equilibrium one, then the deposition rate.

8.3.5 Transport of POM with sediment

The field observation was conducted to clarify the deposition mechanism of POM behavior. Based on the field observation results, deposition characteristics of various POM with sand on sand bar with riparian vegetation in field can be discussed as below.

1. Investigation was conducted on Yahagi river (Chubu region, Japan). We selected a conspicuous island sandbar covered with vegetation. The whole sandbar is submerged during flood. The bed was composed mainly cobbles and boulders as basement rock. Tasks included measuring the topography of

sandbar and the thickness of sediment deposition layer, observing the spatial distribution of vegetation, analyzing the grain size distribution of deposited sediments and the quantity of particulate organic matters contained the deposited sediments.

2. Elevation difference increase from upstream toward center of sandbar. It is shaped like a mountain which elevation difference appears to become smaller toward downstream. The largest part of elevation difference is slightly below the center of sandbar.
3. Variation of elevation difference appeared gently at the upstream and downstream. However, Variation of elevation difference appeared rapidly at the center of sandbar.
4. Deposition thickness and relative height of sandbar is the highest slightly backward from center of sandbar. It is possible to surmise that this deposition phenomenon is caused the deceleration of flow velocity by vegetation worked the resistance of longitudinal water flow.
5. The grain size of deposited sediment in longitudinal direction was coarse in upstream part, became finer from up to downstream part of sandbar. Their distribution in transverse direction was coarser in water-line than inland part as same tendency with longitudinal direction.
6. The POM content become increasing from upstream to downstream part. Details of POM content shows that upstream part of sandbar are mainly composed of CPOM, on the other hand FPOM is mainly deposited at downstream part. The reason why POM size smaller than 0.16mm did not deposited is that flood transported all of them.

After the basic deposition characteristics were extracted by the field observation, We observed the deposition mechanisms by the laboratory experiment. The conclusions are summarized that ripples are formed by the bed load in the riparian vegetation. And CPOM is captured by through of ripples formed by the wave action.

In contrast, their multifunction of movement of both sample were decreased the propagation velocity of wave height and length of ripples. Then, POM behavior with ripples is described by a conceptual model which will affect other aspects in ecosystem management based on fluvial processes.

APPENDIX A

NUMERICAL ANALYSIS METHOD

A.1 General

The simple method is reported many kinds of manual. Appendix reported that because in this study made mention of slight modification about depth correction equation that can be obtained from depth-averaged continuity equation.

A.2 Discretization of basic equation

Discretization of basic equation is carried out by integrating control volume above the staggered grid as shown in Fig. a-1.

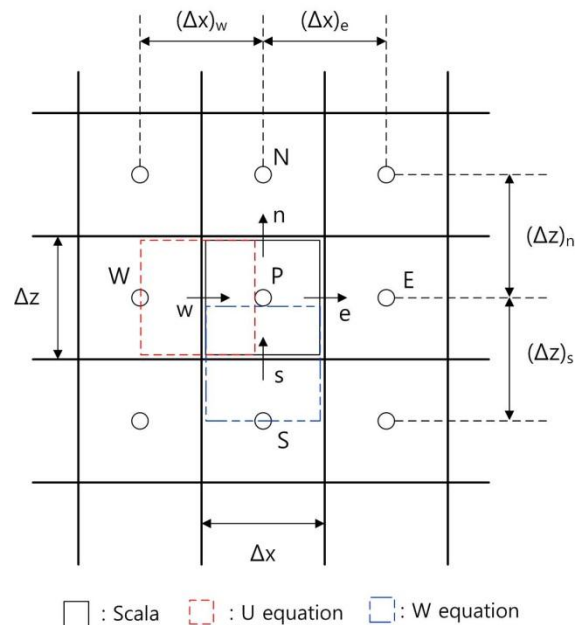


Fig. A.1 Staggered grid

The general conservation equation in the scala cell integrates in control volume.

$$\int_s^n \int_w^e \left[\frac{\partial}{\partial x} \left(\phi h U - h \Gamma \frac{\partial \phi}{\partial x} \right) + \frac{\partial}{\partial z} \left(\phi h W - h \Gamma \frac{\partial \phi}{\partial z} \right) \right] dx dz = \int_s^n \int_w^e S_\phi dx dz \quad (\text{A.1})$$

At this time, the following discretized equation is obtained by replacing volume with square measure.

$$\begin{aligned} \text{left side} = \Delta z & \left[h_e U_e \frac{\phi_E + \phi_P}{2} - \frac{h_e \Gamma_e (\phi_E - \phi_P)}{(\delta x)_e} - h_w U_w \frac{\phi_W + \phi_P}{2} + \frac{h_w \Gamma_w (\phi_P - \phi_W)}{(\delta x)_w} \right] \\ & + \Delta x \left[h_n W_n \frac{\phi_N + \phi_P}{2} - \frac{h_n \Gamma_n (\phi_N - \phi_P)}{(\delta z)_n} - h_s W_s \frac{\phi_S + \phi_P}{2} + \frac{h_s \Gamma_s (\phi_P - \phi_S)}{(\delta z)_s} \right] \end{aligned} \quad (\text{A.2})$$

$$\text{Right side} = (S_c + S_p \phi_P) \Delta x \Delta z \quad (\text{A.3})$$

The capital letter in subscript refer to central value of the control volume, small letter denotes boundary value of the control volume.

Equation(A.4) be obtained after arrangement.

$$a_P \phi_P = a_E \phi_E + a_W \phi_W + a_N \phi_N + a_S \phi_S + b \quad (\text{A.4})$$

Where,

$$a_E \equiv -F_e + \frac{h_e \Gamma_e \Delta z}{(\Delta x)_e} \quad (\text{A.5})$$

$$a_W \equiv -F_w + \frac{h_w \Gamma_w \Delta z}{(\Delta x)_w} \quad (\text{A.6})$$

$$a_N \equiv -F_n + \frac{h_n \Gamma_n \Delta x}{(\Delta z)_n} \quad (\text{A.7})$$

$$a_S \equiv -F_s + \frac{h_s \Gamma_s \Delta x}{(\Delta z)_s} \quad (\text{A.8})$$

$$F_e \equiv h_e U_e \Delta z \quad (\text{A.9})$$

$$F_w \equiv h_w U_w \Delta z \quad (\text{A.10})$$

$$F_n \equiv h_n U_n \Delta x \quad (\text{A.11})$$

$$F_s \equiv h_s U_s \Delta x \quad (\text{A.12})$$

$$a_p \equiv a_E + a_W + a_N + a_S + F_e - F_W + F_n - F_S - S_p \Delta x \Delta z \quad (\text{A.13})$$

$$b \equiv S_C \Delta x \Delta z \quad (\text{A.14})$$

However, In the place where advection and diffusion coexist, using a central difference in advection term is known to cause fatal consequences due to increased reynolds number.

Therefore, In this study use hybrid method. Hybrid method use a central difference in case of same or less than level for advection and diffusion. In case of over level, the hybrid method use upwind differential scheme.

Here, the coefficient such a_s , a_e , a_w , a_n , a_s represented by the Equation (a.5)-(a.8) is modified as follow:

$$a_E = \max(a_E, -F_e, 0) \quad (\text{A.15})$$

$$a_W = \max(a_W, -F_w, 0) \quad (\text{A.16})$$

$$a_N = \max(a_N, -F_n, 0) \quad (\text{A.17})$$

$$a_S = \max(a_S, F_s, 0) \quad (\text{A.18})$$

A.3 Momentum equation of u,w

Discretization of the momentum equation is equal to scala but it should be noted that the position of control volume contact with each other.

In terms of surface gradient, It deals with taking aside for another generation term.

$$a_p U_p = a_E U_E + a_W U_W + a_N U_N + a_S U_S + g h_p \Delta z (h_w - h_e) + b \quad (\text{A.19})$$

$$a_p W_p = a_E W_E + a_W W_W + a_N W_N + a_S W_S + g h_p \Delta x (h_s - h_n) + b \quad (\text{A.20})$$

A.4 Solution of discretized equation

If we know the depth field, the way to solve the above described discretized equation get an answer, but here we solve the depth field and equation of motion at the same time. Here we shall solve the equation of motion and depth field at the same time by simple method.

Current velocity(u) represent sum of prediction(u) and correction(u') lead from momentum equation in the temporary depth field(h).

$$U = \tilde{U} + U' \quad (\text{A.21})$$

Current depth field(h) also can be expressed as follow.

$$h = \tilde{h} + h' \quad (\text{A.22})$$

A set of prediction values(\tilde{h}, \tilde{U}) note that satisfies the momentum equation of U when Equation (a.21) and (a.22) substituting into the momentum Equation(a.19) as follow:

$$\begin{aligned} a_p U_p' = & g \tilde{h}_p \Delta z (h_w' - h_e') + g \tilde{h}_p \Delta z (\tilde{h}_w - \tilde{h}_e) \\ & + g \tilde{h}_p \Delta z (h_w' - h_e') + [a_E U_E' + a_W U_W' + a_N U_N' + a_S U_S'] \end{aligned} \quad (\text{A.23})$$

First term of right side is dominant, ignore second term.

$$U_p' = d_x (h_w' - h_e') \quad ; \quad d_x \equiv \frac{g \tilde{h}_p}{a_p} \Delta z \quad (\text{A.24})$$

Momentum equation of W is obtained similarly to the following equation.

$$W_p' = d_y (h_s' - h_n') \quad ; \quad d_y \equiv \frac{g \tilde{h}_p}{a_p} \Delta x \quad (\text{A.25})$$

If we recreate them for scala control volume are as follows.

$$W_n' = d_{yn} (h_p' - h_n') \quad ; \quad d_{yn} \equiv \frac{\Delta x}{a_n} g \frac{(\tilde{h}_p + \tilde{h}_n)}{2} \quad (\text{A.26})$$

$$W_s' = d_{ys} (h_s' - h_p') \quad ; \quad d_{ys} \equiv \frac{\Delta x}{a_s} g \frac{(\tilde{h}_p + \tilde{h}_s)}{2} \quad (\text{A.27})$$

$$U_e' = d_{xe} (h_p' - h_e') \quad ; \quad d_{xe} \equiv \frac{\Delta z}{a_e} g \frac{(\tilde{h}_p + \tilde{h}_e)}{2} \quad (\text{A.28})$$

$$U_w' = d_{xw} (h_w' - h_p') \quad ; \quad d_{xw} \equiv \frac{\Delta z}{a_w} g \frac{(\tilde{h}_p + \tilde{h}_w)}{2} \quad (\text{A.29})$$

And it is when continuity equation discretize as follow:

$$h_e U_e' \Delta z - h_w U_w' \Delta z + h_n W_n' \Delta x - h_s W_s' \Delta x = 0 \quad (\text{A.30})$$

u , w , h divided by predicted value and corrected value is substituted in Equation(a.30).

$$\begin{aligned} & \tilde{h}_e U_e' \Delta z + \tilde{h}_e \tilde{U}_e' \Delta z + h_e' \tilde{U}_e' \Delta z + h_e' U_e' \Delta z \\ & - \tilde{h}_w U_w' \Delta z - \tilde{h}_w \tilde{U}_w' \Delta z - h_w' \tilde{U}_w' \Delta z - h_w' U_w' \Delta z + \dots = 0 \end{aligned} \quad (\text{A.31})$$

If high order term omitted between the corrected value when Equation (a.26)~(a.29) substituted in the Equation (a.31), the depth corrected equation is finally obtained.

$$a_P h'_P = a_E h'_E + a_W h'_W + a_N h'_N + a_S h'_S + b \quad (\text{A.32})$$

$$a_E \equiv \left(\tilde{h}_e d_{xe} - \frac{\tilde{U}_e}{2} \right) \Delta z \quad (\text{A.33})$$

$$a_W \equiv \left(\tilde{h}_w d_{xw} - \frac{\tilde{U}_w}{2} \right) \Delta z \quad (\text{A.34})$$

$$a_N \equiv \left(\tilde{h}_n d_{yn} - \frac{\tilde{W}_n}{2} \right) \Delta x \quad (\text{A.35})$$

$$a_S \equiv \left(\tilde{h}_s d_{ys} - \frac{\tilde{W}_s}{2} \right) \Delta x \quad (\text{A.36})$$

$$a_P \equiv a_E + a_W + a_N + a_S + \tilde{U}_e \Delta z - \tilde{U}_w \Delta z + \tilde{W}_n \Delta x - \tilde{W}_s \Delta x \quad (\text{A.37})$$

$$b \equiv \tilde{h}_w \tilde{U}_w \Delta z - \tilde{h}_e \tilde{U}_e \Delta z + \tilde{h}_s \tilde{W}_s \Delta x - \tilde{h}_n \tilde{W}_n \Delta x \quad (\text{A.38})$$

If coefficient such as a_E, a_W, a_N, a_S could be negative in Equation (a.33)~(a.36), The coefficient modified as follow because it will be divergent.

$$a_E = \tilde{h}_e d_{xe} \Delta z + \max \left(-\tilde{U}_e \Delta z, 0 \right) \quad (\text{A.39})$$

$$a_W = \tilde{h}_w d_{xw} \Delta z + \max \left(\tilde{U}_w \Delta z, 0 \right) \quad (\text{A.40})$$

$$a_N = \tilde{h}_n d_{yn} \Delta x + \max \left(-\tilde{W}_n \Delta x, 0 \right) \quad (\text{A.41})$$

$$a_S = \tilde{h}_s d_{ys} \Delta x + \max \left(\tilde{W}_s \Delta x, 0 \right) \quad (\text{A.42})$$

Procedure of solution are as follows:

- 1) Assuming the depth field, u,w calculated in Equation (a.19)~(a.20)
- 2) It will require a depth correction amount in Equation (a.32) by using such a quantity.
- 3) Solve the k,ε equation
- 4) Correction of depth
- 5) If the error of continuity and momentum equation below a certain value, finish the calculation. Otherwise, the calculation return to the first.

Convergence tests was to determine if sum of the residuals of continuity equation and momentum equation are satisfied criteria. Be solved discretized equation using TDMA. In addition, basic equation of flow has strong non linearity and iteration is unstable. Next step to solve this performed as follows.

$$\phi_p = \alpha \phi_p^M + (1 - \alpha) \phi_p^{M-1} \quad (A.43)$$

Where, α : relaxation coefficient, Subscript M: result of m number iteration.

APPENDIX B

REFERENCE OF BED MATERIAL SUSPENSION AND TRANSPORT IN STEADY UNIFORM CURRENTS

B.1 Bed load transport formulas

B.1.1 Meyer-Peter Mueller(1948)

Extensive experiment has carried out by Meyer-Peter and Mueller. The experiment were performed in a laboratory flume with a cross-section of 2*2m² and a length of 50m. Uniform bed material as well as particle mixtures were used in the experiments($d=0.4$ to 29mm, slope $I=0.0004$ to 0.02, depth=0.1 to 1.2m). The bed-load transport rate is expressed

$$\phi_b = 8(\mu\theta - 0.047)^{1.5} \quad (B.1)$$

$$\phi_b = \frac{q_{b,c}}{(s-1)^{0.5} g^{0.5} d_m^{1.5}} : \text{dimensionless bed-load transport rate}$$

$$\theta = \frac{\tau_{b,c}}{(\rho_s - \rho) g d_m} : \text{dimensionless particle mobility parameter}$$

$$q_{b,c} : \text{volumetric bed load transport rate(m}^2/\text{s)}$$

$$\tau_{b,c} = \rho g h I : \text{current-related bed-shear stress(N/m}^2\text{)}$$

$$d_m : \text{mean particle diameter(m)}$$

$\mu = (C / C')^{1.5}$: bed-form factor or efficiency factor

$C = 18 \log(12h / k_{s,c})$: overall Chezy- coefficient($m^{1/2}/s$)

$C' = 18 \log(12h / d_{90})$: grain-related Chezy-coefficient($m^{1/2}/s$)

h : water depth(m)

I : energy gradient(-)

$k_{s,c}$: effective bed roughness(m)

$s = \rho_s / \rho$: relative density(-)

The 0.047- value of Equation (B.1) can be interpreted as the critical mobility parameter(θ_{cr}). Since, the formula is related to coarse material, the authors preferred to use a constant value of 0.047.

Meyer-Peter Mueller proposed to use the mean particle diameter d_m as the characteristic particle diameter, defined as: $d_m = \sum p_i d_i$. The d_m -parameter is about 1.1 to 1.3 times larger than the d_{50} -parameter for nearly uniform material.

B.1.2 Frijlink(1952)

The formula of Frijlink essentially is an approximation of the formula of Meyer-Peter and Mueller(1948) and that of Einstein(1950).

$$q_{b,c} = 5\mu^{0.5} u_{*,c} d_{50} e^{-0.27/(\mu\theta)}$$

The parameters are identical to those of Meyer-Peter-Mueller(1948).

B.1.3 Bagnold(1966)

$$\tau_b = \rho g h I : \text{bed shear stress} \tag{B.2}$$

$$\tau_g = \left(\frac{\rho_s - \rho}{\rho_s} \right) g m \sin \beta : \text{gravity component} \tag{B.3}$$

$m = \rho_s V_b$: mass of bed load particle per unit area(kg/m^2)

β : slope angle

V_b : solid volume of bed load particles per unit area(m)

ρ_s : sediment density(kg/m^3)

The moving grains exert a normal stress on bed.

$$\sigma_s = (\rho_s - \rho) V_b g \cos \beta = \left(\frac{\rho_s - \rho}{\rho_s} \right) g m \cos \beta \quad (\text{B.4})$$

The tangential stress at the bed resisting the moving bed-load grains is:

$$\tau_s = \left(\frac{\rho_s - \rho}{\rho_s} \right) g m \cos \beta \tan \phi \quad (\text{B.5})$$

$\tan \phi$: dynamic friction coefficient

The applied bed shear stress(at the base of moving bed load layer) consist of a dispersive grain shear stress($\tau_{b,s}$) and an intergranular fluid bed-shear stress($\tau_{b,f}$)

$$\tau_b = \tau_{b,s} + \tau_{b,f} \quad (\text{B.6})$$

The dispersive stress($\tau_{b,s}$) is a shear stress which is transferred by grain to grain interaction. Since, the moving grains have a velocity smaller than the local fluid velocity, the grains receive their momentum from the fluid motion. Thus, the grains by receiving momentum resist the fluid motion. The $\tau_{b,f}$ -parameter is the residual fluid shear stress exerted directly on the bed by drag and skin friction. The $\tau_{b,f}$ -parameter is negligible small in the near-bed layer where the grain concentration is high. According to Bagnold, grains are set in motion only by the fluid shear stress($\tau_{b,f}$). As many layers of bed-load particles will be eroded as necessary to develop a dispersive grain shear stress which just keeps the fluid shear stress at the immobile bed below the critical bed shear stress for initiation of motion. Thus, the bed load layer acts as a protective layer to obtain a stable bed. When there is no bed load layer, each successive layer of bed particles will be eroded and suspended because the fluid bed

shear stress remains always larger than the critical shear stress.

Equilibrium of shear stress at the bed requires:

$$\tau_{b,s} = \tau_g + \tau_s \quad (\text{B.7})$$

$$\tau_{b,s} + (\rho_s - \rho) g v_b \sin \beta = (\rho_s - \rho) g v_b \cos \beta \tan \phi \quad (\text{B.8})$$

$$\tau_{b,s} = (\rho_s - \rho) g v_b \cos \beta (\tan \phi - \tan \beta) \quad (\text{B.9})$$

The work(W_r) required to be done by the grain shear stress in moving the bed load particles is:

$$W_r = \tau_{b,s} u_b = (\rho_s - \rho) V_b u_b \cos \beta (\tan \phi - \tan \beta) \quad (\text{B.10})$$

Defining the volumetric bed load transport(m^2/s) as $q_{bn,c} = V_b u_b$, it follows that:

$$W_r = (\rho_s - \rho) g q_{b,c} \cos \beta (\tan \phi - \tan \beta) \quad (\text{B.11})$$

The available fluid energy per unit area and time is:

$$W_a = \tau_b \bar{u} = \rho g h I \bar{u} \quad (\text{B.12})$$

Bagnold assumed that: $W_r = e_b W_a$, yielding:

$$q_{b,c} = \frac{e_b \tau_b \bar{u}}{(\rho_s - \rho) g \cos \beta (\tan \phi - \tan \beta)} \quad (\text{B.13})$$

$q_{b,c}$: volumetric bed load transport(m^2/s)

$\tau_b = \rho g h I$: overall bed shear stress(N/m^2)

\bar{u} : depth averaged velocity(m/s)

I : energy gradient

e_b : efficiency factor(0.1-0.2)

$\tan \phi = 0.6$: dynamic friction coefficient

$\tan \phi = I_b$: bed slope

h : water depth(m)

g : gravity acceleration(m/s^2)

v_b : volume of bed load per unit area(m^3/m^2)

B.2 Suspended load transport rates

B.2.1 Einstein(1950)

The method of Einstein is based on a parabolic distribution of the fluid mixing coefficient and a logarithmic distribution of the velocity.

The suspended sediment transport rate can be expressed as:

$$q_{s,c} = 11.6u_*'c_a a \left[I_2 + I_1 \ln(30.2eh/d_{65}) \right] \quad (B.14)$$

$$I_1 = 0.216 \frac{A^{Z-1}}{(1-A)^Z} \int_A^1 \left(\frac{1-X}{X} \right)^Z dX \quad (B.15)$$

$$I_2 = 0.216 \frac{A^{Z-1}}{(1-A)^Z} \int_A^1 \left(\frac{1-X}{X} \right)^Z \ln(X) dX \quad (B.16)$$

$q_{s,c}$: volumetric current related suspended load transport(m^2/s)

u_* : current related bed shear velocity due to the grains(m/s)

c_a : reference concentration(volume) $q_b / (11.6u_*'a)$

a : reference level($=2d$)(m)

h : water depth(m)

d : particle diameter(m)

$A=a/h$: dimensionless reference level

$X=z/h$: dimensionless vertical coordinate

$Z = w_s / (\kappa u_*)$: suspension number

e = correction factor

According to Einstein, the suspended load transport is related to the grain shear velocity (u_*) and not to the overall shear velocity(u_*). The reference concentration is determined from the bed load transport, assuming a bed load layer thickness equal to 2 particle diameters. For almost uniform bed material the d_{65} is taken as the representative particle diameter. For graded bed material the size fraction method should be used. The I_1 and I_2 integrals can be determined graphically(see Einstein,

1950) or numerically. The method of Einstein is not given in full detail here, because of its complexity. Furthermore, an extensive verification study of white et al(1973) has shown that the predicting ability of the Einstein method is much less than other(more simple) methods.

B.2.2 Bijker(1971)

Based on the concept of Einstein(1950), Bijker(1971) proposed:

$$q_{s,c} = 1.83q_{b,c} [I_2 + I_1 \ln(33h / k_s)] \quad (\text{B.17})$$

$q_{s,c}$: suspended sediment transport rate(m^2/s)

$q_{b,c}$: bed load transport rate(m^2/s)

I_1 : integral according to Equation (B.15)

I_2 : integral according to Equation (B.16)

$a = k_s$: reference level

The current related bed load transport rate(m^2/s) is expressed as:

$$q_{b,c} = bu_* d_{50} e^{-0.27/(\mu\theta)} \quad (\text{B.18})$$

u_* : overall bed shear velocity

θ : mobility parameter

$\mu = (C / C')^{1.5}$: bed form factor

C : overall Chezy coefficient

C' : grain related Chezy coefficient($=18\log(12h/d_{90})$)

b : coefficient($=1$ to 5)

Because the reference level is assumed to be equal to the bed roughness height($a=k_s$), the ratio $q_{s,c}/q_{b,c}$ can be expressed as a function of the parameter Z and k_s/h .

B.2.3 Van Rijn(1984)

The suspended load transport can be described below:

$$q_{s,c} = F \bar{u} h c_a \quad (\text{B.19})$$

$$c_a = 0.015 \frac{d_{s0}^{1.5}}{a D_*^{0.3}} : \text{reference concentration}$$

$$D_* = d_{s0} \left(\frac{(s-1)g}{\nu^2} \right)^{1/3} : \text{particle parameter}$$

$$T = \frac{\tau_b' - \tau_{b,cr}}{\tau_{b,cr}} : \text{bed shear stress parameter}$$

$$\tau_b' = \rho g \left(\frac{\bar{u}}{C'} \right)^2 : \text{current related effective bed shear stress (N/m}^2\text{)}$$

$$u_* = \frac{g^{0.5}}{C} \bar{u} : \text{current related overall bed shear velocity (m/s)}$$

$$C' = 18 \log \left(\frac{12h}{3d_{90}} \right) : \text{grain related Chezy coefficient (m}^{0.5}\text{/s)}$$

$$C = 18 \log \left(\frac{12h}{k_s} \right) : \text{overall Chezy coefficient (m}^{0.5}\text{/s)}$$

$$\tau_{b,cr} = (\rho_s - \rho) g d_{s0} \theta_{cr} : \text{critical bed shear stress (N/m}^2\text{)}$$

$$Z' = Z + \psi : \text{suspension number}$$

$$Z = \frac{w_s}{\beta k u_*} : \text{suspension number}$$

$$\psi = 2.5 \left(\frac{w_s}{u_*} \right)^{0.8} \left(\frac{c_a}{c_0} \right)^{0.4} : \text{stratification correction}$$

$$\beta = 1 + 2 \left(\frac{w_s}{u_*} \right)^2 : \text{ratio of sediment and fluid mixing coefficient}$$

$$d_s = [1 + 0.011(\sigma_s - 1)(T - 25)] d_{s0} : \text{representative particle size of suspended sediment}$$

$$q_{s,c} : \text{volumetric current related suspended load transport (m}^2\text{/s),}$$

u : depth averaged velocity(m/s), h : water depth(m), a : reference level, k_s : overall roughness height(m), Δ : bed form height(m), d_{s0} : median particle diameter of bed

material(m), d_{16} , d_{84} , d_{50} : characteristic diameter of bed material(m), w_s : fall velocity of suspended sediment, d_s : representative particle size of suspended sediment, σ_s : geometric standard deviation of bed material, c_0 : maximum concentration(=0.65), s : specific density, ρ_s : sediment density, ρ : fluid density, ν : kinematic viscosity coefficient, κ : constant of Von karman, g : acceleration of gravity.

The F-factor is:

$$F = \frac{u_*}{\kappa u} \left(\frac{a}{h-a} \right)^Z \left(\int_{a/h}^{0.5} \left(\frac{h-z}{z} \right)^{z'} \ln(z/z_0) d(z/h) + \int_{0.5}^1 e^{-4z'(z/h-0.5)} \ln(z/z_0) d(z/h) \right) \quad (B.20)$$

Equation (B.20) cannot be integrated analytically. An approximate solution accurate to about 25% for $0.3 \leq Z' \leq 3$ and $0.01 \leq a/h \leq 0.1$ is given by:

$$F = \frac{(a/h)^{z'} - (a/h)^{1.2}}{(1-a/h)^{z'} (1.2 - z')} \quad (B.21)$$

The β -factor yields an increase of the suspended load transport rate, whereas the ψ -factor yields a decrease of the transport rate. In the lower regime both effects cancel out($\beta=1$, $\psi=0$).

References

1. Meyer-Peter, E. and Mueller, R., 1948. Formulas for bed-load transport. Sec. *Int. IAHR congress*, Stockholm, Sweden.
2. Frijlink, H.C., 1952. Discussion of bed load movement formulas. Report No. X2344/LV, Delft, The Netherlands.
3. Bagnold, R.A., 1966. An Approach to the Sediment Transport Problem from General Physics. *Geological Survey Prof. Paper* 422-I, Washington.
4. Einstein, H.A., 1950. The Bed-Load Function for Sediment Transportation in Open Channel Flow. *Technical Bulletin* No. 1026, U.S. Dep. of Agriculture, Washington, D.C.
5. White, W.R., Milli, H. and Crabbe, A.D., 1973. Sediment Transport, An Appraisal of Available Methods. *Int. Report* 119, Wallingford, England.

6. Bijker, E.W., 1971. Longshore Transport Computations. *Journal of the waterways, Harbours and Coastal Engineering Division*, Vol.97, No. WW4.
7. Van Rijn, L.C., 1984. Sediment Transport, PartII: Suspended Load Transport. *Journal of Hydraulic Engineering, ASCE*, Vol. 110, No. 11.